INVESTIGATION OF POLARIZATION MODE DISPERSION MEASUREMENT PERFORMANCE IN OPTICAL FIBRE WITH A FOCUS ON THE FIXED ANALYZER TECHNIQUE

Romeo Reginald Gunther Gamatham

Submitted in partial fulfilment of the requirements for the degree of

MAGISTER SCIENTIAE

in the Faculty of Science at the Nelson Mandela Metropolitan University

August 2008

Supervisor: Professor A. W. R. Leitch

Co-supervisor: Dr Tim Gibbon

To my parents, Salomon and Maggie Gamatham

ACKNOWLEDGEMENTS

My sincere thanks and gratitude is extended to my supervisor, Professor Andrew Leitch, and co-supervisor, Doctor Timothy Gibbon for their prudent guidance and tremendous support throughout this study.

I also thank Doctor Lorinda Wu for discussions and for proofreading this dissertation.

My thanks are extended to staff and students both in the fibre optics laboratory and within the Physics department for their wisdom, experience and general support.

I thank the Nelson Mandela Metropolitan University research partners and the Fibre Optics research group project Funders:
Aberdare Fibre Optics Cables
African Laser Centre
South African National Research Foundation (NRF)
Technology and Human Resources for Industrial Programme (THRIP)
Telkom South Africa
INGOMA Communication Services
MCT Telecommunications
Corning Optical Fibre

Special thanks go out to Telkom South Africa based in Port Elizabeth for allowing us to carry out measurements on their deployed optical fibre cables.

I thank the Nelson Mandela Metropolitan University for their financial support.

Finally I thank all my friends and my family for their continuous support and encouragement during this study.

TABLE OF CONTENTS

CHAPTER 5: POLARIZATION MODE DISPERSION MEASUREMENT TECHNIQUES

CHAPTER 6: INSTRUMENTATION

CHAPTER 7: AUTOMATION OF DATA COLLECTION AND PMD CALCULATION

CHAPTER 8: FIXED ANALYZER LAB RESULTS

CHAPTER 9: A COMPARISON OF PMD MEASUREMENT RESULTS OF BURIED DEPLOYED FIBRE, FIXED ANALYZER VS COMMERCIALLY BASED TECHNIQUES

SUMMARY

The work presented in this dissertation is a comparative study of polarization mode dispersion (PMD) measurement performance where the fixed analyzer (FA) technique was built and tested for the first time in South Africa. Techniques involved in the study are: the Jones matrix eigenanalysis (JME), generalised interferometric technique (GINTY) and the FA technique, with a particular focus on the FA technique.

The FA PMD measurement technique determines the average differential group delay (DGD) from the transmitted intensity spectrum through a polarizer and has three analysis methods (extrema counting, mean level crossing and Fourier analysis) which were all evaluated. PMD measurements were performed in the laboratory on several different fibre types and in the field on buried deployed Telkom fibre links (28.8 km).

The techniques showed good agreement in the measured PMD value, both in the laboratory and field measurements. In particular very good agreement was found between the JME average DGD and the extrema counting analysis PMD value. The GINTY and FA Fourier analysis method also gave very similar PMD values. It was found that the fibre birefringence and the mode coupling manifest in different ways on the intensity spectrum. By using the FA ratio method, the length regimes of the different fibre types were determined.

Three characteristics of the FA technique were investigated, namely: wavelength window variation, sampling and input SOP scrambling. It was found that the wavelength window and the PMD are inversely proportional. Correct sampling plays a significant role in determining the correct measured PMD value. Lastly an average PMD value over the PMD values for different input SOPs serves as a better representation of the true PMD value.

An additional study showed that the FA technique and a developed Poincaré sphere analysis method agree very well regarding the PMD value.

Keywords: polarization mode dispersion (PMD), state of polarization (SOP), mode coupling, birefringence, fixed analyzer (FA) method, Jones matrix eigenanalysis (JME), generalized interferometric technique (GINTY).

ABBREVIATION LIST

DFB distributed feedback laser
DGD differential group delay
DOP degree of polarization
DUT device under test
DWDM dense wavelength division multiplexing
EDFA erbium doped fibre amplifier
FA fixed analyzer
FUT fibre under test
GINTY generalized interferometric
JME Jones matrix eigenanalysis
MMM Mueller matrix method
OSA optical spectrum analyzer
PBS polarization beam splitter
PDF probability distribution function
PDL polarization dependent loss
PMD polarization mode dispersion
PMF polarization maintaining fibre
PSA Poincaré sphere analysis
PSP principal state of polarization
RMS root mean square
SOP state of polarization
TINTY traditional interferometric
WDM wavelength division multiplexing

CHAPTER 1

INTRODUCTION

In the 1830s electrical communication started gaining popularity, where the first transatlantic telegraph cable went into operation in 1866 [1]. After this analogue transmission of electrical signals were being used with the invention of the telephone. New means of increasing the communication systems capacity were constantly being developed. In the 1940s this came in the form of coaxial cables which operated at 3 MHz [1]. The load that communication systems could carry was further increased by using microwaves as carriers. During the second half of the twentieth century it was realized that a lot more information could be transmitted if the carrier was an optical signal. At the time it was not possible because first the laser needed to be invented, after which a medium that could confine the light being transmitted was required. In 1966 it was suggested that optical fibre be used [1].

High attenuation of the light signal and several dispersive effects, like chromatic dispersion and modal dispersion needed to be overcome. The invention of low loss single mode fibre and dispersion shifted fibre solved these problems. Both the transmission distance and the bit rate improved considerably. In 1990 third generation lightwave systems operating at 2.5 Gb/s became available commercially [1]. Fourth generation lightwave systems make use of optical amplification to increase the repeater spacing distance and of wavelength division multiplexing (WDM) systems to increase the bit rate.

As the bit rate continues to increase a major limiting factor is polarization mode dispersion (PMD). PMD refers to the time delay that occurs between two orthogonal polarization modes, and is caused by the joint effects of birefringence and mode coupling. PMD has the effect of broadening the input light pulse. This broadening effect may result in the overlap between adjacent bits causing signal distortion. Due to the broadened input pulse, PMD also causes power fading. Power fading occurs because of the power distribution which takes place as the pulse spreads out. Hence a

lower power reaches the detector as it is no longer confined to the centre of the bit. Due to the fact that the fibre PMD has a temperature dependence and is affected by external mechanical vibrations, PMD is a stochastic phenomenon which varies with time. Therefore routine PMD measurements need to be conducted. This demands for easy to implement PMD measurement techniques.

The Nelson Mandela Metropolitan University (NMMU) Fibre Optics research group has investigated the PMD measurement performance of several interferometric PMD measurement techniques, the P-OTDR (polarization optical time domain reflectometer) and the Jones matrix eigenanalysis (JME) technique. This document presents the first FA technique PMD measurements conducted in South Africa. The PMD measurement performance of the technique is thoroughly investigated by means of a comparative study with several different commercially available measurement techniques. Several characteristics pertaining to PMD measurements of the FA technique are also examined.

The structure of this dissertation is as follows: Chapter 2 presents a background to the field of fibre optics. The structure and geometrical properties of optical fibre is discussed. This is followed by a discussion of the mathematical details of the transmission of a light pulse through the fibre and the various modes which arise as a result of this. The chapter ends with an overview of various optical effects which take place throughout the fibre. Chapter 3 provides the polarization concepts required when dealing with light. The chapter deals with various methods of representing polarization states and measuring the state of polarization of light. Chapter 4 focuses on PMD and discusses the dispersive effect in detail.

Chapter 5 concentrates on the various PMD measurement techniques. The FA measurement technique, the interferometric techniques and the JME technique are all discussed in detail. The chapter presents the operating principle of each measurement technique and places a particular focus on the FA measurement technique. Chapter 6 offers information pertaining to all the instruments used to carry out this study. In chapter 7 the operating principle and the user interface of the program written in LabVIEW is explained.

The dissertation then moves on to presenting the results. In chapter 8 measurements done using the FA technique are illustrated. All the measurement results presented in chapter 8 were performed in the laboratory. PMD measurements of the FA technique are compared with those of GINTY and JME. The length regime of the fibre under test (FUT) is also determined using a method related to the FA technique. Chapter 9 explores PMD measurements performed in the field using the FA, GINTY and JME techniques. A comparative study is presented between these techniques. The characteristics of the FA technique (wavelength window size, sampling and SOP scrambling) are presented and discussed in detail. Chapter 10 briefly looks into a comparison of the FA technique and our developed PSA method. Thereafter the conclusions follow.

CHAPTER 2

FIBRE OPTICS BACKGROUND

Optical fibre technology has advanced at a tremendous pace over the last ten years. In the year 1992, transmission systems were limited to a data transfer speed of 2.5 Gb/s. Now optical networks have exceeded bit rates of 10 Gb/s and network operators are looking at 40 Gb/s over a single fibre in operational telecommunication networks. Hence by using wavelength division multiplexing (WDM) for 64 WDM channels at 10 Gb/s over 4 fibre pairs the total network capacity becomes 2.56 Tb/s [1]. The backbone of optical communication systems is optical fibre. With its many advantages optical fibre has proven to be a great benefit to the telecommunications industry. This chapter serves to introduce optical fibre communication, with the light on transmission of optical signals through optical fibre. The optical fibre structure is presented with an explanation regarding the phenomena of total internal reflection, which is responsible for guiding light in optical fibres. Various fibre core structures, together with their characteristics have also been included. The chapter then places focus on several phenomena, which manifest as limiting factors to the transmitted signal or signals.

2.1 Optical fibre structure

Optical fibres have been constructed to act as optical guides used for transferring light signals from one place to another. The transmitted light is used as a communication signal in order to transfer data, hence by modulation of the light signal a range of bits may be sent through the fibre. The light transmission takes place over long distances. Therefore it is necessary for the light to remain within the optical fibre with minimal signal degradation.

An optical fibre section is made up of thinly drawn highly purified glass SiO_2 consisting of a core region, surrounded by and a cladding which differ in their

refractive indices (see figure 2.1). The refractive index of the core is higher than that of the cladding. This is achieved by doping the core with germanium. The preference for Germanium (Ge) is that Ge absorbs less energy at 1300 nm and 1550 nm than other possible dopants. This arrangement allows the fibre to confine electromagnetic energy in the form of light within the core region and guide it in the direction parallel to its axis.

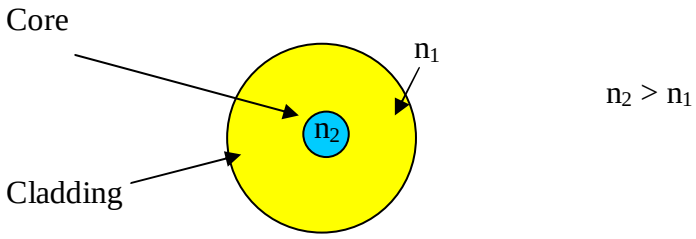

Figure 2.1 Fibre cross-section.

A plastic cover protects the cladding against external stress and strain.

2.2 Geometrical optical properties of fibre

The fibre properties are determined by the dimensions of both the core and the cladding. In addition a specific fibre type may be designed changing how the refractive index (RI) profile in the core varies from the centre of the fibre core.

In general, the core size of a fibre in relation to the wavelength of the light determines the number of guided modes the fibre will support. Standard single mode fibres have a core diameter of 9 μm (micrometer) and a cladding diameter of 125 μm. Ideal single mode fibre supports as the name states, only one single guided mode. A typical multimode fibre core would have a core diameter of approximately 100 μm and a cladding of 140 μm. Multiple stable electromagnetic wave patterns are supported by this fibre type. Hence the fibre's capability for supporting more modes is directly proportional to the size of the core diameter. The number of modes also depends on the wavelength, refer to section 2.3 of chapter 2.

The refractive index profile of a fibre also plays a major role in determining specifications of the fibre. A particular example is a step index profile. In this profile the refractive index remains the same throughout the fibre core and changes abruptly at the core cladding interface [2]. In a graded refractive index profile the refractive index changes gradually from the centre of a fibre core as shown in figure 2.2 (b) [2]. Graded index fibres are used to reduce the effects of material dispersion.

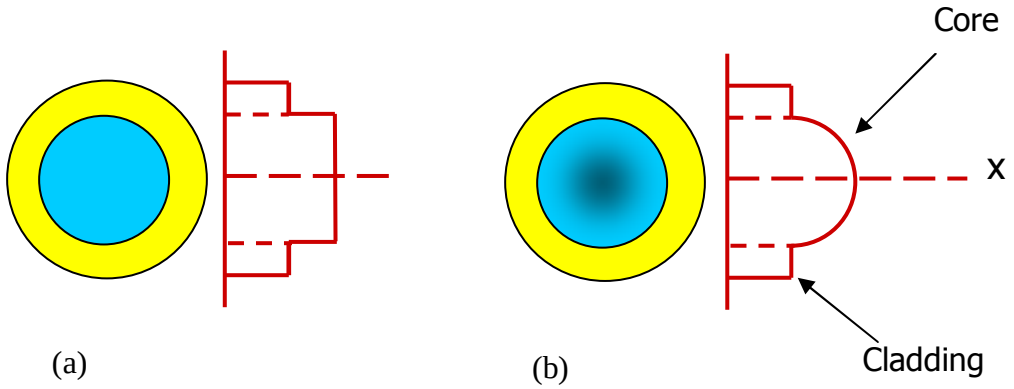

Figure 2.2 Refractive index profile of optical fibre: (a) Step index, (b) Graded index.

2.3 Characteristics of optical transmission through fibre

Governing the confinement of an optical signal within the core of an optical fibre is the total internal reflection phenomenon. Total internal reflection takes place within the fibre core because of the difference in the refractive index between the core and the cladding where the core has a higher refractive index than the cladding. The ray optics model assumes that light travels in a straight line and is either transmitted or reflected, refracted or absorbed at surface contacts. The ray optics model states that light will be reflected back into the fibre core at the core cladding interface depending on the critical angle which is a function of the refractive index of the core (n_2) and that of the cladding (n_1) and is given by

$$\theta_c = \sin^{-1}\left(\frac{n_1}{n_2}\right). \qquad (2.1)$$

Hence according to the ray optics model the light signal is guided throughout the fibre by continuously reflecting off the core cladding interface.

Optical fibre can support several modes. A fibre may be classified as either single mode or multimode fibre depending on the number of modes that the fibre allows to be transmitted. These modes refer to special solutions of the boundary conditions and have the specific property that their spatial distribution must remain unaltered with propagation. A very simple but important cut off condition is the waveguide parameter V [2] of the fibre given by

$$\mathrm{V} = \frac{2\pi \mathrm{a}}{\lambda}\left(n_2^2 - n_1^2\right)^{1/2}, \tag{2.2}$$

where the parameter a is related to the cylindrical radial diameter. Fibres are single mode for values of V less than 2.405. The HE_{11} mode has no cut off and only ceases to exist when the fibre core diameter is zero. The waveguide parameter also serves as an indicator of the number of modes present in multimode fibre [2].

The above theory regarding guided modes may be derived using Maxwell's equations [3]. They constitute a set of coupled, first order, partial differential equations which may be decoupled by applying the curl to both the curl of the electric field component and that of the magnetic field component. For the electric field this yields the wave equation given by

$$\nabla^2 \overline{E}(\bar{r}) + k_0^2 n^2(\bar{r})\overline{E}(\bar{r}) = 0 \tag{2.3}$$

where $k_0^2 \equiv \omega^2\mu\varepsilon_0 = (2\pi/\lambda)^2$, n is the refractive index, ω the frequency, μ is the permeability of free space, ε_0 is the permittivity of free space and $\overline{E}$ the electric field vector. A mode is a solution of the wave equation 2.3 where the solutions must obey the boundary conditions which call for continuity of the tangential components of $\overline{E}$ and $\overline{B}$ at the dielectric interface. Taking the electric field component to have the form

$$\overline{E}(\bar{r},t) = \overline{E}(x,y)e^{i(\omega t - \beta z)} \tag{2.4}$$

equation 2.3 reduces to the form

$$\left(\frac{\partial^2}{\partial x^2}+\frac{\partial^2}{\partial y^2}\right)\overline{E}(x,y)+[k_0^2 n^2(\bar{r})-\beta^2]\overline{E}(x,y)=0 \qquad (2.5)$$

For the sake of mathematical simplicity the discussion is limited to a planar waveguide which gives 2.5 to have the form

Region I (RI is n_1) $$\frac{\partial^2}{\partial x^2}E(x,y)+[k_0^2 n_1^2-\beta^2]E(x,y)=0 \qquad (2.6a)$$

Region II (RI is n_2) $$\frac{\partial^2}{\partial x^2}E(x,y)+[k_0^2 n_2^2-\beta^2]E(x,y)=0 \qquad (2.6b)$$

Region III (RI is n_3) $$\frac{\partial^2}{\partial x^2}E(x,y)+[k_0^2 n_3^2-\beta^2]E(x,y)=0\,. \qquad (2.6c)$$

Assume that $n_2 > n_3 > n_1$. For the first situation suppose $\beta > k_0 n_2$, it then follows that $(1/E)(\partial^2 E/\partial x^2) > 0$ everywhere hence $E(x)$ is exponential in all three layers. Still having to satisfy the continuity at the boundary condition the resulting distribution is as shown in figure 2.3 (a) from Yariv [3]. This solution is not physically realizable as the field keeps on increasing exponentially and thus does not correspond to a real wave.

For the situation $k_0 n_3 < \beta < k_0 n_2$ the solution is sinusoidal in region II as $(1/E)(\partial^2 E/\partial x^2) < 0$ but has exponential solutions in region I and III. This gives rise to two possible distributions shown in figure 2.3 (b and c) where the energy of these modes is confined to region II which has the highest index of refraction.

Situation $k_0 n_1 < \beta < k_0 n_3$ corresponds to exponential behaviour in region I and sinusoidal behaviour in regions II and III shown in figure 2.3 (d). These modes are referred to as substrate radiation modes. Finally $0 < \beta < k_0 n_3$ gives rise to sinusoidal behaviour in all regions where these are the radiation modes as illustrated in figure 2.3 (e).

From this mathematical formulation it can be concluded that the allowed values of β in the propagation region $k_0n_3 < \beta < k_0n_2$ are discrete. The number of allowed confined modes depends on the width (t) of region II, the frequency and the refractive indices. Hence increases in the width t leads to the introduction of more confined modes.

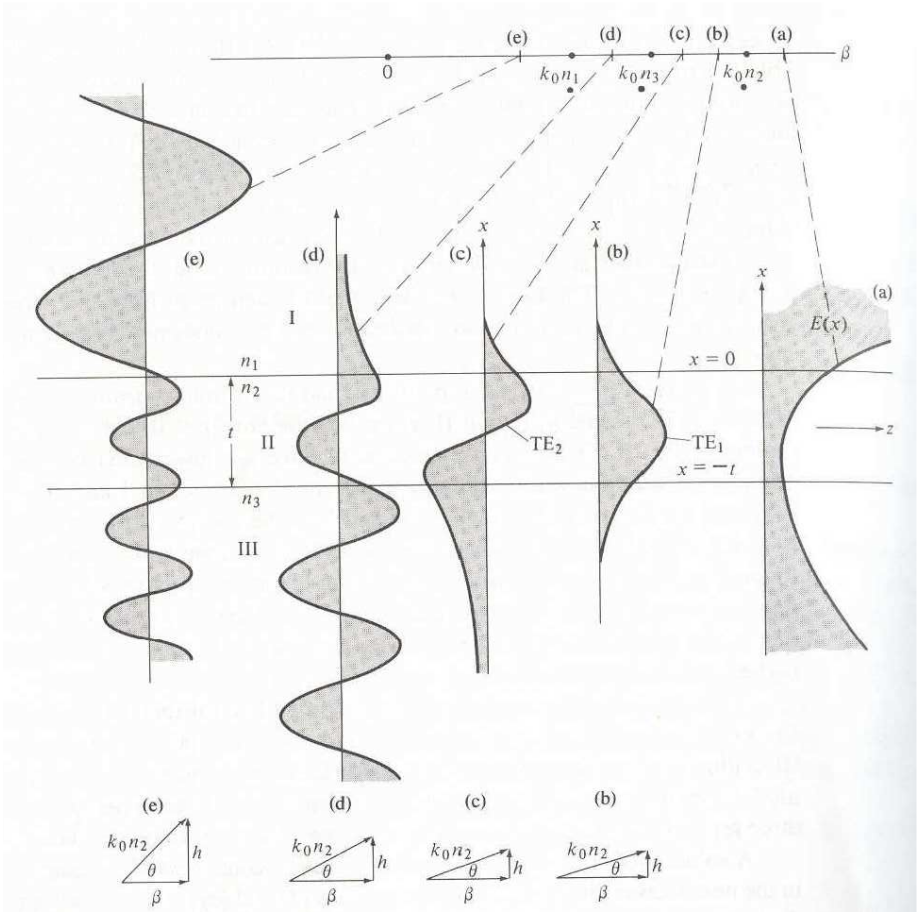

Figure 2.3 Figure from Yariv [3] pg. 494.

2.4 Optical effects within the fibre

When an optical signal is transmitted through the fibre it is crucial that the signal change is minimal. This section discusses how attenuation, dispersion and nonlinear effects all alter the input light signal.

2.4.1 Attenuation

Attenuation refers to the reduction in signal strength by comparing the output power to the input power. Attenuation (α) is expressed in decibels (dB) which is a logarithmic unit and defines the loss as

$$\alpha(\text{dB}) = -10 \times \log_{10}\left(\frac{\text{power out}}{\text{power in}}\right). \tag{2.7}$$

Signal attenuation may also be described by using the attenuation co-efficient which is simply the attenuated signal divided by the fibre length and expressed as dB per kilometre.

Attenuation mechanisms in a fibre are absorption, scattering and radiation loss of the optical signal. These mechanisms arise either as a result of the fibre material or the fibre geometry or both. Absorption in particular is related to the fibre material, while scattering is associated both with the fibre material and with structural imperfections of the fibre. Radiation effects are mainly due to perturbations of the fibre geometry.

Absorption may occur because of atomic defects or impurities in the glass material. Atomic defects of the glass fibre occur when the glass fibre is exposed to radiation, which changes the internal structure of the material. Impurities also act as major absorption centres. The OH ion impurity is known to cause high attenuation where its presence results in major absorption peaks occurring at distinct wavelengths.

Scattering in fibre arises mainly because of variations in the material density, compositional fluctuations and structural in-homogeneities or defects occurring due to fibre manufacture. Variations in the molecular density and compositional fluctuations as a result of several oxides present in the makeup of the fibre results in refractive index variations occurring within the glass over distances small compared to the wavelengths. These index variations result in Rayleigh scattering of the light. Rayleigh scattering has a wavelength dependence of λ^{-4}, hence it decreases considerably with an increase in wavelength. Other losses are fibre bending, core and cladding losses described in Keiser [2].

2.4.2 Dispersion effects in optical fibres

Several dispersive effects occur within optical fibre of which the most common are modal, chromatic and polarization mode dispersion. Their common feature is that they all distort the input optical signal.

In multimode fibres modal dispersion is defined as the dispersive effect which arises due to each mode travelling with a different velocity [4]. Modal dispersion may also be viewed as the dispersive effect caused by the discrete electromagnetic wave patterns travelling through different paths, hence causing a dispersion of the modes in time [1]. The problem of modal dispersion is solved by using single mode fibres.

Chromatic dispersion consists of material and waveguide dispersion. It is a phenomenon which is a result of the group velocity being a function of wavelength. Material dispersion arises from the variation of the refractive index of the core as a function of wavelength. Hence material dispersion causes a wavelength dependence of the group velocity, implying that pulse spreading will still occur even if all the wavelengths follow the same path. Waveguide dispersion occurs as a result of the fibre design. Approximately 80 % of the optical power is confined in the fibre core, while the remaining 20 % propagates at a faster rate through the cladding. Hence the difference in propagation speed causes waveguide dispersion. Since chromatic dispersion is the sum of material and waveguide dispersion, in theory zero chromatic dispersion is achievable by tuning the waveguide dispersion. These types of fibres are called dispersion shifted fibres.

Polarization mode dispersion (PMD) is related to the time delay between the orthogonal polarization modes that transpires from the effect of birefringence. The term PMD encompasses both the effect of birefringence and mode coupling. Birefringence comes about from geometric irregularities of the fibre core or internal and external mechanical stresses. The difference in the refractive indices cause a time delay of the order of pico-seconds between the two orthogonal polarization modes. Other effects which may affect the fibre birefringence are bending, twisting or pinching of the fibre and also temperature changes. Mode coupling further

complicates the effect of birefringence. It refers to the re-coupling of the optical energy from one birefringent fibre section to the other. This thesis concentrates on PMD measurements, hence theory regarding the dispersive effect will be presented in detail in chapter 4.

2.4.3 Non-linear effects

Optical fibres become nonlinear for intense electromagnetic fields. This means that the output and input power are no longer proportional, and the reason is that the power is used to create other effects. In general nonlinear effects increase in strength when the optical energy is confined to a small area and also with an increase in the intensity of the light. All nonlinear effects place limitations on the system performance. Two nonlinear categories are addressed. The first category includes nonlinear inelastic scattering processes and the second nonlinear effects arise from intensity dependent variations of the refractive index in the fibre. When any of these nonlinear effects cause signal impairment, additional optical power will be required at the receiver end to maintain the same BER (bit error rate).

Stimulated Raman scattering (SRS) and stimulated Brillouin scattering (SBS) fall under the umbrella of the nonlinear inelastic scattering category. These effects reduce the intensity of some channels while providing gain to other wavelength channels, thereby producing crosstalk between wavelength channels. SRS describes the interaction of the light waves with the vibrational modes of the molecules. If a photon is incident on a molecule with a bond having a particular frequency, the molecule absorbs some of the energy leaving the photon with a lower energy and a lower frequency. Provided that the new frequency is the same as an already existing frequency, the SRS light is amplified. Therefore SRS causes an intensity reduction for the shorter wavelengths and amplifies that of the longer wavelengths, more detail may be found in reference [2].

SBS comes about from the lightwaves scattering from acoustic waves. SBS is normally backscattered in the lightwave system. The backscattered light is amplified

by the forward-propagating signals, which leads to a depletion of signal power. The frequency of the backscattered light experiences a Doppler shift, which depends on the refractive index and the velocity of sound in the material, for further reading go to reference [2].

Nonlinear effects pertaining to the intensity-dependent variations of the refractive index produces effects such as self-phase modulation (SPM), cross-phase modulation (XPM) and four-wave mixing (FWM). Both SPM and XPM affect the phase of the signal causing chirping in digital pulses. In general the refractive index of many optical materials has a weak dependence on the intensity and is given by

$$n = n_0 + n_2 I = n_0 + n_2 \frac{P}{A_{eff}} \tag{2.8}$$

where n_0 is the ordinary refractive index of the material and n_2 is the nonlinear index coefficient [2]. The refractive index increases with intensity and its nonlinearity is known as the Kerr nonlinearity. The Kerr nonlinearity produces a carrier-induced phase modulation known as the Kerr effect. This may lead to self-phase modulation where the fluctuating optical power in the light wave is converted to phase fluctuations of the same wave. XPM converts the power fluctuations in a particular wavelength channel to phase fluctuations in other co-propagating channels. When SPM and XPM spectral broadening is combined with dispersion, the effect can be a major limitation to very long transmission links. Four-wave mixing arises from the interaction of three co-propagating frequencies to generate a new frequency, whose frequency is dependent on the three original frequencies. This new frequency may result in severe crosstalk.

The field of fibre optics is constantly advancing, with the common purpose of increasing the transmission capacity of the optical network. The introduction of several components, which are constantly being developed, has acted as a catalyst for further advancement. Examples are; WDM (wavelength division multiplexed) components, improved detectors and transmitters, EDFA (erbium doped fibre amplifiers), etc. System limitations are caused by several limiting factors, which were mentioned in this chapter. PMD has proven to act as a major limiting factor as the

transmission rate increases. This calls for detailed studies pertaining to measuring, monitoring and mitigating the problem of PMD. The following chapter touches on relevant polarization concepts of light, required to understand PMD.

CHAPTER 3

POLARIZATION CONCEPTS OF LIGHT

Maxwell's equations for a waveguide may be used to derive the three dimensional wave equation. The electric field component of the light wave propagating down the fibre determines the polarization state of the light wave. Several methods of representing the state of polarization of a light wave will be discussed throughout this chapter.

3.1 Maxwell's equations and electromagnetic wave

The optical fibre core acts like a waveguide for propagating electromagnetic waves since these waves are light waves. In order to analyze the optical waveguide, Maxwell's equations, which give the relationship between the electric and magnetic fields, are required. Maxwell's equations for a linear, isotropic dielectric material having no currents and free charge take the form

$$\nabla \times \overline{\mathrm{E}} = -\frac{\partial \overline{\mathrm{B}}}{\partial t} \tag{3.1a}$$

$$\nabla \times \overline{\mathrm{H}} = \frac{\partial \overline{\mathrm{D}}}{\partial t} \tag{3.1b}$$

$$\nabla \cdot \overline{\mathrm{D}} = 0 \tag{3.1c}$$

$$\nabla \cdot \overline{\mathrm{B}} = 0 \tag{3.1d}$$

where $\overline{\mathrm{D}} = \in \overline{\mathrm{E}}$ and $\overline{\mathrm{B}} = \mu \overline{\mathrm{H}}$ [2]. The parameter $\in$ is the permittivity and μ is the permeability of the medium. Decoupling these equations give

$$\nabla^2 \overline{\mathrm{E}} = \in \mu \frac{\partial^2 \overline{\mathrm{E}}}{\partial t^2}. \tag{3.2}$$

Equation 3.2 is the standard wave equation for the electric field. As has been mentioned in Chapter 2, solutions of the standard electric wave equation satisfying certain boundary conditions give the various modes. These solutions are discrete and quantized, hence such are the modes supported by the fibre as well. Equation 3.2 is a scalar three dimensional wave equation.

3.2 Polarization concepts

The electric field component of a light wave traces out a particular path in the optical waveguide. Suppose that the electric field wave propagates in the z direction, then the electric field vector may be resolved into two orthogonal vectors E_x and E_y. Hence the electric field wave may be represented by two orthogonally polarized electric field waves. The state of polarization of a light wave refers to the time dependent path that the electric field vector traces out in the plane orthogonal to the direction of propagation. This section deals with mathematical and graphical representations of the state of polarization of a particular light wave.

Consider a ray of light travelling in the z direction. This electric field vector will have components in the x- and y-axes respectively. Then in terms of unit vectors

$$\overline{\mathrm{E}}(\mathrm{z},\mathrm{t}) = \hat{e}_x \mathrm{E}_\mathrm{x}(\mathrm{z},\mathrm{t}) + \hat{e}_y \mathrm{E}_\mathrm{y}(\mathrm{z},\mathrm{t}). \tag{3.3}$$

The two orthogonal electric field components have a space and time dependence given by

$$\mathrm{E}_\mathrm{x} = \mathrm{E}_{0\mathrm{x}} e^{i(\mathrm{kz}-\omega t+\varphi_\mathrm{x})} \tag{3.4a}$$

and

$$\mathrm{E}_\mathrm{y} = \mathrm{E}_{0\mathrm{y}} e^{i(\mathrm{kz}-\omega t+\varphi_\mathrm{y})}. \tag{3.4b}$$

E_{0x} and E_{0y} represents the amplitudes, and φ_x and φ_y represents the phase of the waves [5]. Equation 3.3 may thus be written as

$$\overline{\mathrm{E}} = \left[\hat{e}_x \mathrm{E}_{0x} e^{i\varphi_x} + \hat{e}_y \mathrm{E}_{0y} e^{i\varphi_y}\right] e^{i(kz-\omega t)} = \tilde{\mathrm{E}}_0 e^{i(kz-\omega t)} \tag{3.5}$$

where $\tilde{\mathrm{E}}_0$ is the complex amplitude for the polarized wave. The state of polarization is completely determined by the relative amplitudes and phases of these components; hence all that is required is the complex amplitude, which may be written as a Jones vector as

$$\tilde{\mathrm{E}}_0 = \begin{bmatrix} \tilde{\mathrm{E}}_{0x} \\ \tilde{\mathrm{E}}_{0y} \end{bmatrix} = \begin{bmatrix} \mathrm{E}_{0x} e^{i\varphi_x} \\ \mathrm{E}_{0y} e^{i\varphi_y} \end{bmatrix}. \tag{3.6}$$

Jones vectors are usually presented in their normalized form.

The Jones vectors may be used to describe three linear states of polarization with different orientations. Suppose a ray of light propagates in the z-direction and oscillates only in the vertical axis (y-axis). In this case $\mathrm{E}_{0x} = 0$ and $\mathrm{E}_{0y} = \mathrm{A}$ where A is the maximum amplitude. The phase is then also set equal to zero. Therefore

$$\mathrm{E}_0 = \begin{bmatrix} 0 \\ \mathrm{A} \end{bmatrix} = \mathrm{A}\begin{bmatrix} 0 \\ 1 \end{bmatrix}. \tag{3.7}$$

Similarly for horizontally polarized light for which $\mathrm{E}_{0x} = \mathrm{A}$, $\mathrm{E}_{0y} = 0$ and $\varphi_x = 0$,

$$\mathrm{E}_0 = \begin{bmatrix} 0 \\ \mathrm{A} \end{bmatrix} = \mathrm{A}\begin{bmatrix} 1 \\ 0 \end{bmatrix}. \tag{3.8}$$

For both these cases the normalized form of the vector is achieved by setting amplitude A = 1. In general a vector is in its normalized form when its magnitude equals unity. Another example is suppose the phase difference is 0^o for amplitude of A[5]. The Jones vector takes the form

$$\tilde{\mathrm{E}}_0 = \begin{bmatrix} \mathrm{E}_{0x} e^{i\varphi_x} \\ \mathrm{E}_{0y} e^{i\varphi_y} \end{bmatrix} = \begin{bmatrix} \mathrm{A}\cos\alpha \\ \mathrm{A}\sin\alpha \end{bmatrix} = \mathrm{A}\begin{bmatrix} \cos\alpha \\ \sin\alpha \end{bmatrix}. \tag{3.9}$$

The angle α is the angle formed between the x-axis and the path traced out by the electric field vector as shown in figure 3.1 (a). The notation in equation 3.9 describes

different orientations for the linear polarization state [5]. If the phase difference (φ) between the two perpendicular components is 0^o, 360^o or multiples thereof, that is they are in phase, then the electric field traces out the path shown in figure 3.1 (a) in the x,y-plane. If the two orthogonal components are odd integer multiples of 180^o, then superposition of the electric field components trace out the path shown in figure 3.1 (b).

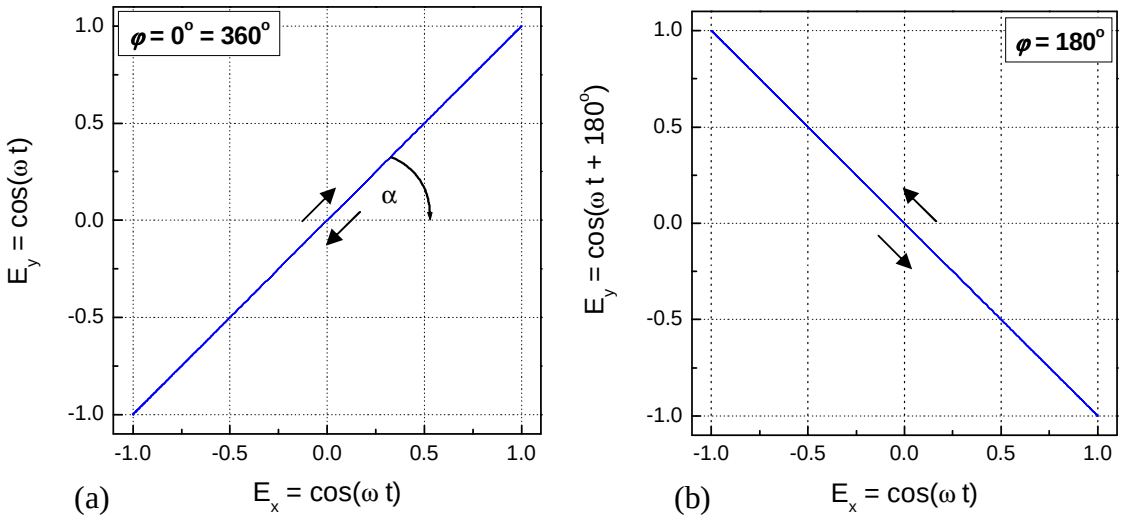

Figure 3.1 Linearly polarized light.

For circular polarization the electric field may either be right or left circularly polarized.

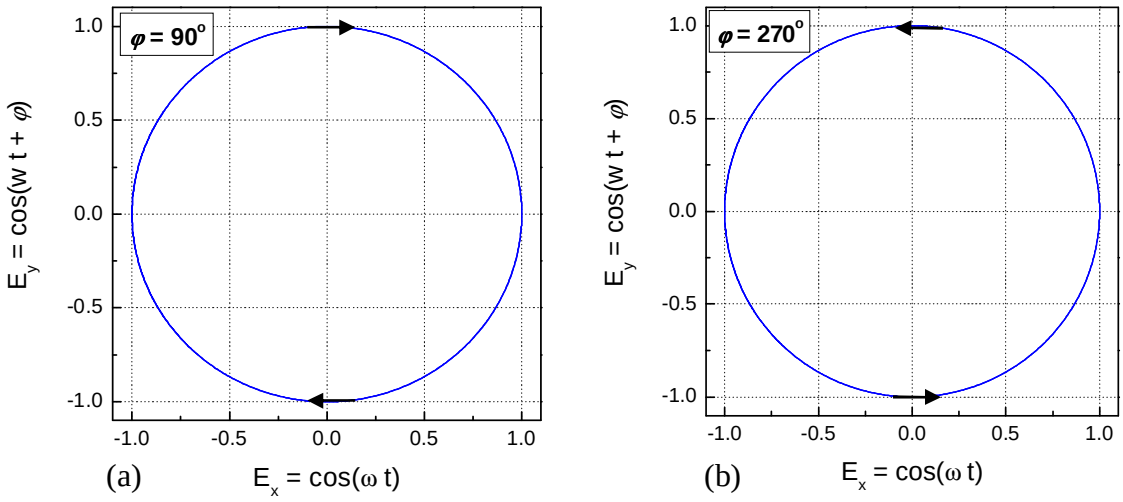

Figure 3.2 Representation of circularly polarized light: (a) Right circular polarized, (b) Left circular polarized

For a phase difference of $-90^{o} + 2m(180^{o})$, with m an integer, the electric field will rotate in a clockwise direction when viewed towards the source. Hence it is right circularly polarized, shown in figure 3.2 (b). When the phase difference is $90^{o} + 2m(180^{o})$ then the electric field is left circularly polarized, as shown in figure 3.2 (a).

For any other phase difference other than those already mentioned the electric field will be elliptically polarized. Figure 3.3 shows specific examples for the angles 45^{o}, 315^{o} and 135^{o}, 225^{o}; which are all elliptical polarization states. The difference between the phase differences 45^{o} and 315^{o} is the direction of rotation, where the phase difference 45^{o} has a left sense of rotation and 315^{o} rotates clockwise. Similarly the difference between 135^{o} and 225^{o} is that 135^{o} rotates anticlockwise while 135^{o} rotates in a clockwise direction.

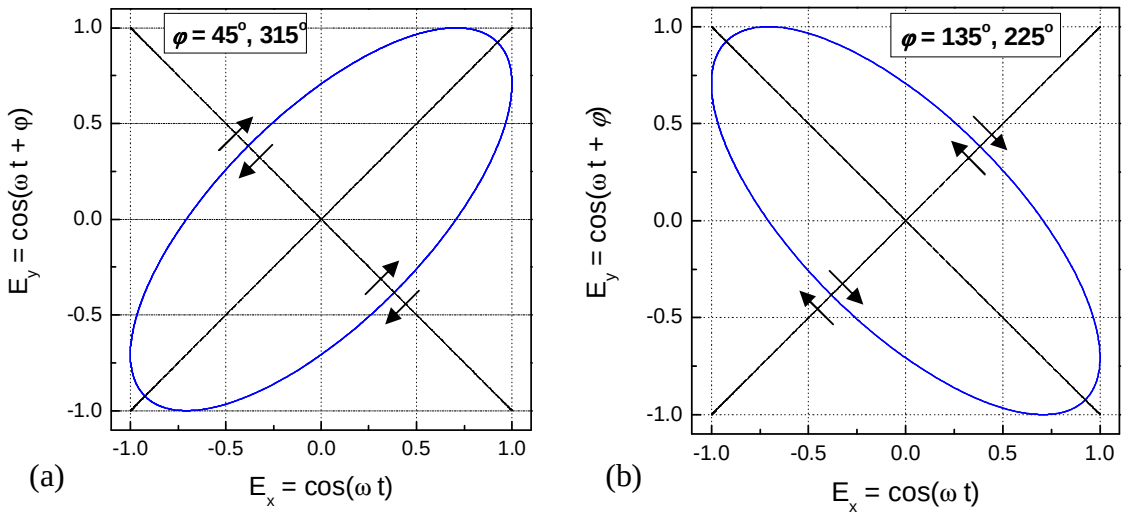

Figure 3.3 Representation of elliptical polarized states: (a) For a phase difference of 45^{o} the electric field rotates clockwise in the direction of travel and rotates anti-clockwise for 315^{o}, (b) The electric field rotation is clockwise for 135^{o} and anti-clockwise for 225^{o}.

This system of the polarization ellipse may be used to describe the state of polarization of the light. Basically as has been shown in the particular examples with the light wave taken to be propagating in the z-direction the ellipse is traced out in the transverse plane, that is the x-y plane. The components defining the ellipse are the magnitudes of the two orthogonal electric field components and their phase difference.

3.3 Stokes parameter formalism

Another method of describing the state of polarization of the light is the Stokes formalism. The Stokes formalism has the added advantage of being able to deal with partially polarized light unlike the Jones vectors. It is not possible to directly measure the electric field of the light, but the irradiance can be measured. The Stokes parameters are an array which describes the optical power values in which the elements describe the optical power under particular reference polarization states. The Stokes parameter array has the form

$$\begin{bmatrix} S_0 \\ S_1 \\ S_2 \\ S_3 \end{bmatrix}. \tag{3.10}$$

The following abbreviations are used below in the description of Stokes parameters: LH (linear horizontal), LV (linear vertical), RC (right circular), LC (left circular), L±θ (linear polarized light at a particular angle).

Description of Stokes parameters found in Derickson [6]:
S_0 = Total power (polarized + unpolarized)
S_1 = Power through LH polarizer – power through LV polarizer
S_2 = Power through (L + 45^o) polarizer – power through (L – 45^o) polarizer
S_3 = Power through RC polarizer – power through LC polarizer

These co-ordinates may be assigned to a xyz-coordinate system where the normalized Stokes parameters are obtained by dividing each Stokes parameter by the total optical power:

$$s_1 = \frac{S_1}{S_0},\ s_2 = \frac{S_2}{S_0},\ s_3 = \frac{S_3}{S_0}. \tag{3.11}$$

The degree of polarization (DOP) gives an indication of the extent to which the light is polarized. It is given by

$$\mathrm{DOP} = \frac{\sqrt{S_1^2 + S_2^2 + S_3^2}}{S_0} = \sqrt{s_1^2 + s_2^2 + s_3^2}\ . \qquad (3.12)$$

The four Stokes parameters are related to the two perpendicular electric field components as follows:

$$S_0 = {E_{0x}}^2 + {E_{0y}}^2 \qquad (3.13a)$$

$$S_1 = {E_{0x}}^2 - {E_{0y}}^2 \qquad (3.13b)$$

$$S_2 = 2E_{0x}E_{0y}\cos\varphi \qquad (3.13c)$$

$$S_3 = 2E_{0x}E_{0y}\sin\varphi \qquad (3.13d)$$

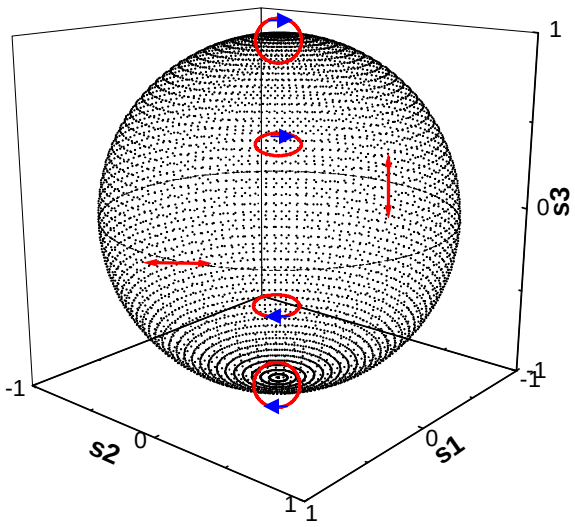

Figure 3.4 Poincaré sphere with representations of various polarization states.

The Stokes parameters are used as co-ordinates for a unit sphere, named the Poincaré sphere, shown in figure 3.4. It is a graphical tool in real, three dimensional space. This sphere represents all possible states of polarization and also shows the DOP. Hence the sphere makes it possible to view polarization transformation caused by propagation through devices. Figure 3.4 also gives an indication of the state of polarization on various sights on the sphere. Circular states are located at the poles, linear states on the equator and elliptical states continuously distributed between the

equator and the poles. Right hand circular states are located at the Northern pole while left circularly polarized states are located at the south pole of the Poincaré sphere. When the light is fully polarized with a DOP of 1 then it is represented by a point on the surface of the Poincaré sphere. In general the DOP is given by the distance from the centre of the sphere to the point representing the SOP. Partially polarized consisting of both polarized and un-polarized light is represented by a point within the volume of the sphere.

The state of polarization of light is determined by its electric field component. In general the phase difference between the two orthogonal electric components dictates the states of polarization of the light. In this chapter various methods of representation of the SOP of the light have been discussed. The Jones vectors, the elliptical method, and the Stokes parameters which may be used to construct a Poincaré sphere are all methods of representing the state of polarization.

CHAPTER 4

POLARIZATION MODE DISPERSION BACKGROUND

Polarization mode dispersion (PMD) is the combined effect of birefringence and mode coupling. PMD causes serious capacity impairments, including pulse broadening in digital systems and distortions in analogue systems. In the course of data transmission the fibre PMD changes the state of polarization of each frequency differently, adding a polarization modulation component to the signal. It is a stochastic phenomenon that varies with time. It is this very characteristic that complicates PMD characterization. This chapter looks into the definition of PMD and moves to discussing the characteristics of PMD.

4.1 Origin of PMD

PMD is an optical effect which is present in concatenations of birefringent elements. It is found in many optical components and in particular in optical fibre. Birefringence refers to the small differences in the refractive index for a particular pair of orthogonal polarization states. Consider a birefringent segment as shown in figure 4.1.

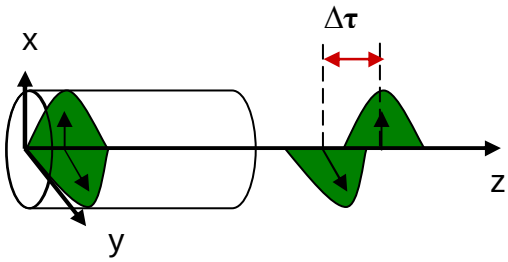

Figure 4.1 Birefringent fibre segment used to illustrate the time delay between the two orthogonal polarization modes caused by birefringence.

As the input light pulse propagates through the birefringent segment, the difference in the refractive index experienced by the two orthogonal polarization states results in a time delay between the two orthogonal modes. The time delay shown in figure 4.1 is

known as the differential group delay (DGD), $\Delta\tau$. Strictly the DGD is the difference between the two principal states of polarization (PSPs) [7]. The PSPs are defined as the two states of polarization (SOPs), having the property that the output SOP remains unchanged with frequency to first order for any input SOP aligned to these PSPs. In single mode fibre, birefringence results from the non-circularity of the fibre core. This occurs because an oval waveguide is inherently birefringent and the mechanical stress field set up by the oval core induces additional birefringence.

Mode coupling further complicates the effect of PMD, making the dispersive effect susceptible to environmental variations. A length of fibre may be represented as a concatenation of a series of random length birefringent segments. Each segment exhibits fast and slow polarization modes. Mode coupling refers to the re-coupling process that takes place between two adjacent birefringent segments. This process occurs because each birefringent segment has distinct PSPs, and the electric field emerging from each segment is projected onto the polarization modes of the following segment. Mode coupling causes the DGD of most fibre systems to show a dependence on wavelength and environmental conditions.

4.2 Representation of PMD

PMD may be represented by using the polarization dispersion vector, $\hat{\Omega}$, and the birefringence vector, $\Delta\hat{\beta}$ [7]. A frequency sweep results in a change in the output state of polarization, which is caused by PMD. Hence each frequency component has a different output state of polarization. Figure 4.2 shows how as the frequency is swept across a specified range, the output state of polarization traces out a path on the Poincaré sphere. The variation of the SOP, $\hat{s}$, with angular optical frequency, ω, obeys the following equations of motion,

$$\frac{d\hat{s}(\omega)}{d\omega} = \hat{\Omega}(\omega) \times \hat{s}(\omega) \tag{4.1}$$

and

$$\frac{d\hat{s}(\omega)}{dz} = \Delta\hat{\beta}(\omega) \times \hat{s}(\omega), \tag{4.2}$$

where z represents the fibre length and $\Delta\hat{\beta}(\omega)$ is the birefringence vector.

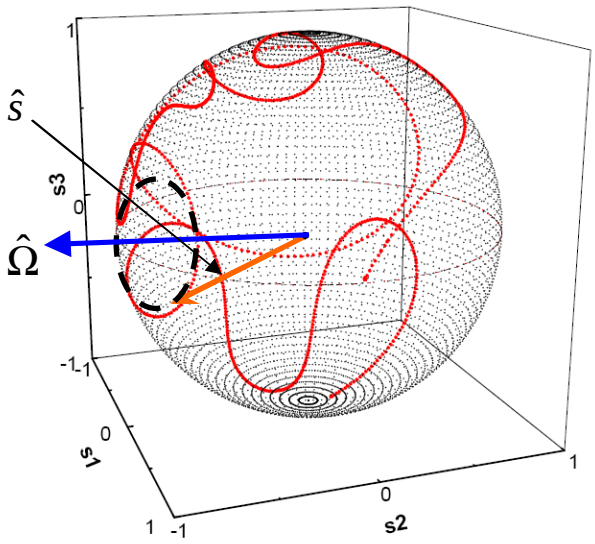

Figure 4.2 SOP path traced out on a Poincaré sphere as the wavelength is changed.

The relationship between the polarization dispersion vector and the birefringence vector has the form

$$\frac{d\hat{\Omega}}{dz} = \frac{d\Delta\hat{\beta}}{d\omega} + \left(\Delta\hat{\beta} \times \hat{\Omega}\right) \tag{4.3}$$

where is $\frac{d\Delta\hat{\beta}}{d\omega}$ is the modal birefringence, B, at position z along the DUT (device under test) and has units of time delay per unit length. $\Delta\hat{\beta} \times \hat{\Omega}$ is the term which indirectly affects the increase of the polarization dispersion by causing the polarization dispersion vector to change direction with $\frac{d\Delta\hat{\beta}}{d\omega}$, resulting in dephasing between the two vectors. The modal birefringence is responsible for causing the increase of the polarization dispersion vector along the DUT length. When considering the frequency domain, the direction of the polarization dispersion vector is co-linear with the slow PSP [8] and its magnitude is equal to the DGD.

$$\hat{\Omega}(\omega) = \Delta\tau(\omega) \cdot \hat{s}_p(\omega) \tag{4.4}$$

where

$$\hat{s}_p^{slow}(\omega) = -\hat{s}_p^{fast}(\omega) \tag{4.5}$$

and

$$\left|\hat{\Omega}(\omega)\right| = \Delta\tau(\omega) = DGD\,. \tag{4.6}$$

The fast PSP direction is represented by $\hat{s}_p^{fast}(\omega)$ and the slow PSP direction by $\hat{s}_p^{slow}(\omega)$. As shown in figure 4.2 with the addition of random mode coupling the SOP path becomes complicated and is no longer simple. Hence there is a fluctuation in both the PSP and the DGD with wavelength.

4.3 PMD characteristics

The modal birefringence is given by $B = \frac{1}{v}\left(\frac{\Delta v}{v}\right)$ where v is the average group velocity and Δv is the differential group velocity between the fast and the slow polarization modes. The PMD may be expressed as the RMS (root mean square) width of the polarization mode time of flight distribution in ps (pico-second) as

$$PMD = \frac{Bh}{\sqrt{2}}\left(\frac{2L}{h} - 1 + e^{-2L/h}\right)^{1/2}, \tag{4.7}$$

where h is the polarization mode coupling length [7]. For fibre length $L << h$, the PMD distribution function is level; $PMD = BL$ and increases linearly with length. For the case where $L >> h$, the PMD distribution function becomes Gaussian and is given by [7]

$$PDF(\tau) = \left(\sqrt{\frac{1}{2\pi\langle\tau^2\rangle}}\right) e^{-\tau^2/2\langle\tau^2\rangle}. \tag{4.8}$$

The PMD delay is $\langle \tau^2 \rangle^{1/2}$ and increases with the square root of length. For random mode coupling the DGD obeys a probability distribution function (PDF) following a Maxwellian distribution

$$PDF(\Delta\tau) = 3\left(\sqrt{\frac{6}{\pi}}\right)\frac{\Delta\tau^2}{\langle \Delta\tau^2 \rangle^3} e^{-3\Delta\tau^2/2\langle \Delta\tau^2 \rangle}, \tag{4.9}$$

where the PMD is equal to the RMS DGD [7]. The RMS DGD, $\langle \Delta\tau^2 \rangle^{1/2}$, and the mean DGD $\langle \Delta\tau \rangle$ are related as follows, from [7],

$$\langle \Delta\tau^2 \rangle = \frac{3\pi}{8}\langle \Delta\tau \rangle^2. \tag{4.10}$$

A higher order of PMD is the second order PMD, which is the variation of the DGD and PSP with angular optical frequency. It occurs with an increase in random mode coupling.

CHAPTER 5

POLARIZATION MODE DISPERSION MEASUREMENT TECHNIQUES

This chapter introduces the theory concerning PMD measurements and provides a brief overview of several PMD measurement techniques. It then moves to describe the Jones matrix eigenanalysis (JME), interferometric and fixed analyzer (FA) measurement techniques in more detail using actual PMD measurement results to aid the discussion. The chapter ends with a summary of the comparison of PMD measurement performance between the different techniques as documented in literature.

5.1 PMD measurement performance overview

Most optical components have a specific PMD value depending on the magnitude of the birefringence and the number of mode coupling sites within the component. Both these effects play a major role in determining the true and measured PMD values. PMD produces observable effects in both the time and the frequency domain, hence PMD measurement techniques operating either in the time or the frequency domain have been developed.

Time domain PMD measurement techniques directly measure the effect of the time delay between the two orthogonal polarization modes. The frequency PMD measurement techniques determine the PMD from the evolution of the state of polarization of the light as a function of wavelength. PMD causes the output state of polarization to precess about the principal state of polarization as the angular optical frequency is changed [9]. The rate of rotation with angular optical frequency gives the local polarization mode dispersion known as the differential group delay (DGD).

There exist several time and frequency domain PMD measurements. The most common time domain measurements are the time-of-flight and the interferometric techniques. The time-of-flight or optical pulse method makes use of an oscilloscope which plots the arrival time of narrow pulses sent through the fibre with different launch polarization states. Two received pulses due to the mean DGD are observed for launch polarizations between the two PSPs [10, 11]. Interferometric PMD measurements deduce the PMD of the optical component from an interferogram generated by a Michelson interferometer. Interference patterns are observed when the time difference of the light between the two arms match the delay caused by the PMD in the test device to fall within the coherence time of the source [10]. Broadband sources provide a suitable coherence time which will resolve into interference fringes predominantly from PMD. Other causes of the interference fringes is the initial source phase difference.

Common frequency domain measurement methods are; the Jones matrix eigenanalysis (JME) technique, Mueller matrix method (MMM), Poincaré sphere arc method and the wavelength scanning or fixed analyzer (FA) technique as it is also known. The former three techniques fall under the umbrella of polarimetric measurement of DGD. These methods determine both the DGD and the PSP (principal states of polarization) by measuring the rate of rotation of the states of polarization around the PSP with a change in frequency. The same experimental setup can be used for all three techniques; hence the only difference is in the analysis method. By using the same measurement data it has been shown that JME and Poincaré sphere analysis (PSA) give similar results within measurement error [12].

The Jones matrix technique relies on the evolution of the output state of polarization as a function of wavelength for three different linear input states of polarization to determine the Jones matrix of the DUT. The 2×2 Jones matrix relates the input and output Jones vectors of the device under test (DUT). The output Jones vector is determined via measurement and is used together with the input Jones vector to establish the Jones matrix of the DUT, which is then used to extract the DGD.

The Mueller matrix method is very similar to the JME method in its determination of PMD except for the fact that it uses a 3×3 polarization transfer matrix in its

computation and operates in Stokes space. A 3×3 polarization transfer matrix is determined for very closely-spaced frequencies. The method makes the assumption of the absence of Polarization Dependent Loss (PDL), making the transfer matrix a rotation matrix. The precession angle of the output polarization may then be computed using the trace of the rotation matrix and the PSP as the eigenvector which corresponds to an eigenvalue of unity [10].

The Poincaré sphere analysis (PSA) measurement technique is based on Stokes parameter evaluation. As with the JME measurement technique the polarization transformation of three distinct input SOPs are recorded with a change in wavelength across a wavelength range. The DGD is related to the change of three output Stokes vectors with a change in optical frequency and may thus be calculated. PSP calculation is done in a similar manner where an equation relates the Stokes vectors and their change to the PSP [6].

Various other polarimetric measurement techniques similar to JME, PSA and the MMM techniques exist. These techniques are often not mentioned in literature references but share the principle of measuring the DGD by measuring the rate of change of the output SOP with wavelength. This is applicable when the input polarization state is launched such that both PSP are equally illuminated [10].

The fixed analyzer (FA) technique also known as the wavelength scanning technique, takes a different approach to the polarimetric measurement techniques by measuring the PMD indirectly. The transmitted power through a polarizer is measured as a function of wavelength. The average DGD is related to the number of extrema and mean-level crossings of a normalized intensity trace, where the intensity is measured through a polarizer as a function of wavelength [13]. Fourier analysis of the intensity spectrum also yields the PMD of the DUT [7].

This work focuses on the investigation of PMD measurement performance of the fixed analyzer (FA) technique in comparison with the JME, Generalized interferometric and Poincaré sphere arc PMD measurement techniques. Hence the following sections discuss the FA technique in great detail and, also the JME and

interferometric PMD measurement techniques. The specific Poincaré sphere arc technique will be introduced and presented in detail at a later stage, in chapter 10.

5.2 Fixed analyzer (FA) PMD measurement technique

The fixed analyzer (FA) PMD measurement technique is also known as the wavelength scanning PMD measurement technique. It is based on measuring the transmitted intensity through a polarizer, known as the fixed analyzer, as the wavelength is changed. The section starts off with the general setup of the FA method and offers an intuitive understanding of the operating principle of the technique. It then concentrates on the theory of the fixed analyzer and presents a detailed explanation of the various analysis methods of the FA transmission spectra.

5.2.1 FA technique background

In 1994 C. D. Poole and D. L. Favin released a paper presenting the FA technique and the derivation of two PMD analysis methods [13]. The technique was compared with commercial PMD measurement techniques, Jones matrix eigenanalysis and general analysis method, and it compared very well. It is now a standard PMD measurement technique and is presented in the IEC technical report [7].

Generally there are two setups for the FA method. In the one setup a polarized broadband source is used and thus this requires an optical spectrum analyzer as a detector, figure 5.1 (a). The other setup uses a tuneable polarized laser source where a power meter is used as a detector, figure 5.1 (b).

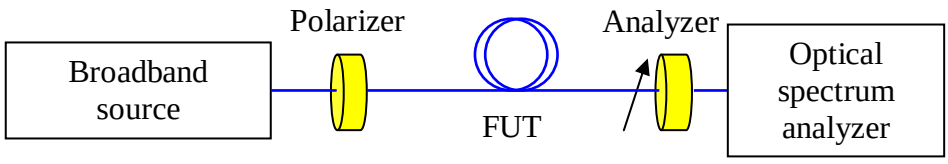

(a)

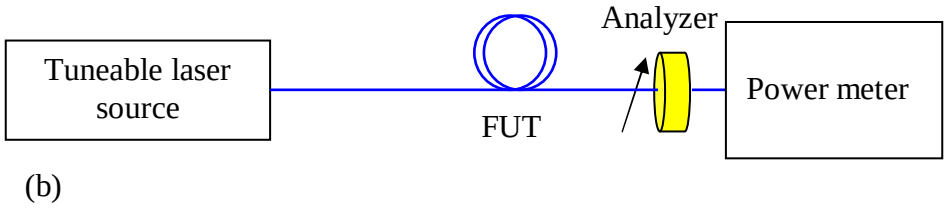

(b)

Figure 5.1. General configuration of the FA PMD measurement technique, (a) with a broadband source and (b) with a tuneable laser.

When a broadband source is used, a specified range of wavelengths is transmitted through the fibre under test (FUT) or device under test (DUT) after passing through a polarizer. The transmitted intensity through an analyzer (polarizer) is measured as a function of wavelength. The setup viewed in figure 5.1 (a) represents the basic FA setup without any extra accessories. The broadband light source transmits a selected wavelength band through a polarizer which polarizes the light being passed through the DUT. PMD in the DUT changes the state of polarization (SOP) of the light as the wavelength is swept. By taking advantage of this phenomenon the magnitude of PMD and fluctuation of the DGD can be linked to this variation of the SOP with wavelength. The fixed analyzer technique uses a fixed polarizer coupled with a power meter or an optical spectrum analyzer to track this behaviour by monitoring the intensity fluctuation of the transmitted light signal through a polarizer. The setup shown in figure 5.1 (b), shows a tuneable laser which sweeps across a selected wavelength range in small wavelength steps, where a power meter records the light intensity.

The FA technique requires the calculation of the intensity ratio $R(\lambda)$, which is a ratio of the spectrum obtained without the polarizer in place $P_{TOT}(\lambda)$ and the spectrum obtain with the polarizer in the path of the light $P_A(\lambda)$.

$$R(\lambda) = \frac{P_A(\lambda)}{P_{TOT}(\lambda)} \tag{5.1}$$

Alternatively the normalized intensity ratio $R(\lambda)$ may be determined by leaving the analyzer in place during both scans but with the difference of rotating the analyzer by 90^o during the second scan, $P_B(\lambda)$

$$R(\lambda) = \frac{P_A(\lambda)}{P_A(\lambda) + P_B(\lambda)}. \tag{5.2}$$

In this study equation 5.1 was used to normalize the intensity spectrum in the FA setup where a broadband source was used with an optical spectrum analyzer as a detector.

Figure 5.2 shows two signatures which have the same domain but differ in the variable recorded. The evolution of the SOP and the corresponding intensity fluctuation through the polarizer with wavelength are represented.

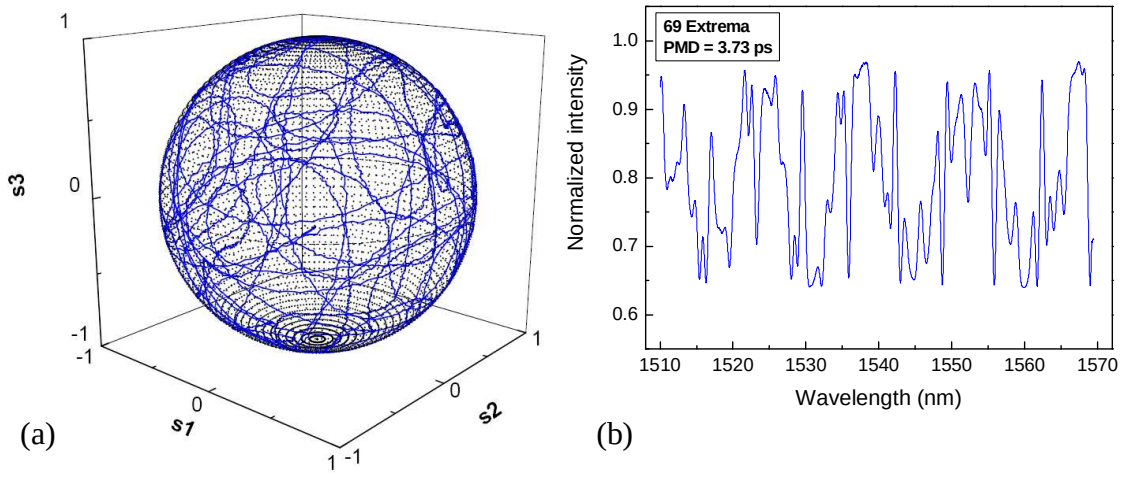

Figure 5.2. (a) SOP transformation when the angular optical frequency is changed represented on the Poincaré sphere. (b) The intensity fluctuation through a polarizer due to the same SOP transformation as a result of the change in angular optical frequency.

These results are from an actual PMD measurement of an emulator, where both the SOP change and the transmitted intensity were monitored and recorded simultaneously. The emulator is made up of a concatenation of four polarization maintaining fibre (PMF) sections hence it has mode coupling explaining the non-periodic signature. If a fixed polarizer (analyzer) is in the path of this SOP fluctuating signal then, depending on the SOP input to the analyzer, a fraction of the light intensity will be allowed to pass through the analyzer. The fraction of the light intensity allowed to pass through depends on the SOP of the polarizer and the SOP of the light. The SOP of the polarizer is fixed but, the SOP of the light exiting the DUT constantly changes due to the birefringence and mode coupling.

When observing the change in the SOP on the Poincaré sphere the peaks and valleys, figure 5.2 (b), may be explained as follows:

1. First the analyzer is simply a polarizer with a specific SOP named SOP1 from now onwards. SOP1 may be identified and marked on the Poincaré sphere as it is a distinct SOP with specific Stokes parameters.

2. A peak occurs in the intensity spectrum when the SOP of the light moves closer to SOP1 and then further away from SOP1. Hence as the SOP of the light approaches SOP1, the output light intensity increases.

3. A further change in wavelength may change the direction of the path of the SOP such that it moves away from SOP1. This dissimilarity between the two SOPs leads to a decrease in the intensity of the light. If the SOP of the light again moves towards SOP1 then an increase in the light intensity traces out a valley in the intensity spectrum.

4. Hence an entire signature is traced out as the SOP transforms depending on the birefringence and the number of mode coupling sites with a change in wavelength over a selected wavelength range.

5. The absolute maximum in the intensity spectrum corresponds to when SOP matches SOP1 and the absolute minimum occurs when SOP and SOP1 are orthogonal, that is 180^{o} apart on the Poincaré sphere.

The results presented later on will show that the intensity spectrum traced out depends both on the magnitude of birefringence and the degree of mode coupling present, hence having an effect on the calculated PMD and also giving an indication of the length regime of the DUT.

The following subsections concentrate on the analysis methods of the data recorded using the FA technique. A detailed derivation of the mean level crossing and extrema counting equations, which may also be found in [13], will be presented. Then a

thorough discussion concerning the Fourier analysis method is undertaken, and presented in the format of theory and a hypothetical example.

5.2.2 FA technique analysis methods

The resultant spectrum from a FA PMD measurement may be analyzed using three different analysis methods to compute the measured PMD value. Two of the analysis methods involve counting the number of a particular feature evident within the spectrum. These techniques were introduced and presented in detail by C. D. Poole and D. L. Favin [13]. This article also suggested a very straightforward method for calculating the particular length regime of the DUT. The third analysis method involves Fourier analysis of the intensity spectrum.

5.2.2.1 Extrema counting and mean level crossing PMD analysis methods

The two FA PMD analysis methods which involve counting are extrema counting and mean level crossings. Extrema counting involves literally counting the number of peaks and valleys in the spectrum, while mean level crossing refers to counting the number of times the transmission spectrum crosses the mean value of the transmitted intensity.

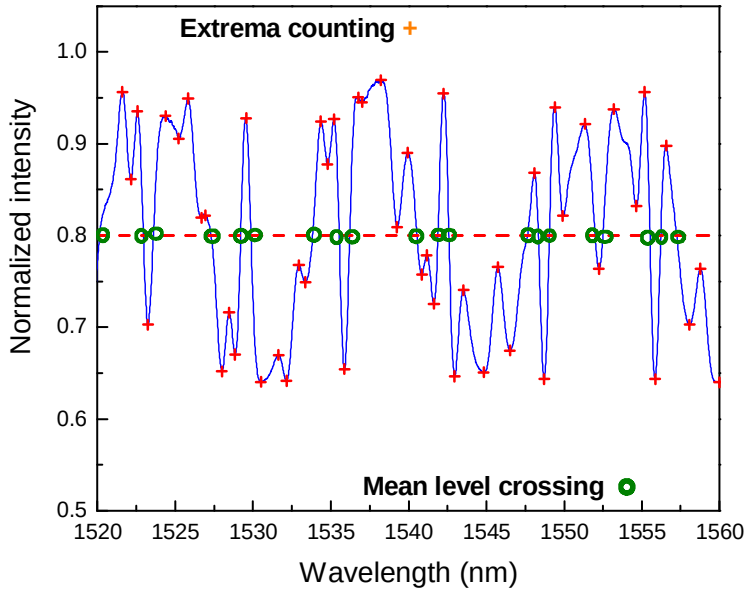

Figure 5.3. Normalized intensity spectrum measured using an OSA indicating the number of extrema and mean level crossings.

For illustrative purposes figure 5.3 shows a smaller window of the PMD measurement of the emulator shown in figure 5.2. Figure 5.3 provides a clear indication of the definition of extrema and mean level crossing numbers. In this spectrum 45 extrema and 20 mean level crossings can be clearly identified.

The extrema density within a wavelength range has been linked to the measured PMD value for both the cases of the presence and absence of mode coupling. In the absence of mode coupling, the measured PMD is given by the equation

$$\langle \Delta\tau \rangle = k\pi \frac{\langle N_e \rangle}{\Delta\omega} = \frac{k\langle N_e \rangle \lambda_1 \lambda_2}{2c(\lambda_2 - \lambda_1)} \tag{5.3}$$

where k is the mode coupling factor. The mode coupling factor has a value of 0.824 in the presence of mode coupling, according to Poole and Favin [13], and takes on the value of 1 in the absence of mode coupling. N_e is the number of extrema, c the speed of light in vacuum, $\Delta\omega$ the angular optical frequency range and λ represents the wavelength in free space. In 1998 Williams and Wang presented an article suggesting a correction to the mode coupling factor [14]. The new value equalled 0.805. This new mode coupling factor was also determined using Monte Carlo simulations but with a difference in the assumptions in the makeup of the simulated fibre. The IEC TR 61282-9 technical report [7] recommends that the value 0.82 be used for the mode coupling factor when mode coupling is present, and was made use of throughout this document. Poole and Favin also managed to link the mean level crossing density to the measured PMD value. This materialised into an equation which may be used to calculate the PMD value by counting the number of mean level crossings. The mean level crossing analysis equation has the form

$$\langle \Delta\tau \rangle = 4 \frac{\langle N_m \rangle}{\Delta\omega} = \frac{2\langle N_m \rangle \lambda_1 \lambda_2}{c\pi(\lambda_2 - \lambda_1)}, \tag{5.4}$$

where N_m represents the number of times the transmission spectrum crosses the mean transmittance. In the absence of mode coupling the two equations described above tend to become equal and take the form

$$\langle \Delta\tau \rangle = \frac{\pi \langle N_e \rangle}{\Delta\omega} = \frac{\pi \langle N_m \rangle}{\Delta\omega}. \qquad (5.5)$$

Poole and Favin further put forward a means of evaluating the length regime of the fibre. That is to investigate whether the fibre is in the long length regime or in the short length regime. In the long length regime PMD scales as the square root of length and shows a Maxwellian probability density distribution and in the short length regime it varies linearly with length. This straightforward method involves determining both the extrema and mean level crossings in a given spectrum and uses their ratio as an indication of the length regime. For example in the case of mode coupling the ratio of equation 5.3 and 5.4 gives

$$\frac{\langle N_e \rangle}{\langle N_m \rangle} = \frac{4}{0.824\pi} = 1.54, \qquad L/l_c \to \infty, \qquad (5.6)$$

where L is the fibre length and l_c the coupling length. Hence the value of this ratio conforms to fibres in the long length regime. Fibres in the short length regime where the fibre length is short compared to the coupling length (l_c), the ratio is just unity,

$$\frac{\langle N_e \rangle}{\langle N_m \rangle} = 1, \qquad L/l_c \to 0. \qquad (5.7)$$

It can be noted that the ratio of extrema to mean level crossing for the long length regime is greater by 54 % compared to the short length regime ratio. Both the extrema counting and mean level crossing analysis methods were used to determine the PMD value of FA PMD measurements.

5.2.2.2 Derivation based on geometrical arguments

C. D. Poole and D. L. Favin derived expressions relating the extrema counting and mean level crossing densities to the measured PMD value. These derivations may be found in article [13] published by them in 1994. The following two subsections show the derivations based on geometrical arguments and fills in the required mathematical details.

(a) Mean level crossing

Consider the frequency dependent transmission through a polarizer represented on a hypothetical unit Poincaré sphere where a path, in red (figure 5.4), is traced out on the sphere as the state of polarization changes with a change in frequency. The state of polarization of light incident on the polarizer is represented by the vector $\hat{s}$ and the high transmission state or pass axis of the polarizer by the vector $\hat{p}$ on the Poincaré sphere.

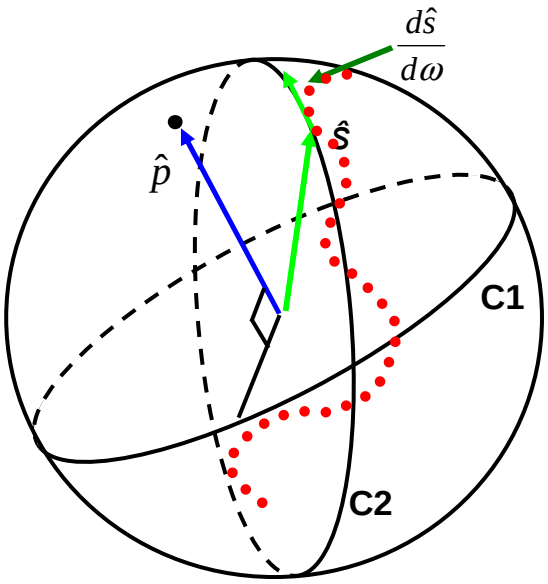

Figure 5.4. Schematic illustration of SOP change with wavelength as the angular optical frequency is varied.

The transmission through a perfect polarizer is given by

$$T(\omega) = \frac{1}{2}\left(1 + \hat{s}(\omega) \cdot \hat{p}\right). \tag{5.8}$$

Since the fibre is in the long length regime, implying the presence of mode coupling, it is expected that all SOPs are equally probable. Therefore, the dot product in equation 5.8 will average to zero and the mean transmission is $\langle T \rangle = 0.5$. Hence this allows us to argue in the following manner: For the transmission $T(\omega)$ to be equal to the mean transmission the dot product must equate to zero. Thus for $T(\omega)$ to cross the mean transmission the vector $\hat{s}$ should cross the circle C1 shown in figure 5.4. Circle C1 is defined as the locus of points on the Poincaré sphere by all vectors orthogonal to vector $\hat{p}$. Hence the expected number of mean level crossings is equal to the number of times vector $\hat{s}$ crosses the circle C1. As can be viewed on the surface of the sphere, vector $\hat{s}$ traces out an arc on the sphere of length

$$\Delta l = \left|\hat{s}_2 - \hat{s}_1\right| = \left|\Delta\hat{s}\right| = \left|\frac{d\hat{s}}{d\omega}\right|\Delta\omega, \tag{5.9}$$

where $\left|\mathrm{d}\,\hat{s}\,/\mathrm{d}\omega\right|$ is the local speed with which the SOP vector changes with frequency. Since $\mathrm{d}\,\hat{s}\,/\mathrm{d}\omega$ is tangential, the arc that $\hat{s}$ traces out lies on a great circle C2 provided the frequency interval is sufficiently small. Since C2 crosses C1 twice, the probability that the vector $\hat{s}$ crosses C1 is twice the ratio of the arc length to the circumference C.

$$C = 2\pi r = 2\pi(1) = 2\pi \tag{5.10}$$

$$\mathrm{Prob}\left(\text{mean level crossing}\right) = 2\times\frac{\Delta l}{2\pi} = \frac{1}{\pi}\left|\frac{d\hat{s}}{d\omega}\right|\Delta\omega \tag{5.11}$$

It is assumed that $\hat{s}$ represents a stationary random process. Hence the probability in equation 5.11 is independent of frequency. The mean level crossing density is then given by

$$\gamma_m = \frac{\langle N_m \rangle}{\Delta\omega} = \frac{\left\langle \mathrm{Prob}\left(\text{mean level crossing}\right)\right\rangle}{\Delta\omega} = \frac{1}{\pi}\left\langle\left|\frac{d\hat{s}}{d\omega}\right|\right\rangle. \tag{5.12}$$

Rotation about the principal states of polarization axis can be written as a cross product relation

$$\frac{d\hat{s}}{d\omega} = \overline{\Omega} \times \hat{s}\,. \tag{5.13}$$

The average speed can then be obtained by making use of equation 5.13,

$$\left\langle \left| \frac{d\hat{s}}{d\omega} \right| \right\rangle = \left\langle \left| \overline{\Omega} \times \hat{s} \right| \right\rangle = \left\langle \Delta\tau \right\rangle \left\langle \left| \sin\theta \right| \right\rangle . \tag{5.14}$$

From the probability density function of sinθ it can be shown that $\langle \,|\, \sin\theta \,|\, \rangle = \pi/4$. Therefore

$$\gamma_m = \frac{N_m}{\Delta\omega} = \frac{\left\langle \Delta\tau \right\rangle}{4} \tag{5.15}$$

and

$$\left\langle \Delta\tau \right\rangle = 4\frac{\left\langle N_m \right\rangle}{\Delta\omega}, \qquad L/l_c \to \infty \tag{5.16}$$

Equation 5.16 shows that the expected PMD value is only four times the mean level crossing density. This equation applies to the case of a DUT with mode coupling sites and only requires that the angular optical frequency range and the number of mean level crossings be within the specified sweep range.

(b) Extrema counting

Extrema occur in the transmission spectrum when the derivative with respect to frequency of the transmission through the polarizer is equal to zero. The derivative of equation 5.8 is

$$T'(\omega) = \frac{dT}{d\omega} = \frac{1}{2}\left(\overline{\Omega} \times \hat{s}\right) \cdot \hat{p}\,. \tag{5.17}$$

A useful substitution is

$$\overline{\Omega} \times \hat{s} = \left| \overline{\Omega} \times \hat{s} \right| \hat{\eta}\,, \tag{5.18}$$

where $\hat{\eta}$ is a unit vector in the direction of the vector cross product.

The derivative of the transmission can then be rewritten as

$$T'(\omega) = \frac{1}{2}\left|\overline{\Omega} \times \hat{s}\right| \hat{\eta} \cdot \hat{p} \,. \tag{5.19}$$

From this equation it should be noted that all the vectors on the right, except for the pass axis vector $\hat{p}$, vary with a change in frequency. As mentioned before extrema occur when the derivative of the transmission is zero; hence there are three possibilities when this can occur:

1) The magnitude of the PMD is equal to zero.
2) The PMD vector is parallel to the SOP vector $\hat{s}$.
3) The vector $\hat{\eta}$ is orthogonal to the vector $\hat{p}$.

Making the assumption that the vectors in equation 5.26 are statistically independent and that the probability density function for the PMD is absent of singularities rules out the first two possibilities, leaving only the third possibility. Consequently this requires that vector $\hat{\eta}$ should cross the great circle C1. The number of times this event occurs is equivalent to the number of extrema found in the transmission spectrum. This is analogous to the previous section, hence the extrema density may be written as

$$\gamma_e = \frac{\langle N_e \rangle}{\Delta\omega} = \frac{1}{\pi}\left\langle \left| \frac{d\hat{\eta}}{d\omega} \right| \right\rangle. \tag{5.20}$$

By making use of equation 5.18, the local speed with which the vector $\hat{\eta}$ traces out an arc on the sphere can then be written as

$$\left| \frac{d\hat{\eta}}{d\omega} \right| = \left| \frac{d\left(\overline{\Omega} \times \hat{s}\right)}{d\omega \left|\overline{\Omega} \times \hat{s}\right|} \right|. \tag{5.21}$$

The complicated interdependence of the terms on the right hand side makes it difficult to obtain an analytical value for the average local speeds. Therefore Poole and Favin turned to Monte Carlo simulations which produced the following result

$$\left\langle \left| \frac{d\hat{\eta}}{d\omega} \right| \right\rangle = 1.21 \langle \Delta\tau \rangle . \tag{5.22}$$

This leads to the final extrema counting equation for mode coupling

$$\langle \Delta\tau \rangle = 0.826\pi \frac{\langle N_e \rangle}{\Delta\omega}, \qquad L/l_c \to \infty . \tag{5.23}$$

5.2.2.3 Fourier analysis of the transmission spectrum

Another important analysis method used to analyze FA intensity spectra for PMD information is the Fourier analysis method. Fourier analysis on the intensity spectrum results in an interference pattern where the PMD information is contained in the spread of the pattern [15]. In this section the transmission equation which includes the PMD term is derived as shown in [7]. Following a brief overview of Fourier analysis theory is a short theoretical experiment. By substituting in a specific PMD value the transmission equation is used to draw an intensity spectrum. Fourier analysis of this spectrum should then yield an interferogram with three peaks where the separation of the satellite peaks should be twice the DGD value used initially.

Suppose a simple birefringent device, implying negligible mode coupling, is placed between two crossed polarizers each at an angle of 45^o to the PSP of the DUT, the light transmission ratio is then given by

$$R' = \sin^2\left(\frac{\pi \Delta n L}{\lambda} \right) = \sin^2\left(\pi\nu \left(\frac{\Delta n \cdot L}{c} \right) \right) \tag{5.24}$$

where R' is the transmitted intensity of the light that passes through the polarizer, Δn the DUT birefringence and L the DUT length.

Suppose $\delta\tau$ is the PMD of the DUT given by

$$\delta\tau = \tau_2 - \tau_1 \tag{5.25}$$

where τ_1 and τ_2 represent the time of flight of the orthogonal state of polarizations. The PMD may then be rewritten as

$$\delta\tau = \frac{L}{v_2} - \frac{L}{v_1} = L\left(\frac{\Delta v}{v_1 v_2}\right). \tag{5.26}$$

Change in the refractive index can be written as

$$n = \frac{c}{v} \quad \Rightarrow \quad \Delta n = c\left(\frac{\Delta v}{v_1 v_2}\right). \tag{5.27}$$

Hence substitution gives

$$\delta\tau = \frac{\Delta n \cdot L}{c}. \tag{5.28}$$

The PMD term may now be included in the transmission equation which, after reformulating using a trigonometric identity, becomes

$$R' = \frac{1 - \cos(2\pi\nu \cdot \delta\tau)}{2}. \tag{5.29}$$

Equation 5.29 shows that R' is a cosine wave with an oscillation frequency $\delta\tau$. Hence the spectral content of R', obtained by Fourier transform will show a single component at $\delta\tau$. Fourier transformation of the spectrum transforms it from a frequency to a time domain. The intensity of the spikes in the Fourier transform spectrum will depend on the orientation of the polarizer and the analyzer with respect to the DUT PSP at the input and output. However this has no effect on the position of the spike, hence PMD measurements may be done independently of fibre splice rotation and polarization position [7].

Fourier transformation is a versatile tool and is often used in physics and engineering to alter the data or problem such that information may be more easily extracted and the problem more easily solved. The Fourier transform separates the waveforms into

sinusoids of different frequency which when added together give the original waveform. The Fourier transform of a function f(x) is defined as

$$F(s) = \int_{-\infty}^{\infty} f(x) e^{-i2\pi xs} dx . \tag{5.30}$$

The transform of F(s) gives

$$f(x) = \int_{-\infty}^{\infty} F(s) e^{-i2\pi xs} ds . \tag{5.31}$$

Experimental work generates discrete data hence a discrete Fourier transform (DFT) is required. The DFT computes the discrete samples of the transform using discrete sample values. The DFT of a dataset x[n] with index n in the range $0 \leq n \leq N-1$ is given by

$$X[k] = \sum_{n=0}^{N-1} x[n] e^{-i2\pi F_k n} \tag{5.32}$$

where F_k = k/N. The inverse or backward Fourier transform is then defined as

$$x[n] = \frac{1}{N} \sum_{k=0}^{N-1} X[k] e^{i2\pi F_k n} \tag{5.33}$$

in the range $0 \leq k \leq N-1$. The DFT requires computation which takes up computer time. Various algorithms have been developed to reduce the number of computations. These efficient algorithms of the DFT are called fast Fourier transforms (FFT). The Origin 6.1 software package used in this study has built-in functions which carry out the FFT of a given set of data. In this work the FFT function based on equations 5.32 and 5.33 are used together with windowing methods.

Suppose a PMD measurement is done on a simple birefringent element (no mode coupling) with a specific PMD value. The theoretical spectrum of the transmitted intensity can then be calculated over a wavelength range using equation 5.29. Figure 5.5 shows the calculated transmission spectrum assuming a PMD value of $\delta\tau$ = 3 ps

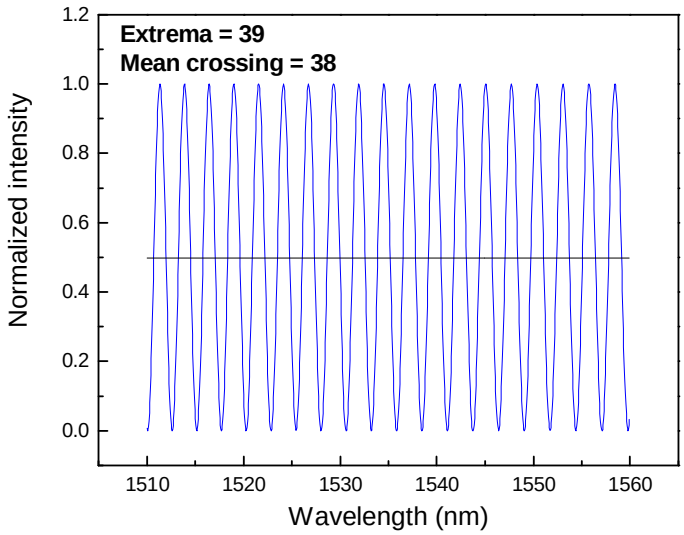

Figure 5.5. Normalized intensity spectrum generated using equation 5.29 for PMD = 3 ps.

and a wavelength window of 50 nm from 1510 nm to 1560 nm. The fast Fourier transform of this spectrum gives evidence of three spikes figure 5.6. As predicted the centroid appears at the PMD value which is 3 ps.

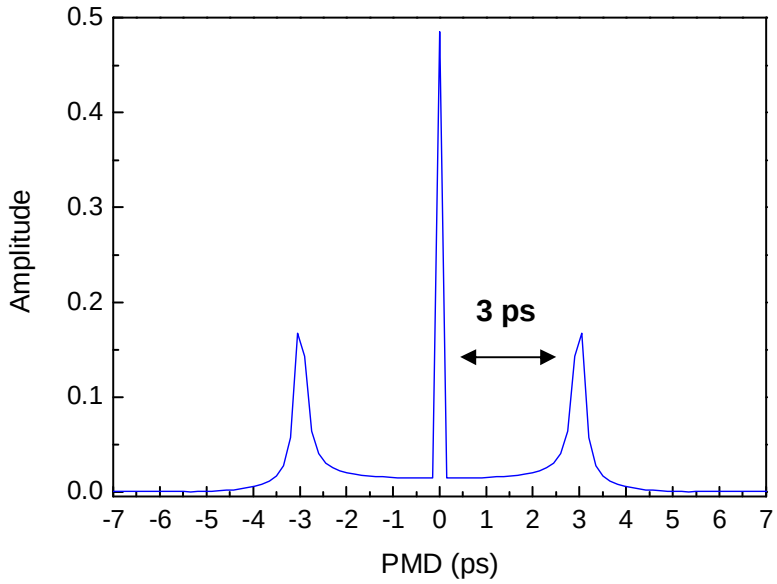

Figure 5.6. Fast Fourier transform of the spectrum shown in figure 5.4.

As a comparison, the extrema and mean level crossing values counted from the transmission spectrum in figure 5.5 are 39 and 38, respectively. Substituting these values into equation 5.5 gives a PMD value of 3.09 ps for extrema counting analysis

and 2.99 ps for mean level crossing analysis. Both these values are in excellent agreement with the PMD computed using Fourier analysis of the transmission spectrum. Similar results may be obtained for any chosen PMD value.

Random mode coupled devices will produce non-periodic transmission spectra. Fourier transforms of these spectra yield many spikes where each spike corresponds to a different DGD value. All the PMD information is contained within the spread of the interferogram [15]. The PMD value is given by half the width of the FWHM of the Gaussian fit to the interferogram.

5.3 Jones matrix eigenanalysis

The Jones matrix eigenanalysis (JME) technique is a highly accurate, well known PMD measurement technique [16, 17]. It is based on determining the transmission Jones matrix of a time invariant optical device. R. C. Jones showed that it is possible to fully describe the properties of an output beam of light using a matrix, named the Jones matrix [18]. The PMD information of the DUT is contained within its Jones matrix, which may be determined experimentally, and be extracted by eigenanalysis of the matrix. This eigenanalysis method is well documented in an article [16] authored by B. L. Heffner where the theoretical background is first described and then applied in an experiment to determine the PMD of a crystal. The JME technique performed well, producing similar results as the theoretical calculations of the DGD and orientation of the PSP over wavelength [16].

A conventional experimental JME measurement setup consists of a tuneable laser source, polarization controller, polarization analyzer (polarimeter) and the link or the DUT under test.

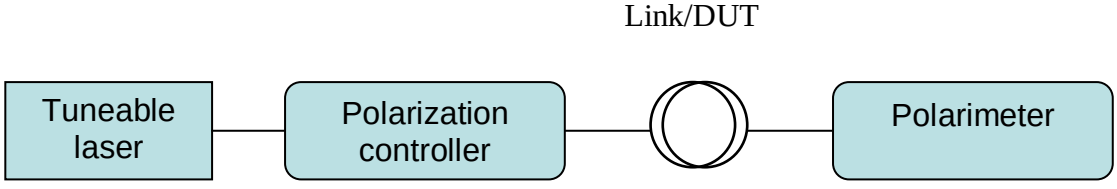

Figure 5.7 Schematic of the JME PMD measurement technique setup.

When a PMD measurement is conducted the laser sweeps across a wavelength range within the specified bandwidth. Determination of the Jones matrix of a DUT requires the evolution of the state of polarization with a change in wavelength for three distinct input states of polarization. Generally the polarization controller is set to transform the state of polarization of the laser light source to three known states of different linearly polarized light. A polarimeter keeps track of the evolution of the output state of polarization of the light through the DUT. Control of the hardware and analysis of the measurement results is done using a computer.

In the year 1947 R. C. Jones suggested a new calculus for the treatment of optical systems [18]. In this article he described how a set of measurements can be used to determine the transmission matrix of a crystalline plate. The Jones vector of a light source has the form

$$E = \begin{pmatrix} A_x \\ A_y \end{pmatrix} = \begin{pmatrix} E_x e^{i\delta_x} \\ E_y e^{i\delta_y} \end{pmatrix} \tag{5.34}$$

where E_x and E_y are the spatial variations of the electric field vectors in the x and y directions respectively and δ_x, δ_y represents the phase of the electric wave [7]. This representation completely describes the amplitude and phase of the light source. As polarized light traverses through any optical device, the light undergoes a transformation. This transformation may be represented by a 2×2 Jones transmission matrix as mentioned before. The input electric field vector and the output electric field vector are related by the Jones matrix, J, as follows:

$$E_{out} = \mathrm{J}E_{in}\,. \tag{5.35}$$

Hence the Jones matrix operates on the input light from the source to give the electric field vector of the output light. Consider the simplest case where the three known polarization states are linear horizontal, linear vertical and linear +45 ^{o}. The three measured output polarization states may then be

$$\begin{pmatrix} E_{x1} \\ E_{y1} \end{pmatrix}, \begin{pmatrix} E_{x2} \\ E_{y2} \end{pmatrix}, \begin{pmatrix} E_{x3} \\ E_{y3} \end{pmatrix}. \tag{5.36}$$

The following complex ratios are then constructed

$$k_1 = \frac{E_{x1}}{E_{y1}}; k_2 = \frac{E_{x2}}{E_{y2}}; k_3 = \frac{E_{x3}}{E_{y3}}; k_4 = \frac{k_3 - k_2}{k_1 - k_3}. \tag{5.37}$$

Giving the Jones matrix as

$$J = C * \begin{bmatrix} k_1 k_4 & k_2 \\ k_4 & 1 \end{bmatrix} \tag{5.38}$$

where C is a complex constant [18].

Once the Jones matrix of the device under test is known the differential group delay (DGD) of the test device can be fully characterised by eigenanalysis of the Jones matrices. The derivative of the representation of the principal state of polarization (PSP) with respect to frequency of an output PSP leads to an equation containing the product $T'T^{-1}$. T' is the first order derivative with respect to frequency, of the transmission Jones matrix T [18]. Measurement of T' and T^{-1} including the absolute phase would allow the direct computation of the two group delays and $\Delta\tau$. In reality however T' is approximated as

$$T' \approx \left[T(\omega + \Delta\omega) - T(\omega)\right] / \Delta\omega, \tag{5.39}$$

provided that the frequency interval is so small that each output PSP suffers nearly the same loss at ω and $\Delta\omega$. A further restriction that the eigenvalues of $T(\omega+\Delta\omega)T^{-1}(\omega)$ can only be determined within a complex constant, prevents determination of the two group delays individually. By making a small approximation, the DGD, $\Delta\tau$, can be expressed as

$$\Delta\tau = \left|\tau_{g,1} - \tau_{g,2}\right| = \left|\frac{Arg(\rho_1/\rho_2)}{\Delta\omega}\right| \tag{5.40}$$

where ρ_1 and ρ_2 are the eigenvalues of $T(\omega+\Delta\omega)T^{-1}(\omega)$ and *Arg* is the argument function, $Arg(\alpha e^{i\theta}) = \theta$. The eigenvectors corresponds to the PSPs of the device under test.

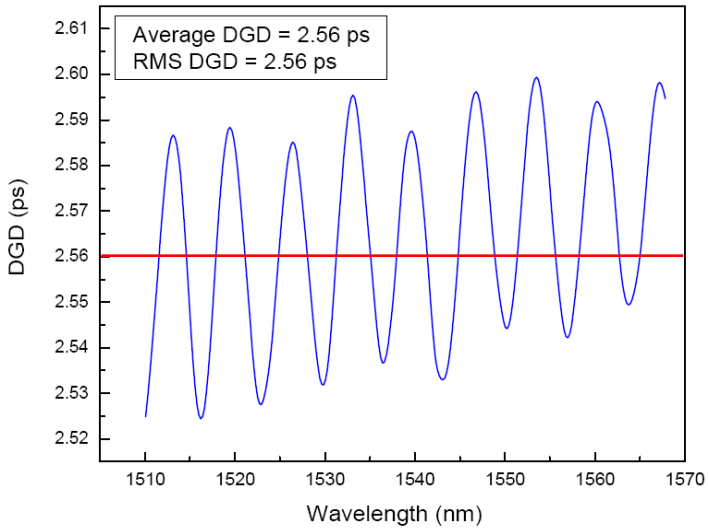

Figure 5.8 Variation of DGD with wavelength obtained from a JME measurement of PMD on polarization maintaining fibre.

The above figure is a representation of an actual PMD measurement result of a 1 m long segment of polarization maintaining fibre. Automated PMD measurements calculated the DGD of every intermediate wavelength. In the absence of mode coupling the range of DGD variation is smaller and more uniform than when mode coupling is present within the DUT. However the DGD still fluctuates periodically. This is because of the slight non-uniformity of the refractive index along the PMF leading to very small differences in the DGD values. The PMD is defined either as the root mean square or average DGD. The presence of mode coupling generates a signature which is more active and unevenly distributed about the mean DGD over wavelength. This can be seen in figure 5.9 which is a representation of a PMD measurement of an emulator consisting of four polarization maintaining fibre spliced sections.

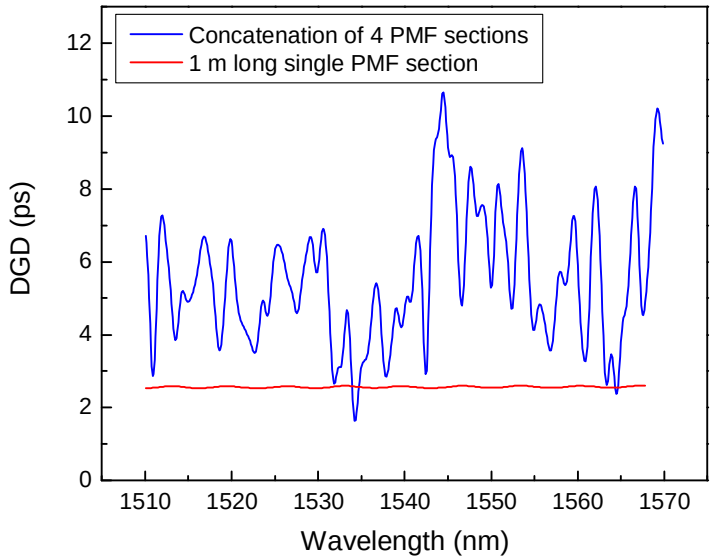

Figure 5.9. JME measurement result of a PMD measurement on a basic emulator. The average DGD for the mode coupled section is 5.53 ps and the RMS DGD value is 5.81 ps. The red line shows the DGD as a function of wavelength of the PMF in figure 5.8.

The average DGD and the root mean square DGD are related by a simple numerical factor of 1.085 = $\sqrt{(3\pi/8)}$ which is close to the ratio 1.05 given by these two quantities for the measurement results represented in figure 5.9. This difference is attributable to the fact that there exist two definitions of PMD and their mathematical formulation leads to a simple numerical relation relating the two [19].

5.4 Interferometric PMD measurement technique

The interferometric PMD measurement technique is based on a polarized broadband source, an analyzer and an interferometer. Light passes through the DUT and an interference pattern known as an interferogram is produced. The desired PMD information is contained within this fringe envelope for the wavelength range associated with the source spectrum. There exist two analysis methods to obtain the PMD delay, namely the traditional analysis (TINTY) method which uses specific operating conditions and a basic setup. The second is known as the general analysis (GINTY) method which does not use any limiting operating conditions and uses a more modified setup as compared to TINTY. At the heart of any interferometric technique is an interferometer, where the Michelson interferometer is generally used.

Hence in this section the Michelson interferometer and the theory regarding interference of light will be presented and covered in detail. The section will further link the fringe pattern interferogram with the PMD delay and present both the traditional and generalized interferometric PMD measurement techniques, placing emphasis on GINTY as it was the interferometric technique used throughout this study.

5.4.1 Interference of light and the Michelson interferometer

Interference of light refers to the superposition of two or more light waves which may either lead to an enhancement, constructive interference, or attenuation, destructive interference, of the waves involved. A Michelson interferometer is a device which splits a single light ray into two separate rays.

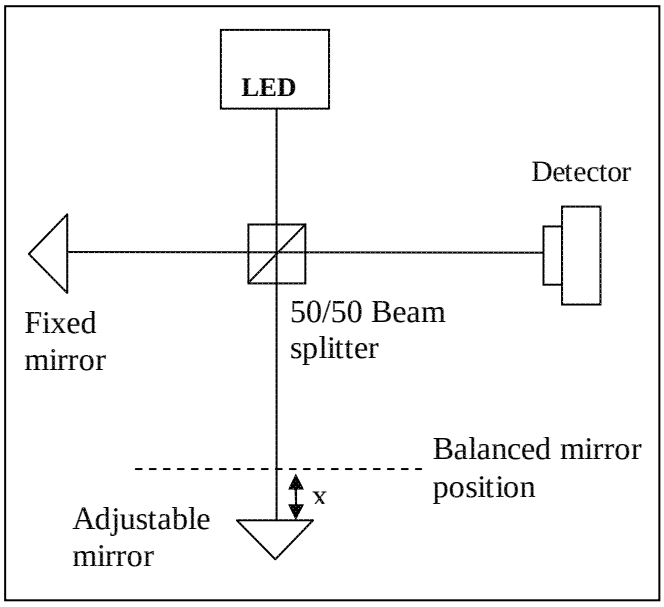

Figure 5.10 Schematic of a basic Michelson interferometer.

As shown in figure 5.10 it is made up of a broadband source, two mirrors, a beam splitter and a detector. The beam slitter splits the incoming light rays into two allowing them to propagate down separate paths. The light rays reflect off the fixed and movable mirror, are recombined and directed to the detector where interference fringes will be evident due to the time delay caused by the path length difference.

If there is an offset distance of x between the movable and fixed mirror then there exist a time delay of 2x/c between the two beams (c represents the speed of light). Interference fringes are a function of the path length difference between the two arms. Depending on the position of the movable mirror the interference of the light beams

may either be constructive or destructive. Hence based on this, a fringe envelope will be created as the movable mirror position is changed.

A Michelson interferometer can be seen as a device which physically performs a Fourier transform on the incoming light source. Hence the spectral distribution in the frequency domain is the Fourier transform of the interferogram in the time domain. After reflection of the mirrors the two electric fields are incident on the detector where interference will occur to produce an output intensity which mathematically consists of an autocorrelation term and a cross-correlation term. The autocorrelation term represents the total irradiance due to the non-interfering beams while the cross-correlation term will cause a positive or negative deviation from the non-interfering term.

The interference envelope produced by the Michelson interferometer for a laser and a broadband source differ. For example for a 1550 nm DFB (distributed feedback) laser the interference envelope will remain strong for interferometer delays of many metres. However for a 1550 nm LED the interferogram is formed only near zero path length difference between the two arms [6]. This difference is attributed to their difference in coherence time. Coherence time refers to the time over which the phase of a particular source remains constant. The DFB laser has a well defined wavelength; hence it is considered a highly coherent source. Whereas the LED is a more incoherent source as it consists of a wider wavelength range. The coherence time of a source may be directly related to the source spectral width by the following expression

$$\tau_c = \frac{{\lambda_0}^2}{c\Delta\lambda}, \tag{5.41}$$

where λ_0 is the central wavelength, $\Delta\lambda$ is the spectral width at half maximum and c is the speed of light in a vacuum [20]. From expression 5.41 it is evident that a narrow spectral width has a greater coherence time than a wider spectrum width, justifying the above statement.

Interference only occurs for time delays shorter than the source coherence time. If a laser source with a narrow spectral width were to be used, according to equation 5.41 it will have a very large coherence time. Therefore this will give rise to a continuous

interference pattern providing very little information about the fibre imposed PMD delay. For a broadband source with an equitable smaller coherence time only one central interference fringe is evident. This maximum intensity is produced when the mirrors are at balanced mirror positions which results in equal path length between the two arms. Interference fringes related to the time delay occur when the path length difference compensates for the differential group delay of the DUT.

Firstly, consider the case of no mode coupling in the DUT. In this particular case two outlying satellite peaks are produced. Consider the Michelson interferometer. If the interferometer is placed after the DUT then both eigenmodes, the fast and the slow light, propagate down the two arms of the interferometer. Therefore as the mirror sweeps from one side of the balanced mirror position to the other side, two compensating events will occur at these opposite ends of the mirror position. The time delay between the two outlying peaks is twice the differential group delay (DGD). If the position of the interferometer and the DUT were reversed, then the same compensation resulting into interference would take place. Secondly, consider the PMD measurement of a device with mode coupling. Due to the presence of mode coupling the interference envelope will be filled with interference patterns. The central peak of the interference envelope will be of high intensity as a result of the balanced mirror position. As the adjustable mirror shifts away from the balanced mirror position the DGD and the coherence time become more similar. Hence the intensity of the interference fringes diminishes and fades out until no more fringes are evident.

PMD is determined from the interferogram via either one of two methods; direct fitting of the Gaussian or calculation of the second moment [6]. The fitted Gaussian curve is related to the differential group delay by

RMS DGD: $$\left\langle \Delta\tau^2 \right\rangle^{1/2} = \sqrt{\frac{3}{4}}\sigma \qquad (5.42)$$

Mean DGD: $$\left\langle \Delta\tau \right\rangle = \sqrt{\frac{2}{\pi}}\sigma \qquad (5.43)$$

where σ is the standard deviation of the Gaussian to best fit the interferogram excluding the central peak, and RMS implies root mean square [6]. The PMD may also be determined using an algorithm based on the square root of the second moment of the photocurrent response. The algorithm involves amplitude shifting of the response to reduce the noise, removal of the central autocorrelation peak, truncation of the interferogram, computation of the second moment of the truncated interferogram and determination of the Gaussian [6].

5.4.2 Autocorrelation PMD measurement technique

This section describes both the autocorrelation PMD measurement setup and its operational principles. Figure 5.11 shows the main components of a TINTY setup during a PMD measurement. As illustrated the adjustable mirror scans from position a, past the balanced mirror position, until position b. A detector at the output end of the fibre senses the light intensity through an analyzer (polarizer) as a function of mirror position. Interference fringes occur when the path length difference compensates for the DGD, as mentioned before.

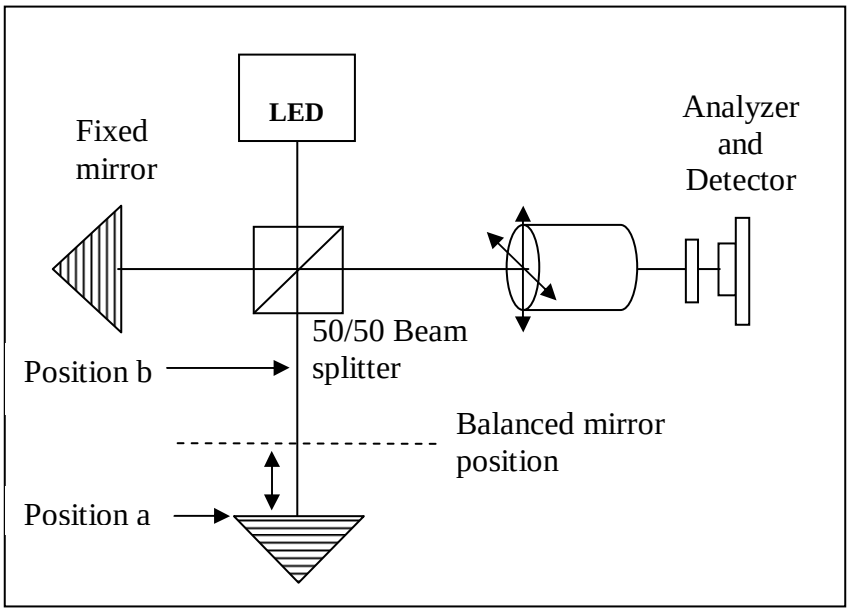

Figure 5.11. Autocorrelation PMD measurement interferometer.

This traditional analysis method setup generates interferograms consisting of both the source autocorrelation and cross-correlation functions. The autocorrelation peak is the central interference fringe with the highest intensity and occurs when the path length difference between the arms of the interferometer are equal in distance. This autocorrelation function does not house any PMD information and may thus act as a limiting factor when small PMD values are measured. All the PMD information of the DUT is contained in the cross-correlation term.

The interferogram produced by the TINTY PMD measurement technique for a test device with no mode coupling has three distinct interference peaks, where the two offset peaks separated by the central autocorrelation peak is due to birefringence. The DGD of the test device is the time delay between the autocorrelation peak and one of the satellite peaks. This feature of the TINTY PMD measurement technique is clearly shown in figure 5.12 for half a metre of PMF. As mentioned previously, the two satellite peaks at the side are a result of the mirror position compensating for the light propagating in the fast axis and also for light propagating in the slow axis. In the TINTY technique the autocorrelation peak is omnipresent and is the most intense, occurring when the adjustable mirror is at the balanced mirror position.

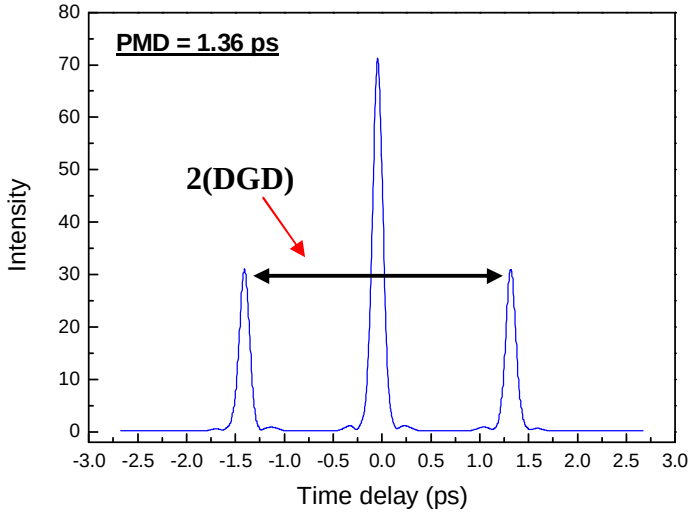

Figure 5.12. Autocorrelation interferogram of polarization maintaining fibre.

TINTY and GINTY diverge in their analysis method depending on the assumptions made when mode coupling is present in the DUT. The presence of random mode coupling requires analysis of the entire envelope making up the interferogram. Figure

5.13 shows the interference pattern of a concatenation of three PMF sections. It is clearly evident that the introduction of the mode coupling sites induces the presence of more interference peaks.

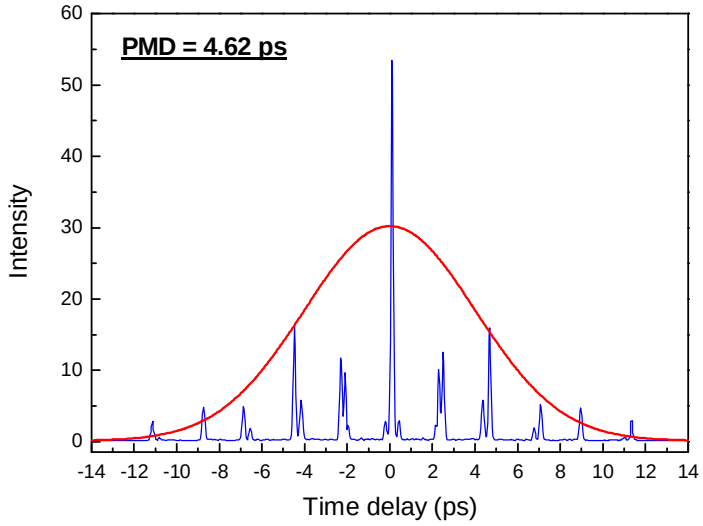

Figure 5.13. Autocorrelation interferogram of concatenation of PMF sections.

TINTY retains its characteristic and highlights the equal path length occurrence with the high intensity autocorrelation peak. A Gaussian fit which excludes the autocorrelation peak is fit to the interference envelope and the PMD delay computed from the second moment (RMS width) of the cross-correlation of the interferogram using equation 5.42 [7]. The PMD coefficient is then given as the time delay per square root length of the device under test as the PMD no longer increases with length but with the square root of length.

The traditional analysis (TINTY) used in the PMD measurement technique makes a few assumptions which present some limitations regarding PMD measurements. The first assumption is that equation 5.42 relating the PMD to the RMS width of the interferogram is based on the assumption that the device under test is an ideal random mode coupled device of infinite coupling ratio [21]. The coupling ratio is the ratio of the fibre length and the coupling length, which is equal to the fibre length over which the polarization of a lightwave becomes uncorrelated due to polarization mode coupling. Secondly the PMD to be measured must be much larger than the source coherence time [21]. Thirdly the interferogram is a statistical average over all possible PMD values for a theoretical PMD value [21]. Having made these assumptions the formula thus refers to a theoretical interferogram which is Gaussian in shape. TINTY

is a good PMD measurement technique provided certain requirements are met. Due to the assumptions mentioned TINTY has two clear limitations regarding PMD measurements. Firstly the measured PMD value obtained using TINTY deviates from the true PMD value of the DUT when limited mode coupling sites are present and secondly the TINTY technique lacks the ability to measure extremely low PMD values due to the presence of the autocorrelation peak.

5.4.3 Cross-correlation PMD measurement technique

The cross-correlation PMD measurement technique differs from the autocorrelation PMD measurement technique by only considering the cross-correlation function and extracting the PMD from it. The Santec 6000B is such an interferometric PMD measurement instrument. Figure 5.14 shows a schematic illustration of the Santec 6000B cross-correlation instrument.

Several differences between the autocorrelation and the cross-correlation techniques are apparent in the setup. The cross-correlation technique has the same setup as the autocorrelation technique except for three polarization beam splitters (PBS), a half wave plate and a quarter wave plate placed in the path of the light. As shown in figure 5.14 each arm has a polarizer just before the mirrors. These polarizers are oriented orthogonally relative to each other. A half wave plate is positioned just before the light enters the fibre.

A broadband light source shines light through a polarizer and a quarter wave plate before the light is split into two separate arms by a beam splitter, one with a fixed mirror at the end and one with a movable mirror. The two polarizers in place alter the polarization state of the rays such that they recombine at the beam splitter with states of polarizations orthogonal relative to each other. Two mirror scans are run where the orientation of the half wave plate is changed for each individual scan. Before the first scan a principal axis search (PAS) is run in order to determine the fast and slow axis of the DUT. This works well for PM fibre. The wave plate is then adjusted such that all the incoming light is first coupled into the fast axis of the DUT. A second scan is

then run with the wave plate adjusted such that all the light is coupled into the slow axis of the DUT. The two interference envelopes are then finally combined and the PMD determined from this combined interferogram. The final result is minimal influence of the autocorrelation envelope.

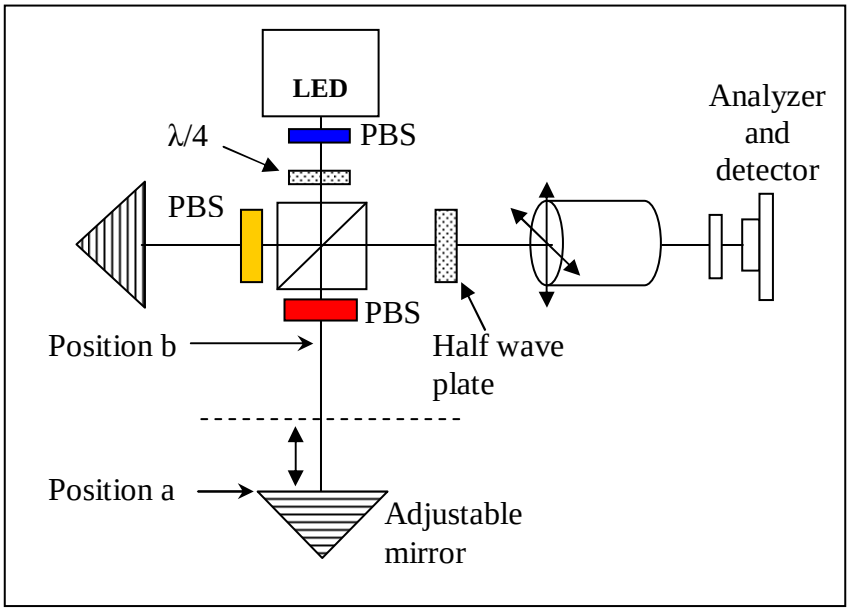

Figure 5.14. Schematic diagram of the Cross-correlation interferometer, polarization beam splitter (PBS).

The resultant interferogram of polarization maintaining fibre (PMF) shows distinct evidence of the reduction of the autocorrelation peak.

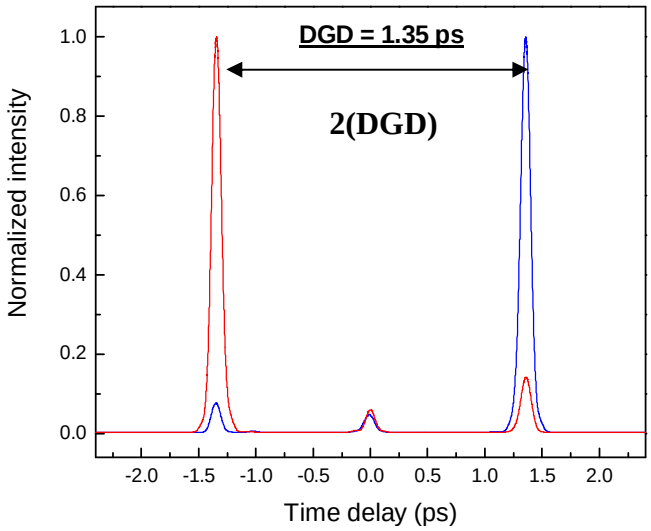

Figure 5.15. Normalized interferogram of PMF of the cross-correlation interferometer.

From the interference pattern, of a measurement done on half a metre of PMF shown in figure 5.15, it can be seen that the central peak (autocorrelation peak) is considerably much weaker in intensity, only the two outlying interference patterns have high intensity. The outer peaks are a result of the fast and slow axis which are maintained throughout in PMF. In the presence of mode coupling the two interference envelopes are still separate and the influence of the autocorrelation function minimized. However the presence of mode coupling implies that the PSPs are no longer fixed hence the PAS search and lining up of the half wave plate no longer plays a significant role. The interference envelope of a concatenation of three PMF sections is shown in figure 5.16.

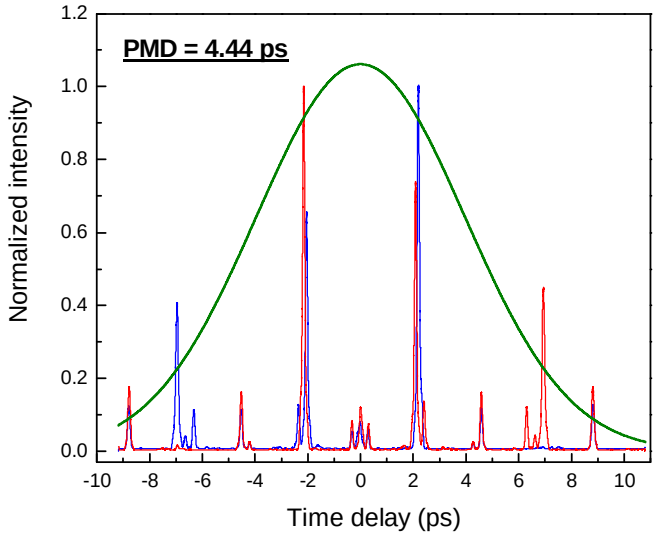

Figure 5.16. Normalized interferogram of a concatenation of PMF sections of the cross-correlation interferometer.

This concatenation is the same emulator used to illustrate the interference envelope generated by TINTY for DUT with mode coupling (figure 5.13). The most common, by now, and most significant feature is the clear absence of the autocorrelation peak. The two techniques do show good agreement in the measured PMD value with only a 1.36 % difference for a FUT without mode coupling and a 3.9 % lower PMD value for the FUT with mode coupling.

5.4.4 GINTY PMD measurement technique

The general analysis interferometric (GINTY) PMD measurement technique deduces the desired PMD from both the autocorrelation, and cross-correlation interferograms. The measured PMD is given by

$$\text{Measured PMD} = \sqrt{\frac{3}{2}\left(\sigma_x^2 - \sigma_0^2\right)} \tag{5.44}$$

where σ_0 and σ_x represent the RMS widths of the auto- and cross-correlation mean square envelopes [22]. The GINTY technique has a setup which measures both the auto- and cross-correlation interferograms separately to obtain the needed RMS widths. In this setup a polarization beam splitter is placed after the interferometer. The beam splitter splits the light to two detectors which separates the auto- and cross-correlation envelopes to determine the PMD.

GINTY may be used to measure the PMD of any DUT of any order of mode coupling, with a linear response and with low PDL. The condition that the RMS width of the cross-correlation envelope must be larger than that of the autocorrelation no longer applies [22]. In principle zero PMD can be measured using this method. In this case the auto- and cross-correlation envelopes have the same width leaving the offset subtraction to be zero. Another enhancement of the GINTY technique is that the source spectral shape does not need to be perfectly smooth and Gaussian. Also of interest is that an estimate of the DGD curve can be generated [22]. This can be done by analysing the same raw data using windowing hence by selecting narrow windows with a central wavelength. There are no theoretical limits provided.

This subsection presents PMD measurement results of three different fibre types using the GINTY PMD measurement technique. Interferograms of the first two fibre types were shown above using the auto- and cross-correlation PMD measurement techniques. Figure 5.17 shows the interference envelope produced by GINTY for the same half metre of PMF as above. The measured PMD value is the same as that generated by TINTY. A similar feature found in the cross-correlation envelope for

PMF is evident in the GINTY envelope for the PMF measured. That is, the significant reduction in peak intensity of the auto-correlation function is also found in the final interference envelope generated by GINTY.

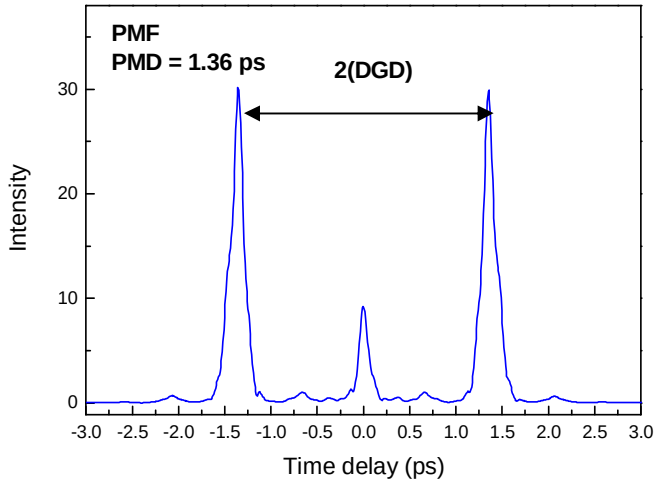

Figure 5.17. Interferogram of PMF from GINTY.

More interference fringes are generated in the interferogram produced by GINTY for a concatenation of PMF sections, which is a common result by now. GINTY determined the PMD of the concatenation to be 4.50 ps, a result not very different to the previous PMD values found by the other two interferometric PMD measurement techniques.

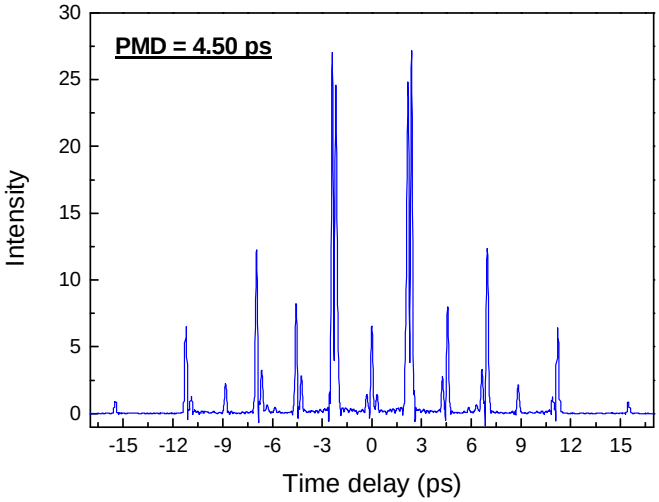

Figure 5.18. Interferogram of a concatenation of PMF sections from GINTY.

An increase in the number of mode coupling sites present in a fibre or DUT, leads to an increase in the number of interference events during a single measurement. Figure 5.19 is such an interferogram attained using GINTY.

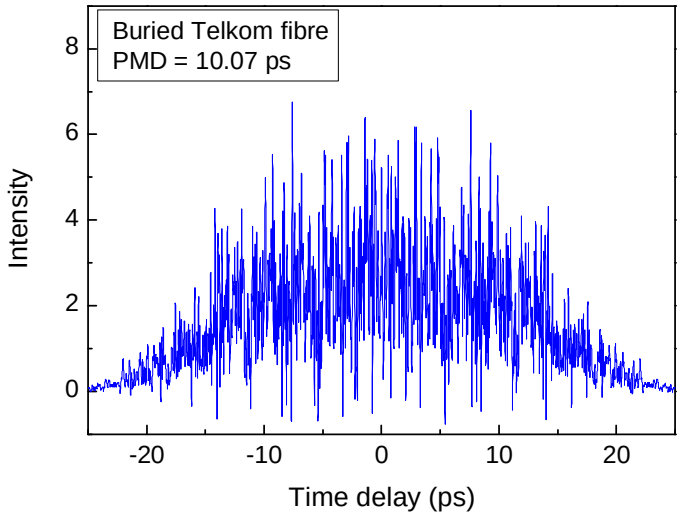

Figure 5.19. Interferogram of buried deployed cable obtained using GINTY.

Measurements were done on buried deployed Telkom optical fibre. The high number of interference fringes gives an indication of the high number of mode coupling sites present in this buried fibre. The measured PMD was a high PMD value of 10.07 ps.

5.5 Comparison of PMD measurement methods

The PMD measurement techniques mentioned above exhibit different capabilities and characteristics, hence their suitability differs among different measurement situations. In general it has been shown that the above mentioned techniques show good agreement in the determination of the average PMD. More specifically, the polarimetric techniques give the DGD and the PSP, whereas the interferometric and the fixed analyzer techniques are only able to deliver the root mean square or average DGD. However the interferometric technique has the advantage of operating under conditions where the SOP is unstable, whereas the resultant DGD is affected in the polarimetric techniques. The interferometric technique is also considerably fast. Fixed analyzer measurements have an advantage of their own in the form of being able to give information regarding the degree of mode couple present in the DUT [13]. N. Gisin *et al.* [19] gives two definitions of PMD and showed that they are related by a simple numerical factor of $\sqrt{(3\pi/8)}$. The first definition relates PMD to the time-dependent intensity and the second definition relates the DGD to the rate of change of

the output state of polarization with frequency over a range of frequencies [19]. Using the wavelength scanning technique and in particular the JME technique, PMD may either be defined as the average DGD or as the root mean square (RMS) DGD. B. Perny *et al.* proved that the RMS value of the DGD compared very well with the interferometric PMD value [23]. A large scale comparison between the measured PMD values resulted in a 3 % difference for components with a PMD value within the range 0.1 – 5 ps between the least square fit to the data and the unity line. A 13 % difference was evident for a bigger range of <0.1 to 10 ps. It is found in literature that the fixed analyzer technique compares well with both the JME and interferometric measurement techniques [24, 25, 26, 27]. In particular the fixed analyzer technique with extrema counting analysis yields a very similar average PMD value to the JME technique whereas the fixed analyzer technique with Fourier analysis compares very well with the interferometric technique [24, 26]. The similarity between the interferometric technique and the FA method is explained by the fact that the Fourier transform of the spectral intensity over wavelength is the same as the fringe envelope produced by the interferometric technique [15, 19]. Other time and frequency domain PMD measurement techniques also showed good agreement with the FA method. Generally the optical pulse method and the Sagnac interferometer produced similar PMD values [24, 28]. The Sagnac interferometer is based on a setup where a 50:50 coupler is closed with a fibre. Light having the same polarization state will interfere in the coupler causing the transmission measured with an Optical Spectrum Analyzer to vary with wavelength. Analysis is done by extrema counting. The number of extrema found in the transmission spectrum of the FA method was found to match those for the Sagnac interferometer for several fibres of various lengths [28]. Polarimetric techniques like the SOP and PS methods were found to compare well with the FA method, in particular with the extrema counting analysis [11, 29, 30] of the transmission spectrum.

CHAPTER 6

INSTRUMENTATION

Different instruments were used to carry out this study. All the equipment and instruments used served a different purpose. Collectively several tools and equipment performed the function of preparing the fibre. A range of other instruments such as laser sources, interferometers, polarimeters, polarization controllers and optical spectrum analyzers were used in PMD measurements to measure and record parameters used to calculate the PMD. This chapter describe the operating principles of the instruments used, sets out to provide important relevant specifications regarding the instruments and also to point out the role played by some of the instruments during PMD measurements.

6.1 Miscellaneous tools and equipment

Optical fibre, various components used in fibre optics and the connector interfaces of instruments need to be clean when in use. This is both for the purpose of preventing any damage to the mentioned parts and also to minimize attenuation and scattering of the light signal.

Optical fibre connectors mainly consist of a connecting body, mechanical retainers and a ferrule where the ferrule houses the glass fibre. The ferrule is made up of metallic or ceramic material and is the part which comes into contact with any other external connection. Hence it needs to be thoroughly cleaned. A combination of wipes, a connector wiper, wrapped

Figure 6.1 Miscellaneous fibre optic equipment.

foam swabs and isopropanol are used to remove dust particles, grease and dirt from the fibre itself, the ferrule and optical input ports to any instrument. In the specific cleaning process of cleaning a ferrule of an optical connector, an optical microscope, figure 6.1, is used to zoom in and get a closer look at the face of the ferrule. This is just to confirm whether the ferrule and fibre core are clear of dust particles and grease.

In any fibre optics work or study a frequently performed task is the splicing of fibre. Splicing refers to the joining of two fibre pieces. It is mainly required for two reasons. Firstly fibre consists of highly purified glass and will thus break when bent beyond a certain angle or as a result of external mechanical stress applied to it. Secondly fibre is also spliced when constructing emulators and when joining fibre pieces together for practical reasons. Before splicing the fibre together the fibre is first stripped with a stripper to remove the plastic coating. A cleaver shown in figure 6.1 is then used to cut the fibre. The cleaver has fibre clamps, a fibre groove to secure the fibre and a sharp blade to make a clean cut. If the fibre is not cut properly so that the end face of the fibre is even and flat then it is not possible to splice the fibre well. Figure 6.2 (a) shows the full view of a Sumitomo electric fusion splicer.

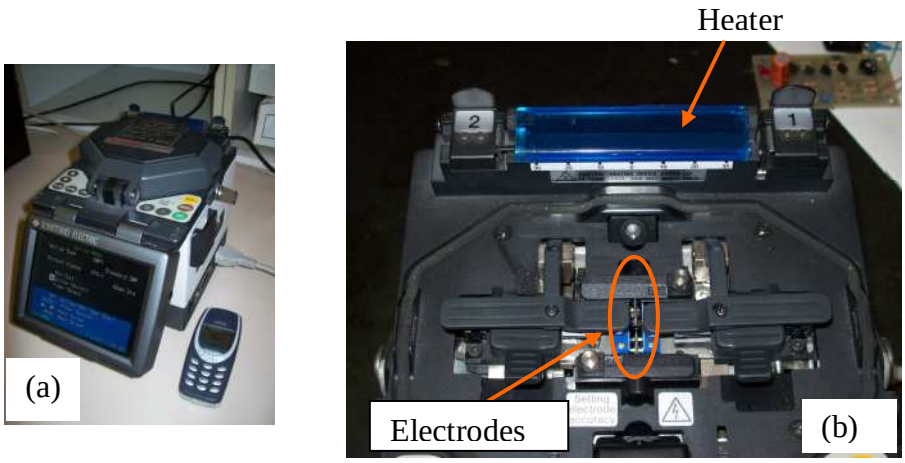

Figure 6.2 Sumitomo electric fusion splicer; (a) full view, (b) close up.

More specifically, this is the TYPE-37/TYPE-37B micro-core fusion splicer. It has been designed to splice nine different fibre types which include single mode fibre (SMF) and multimode fibre (MMF) [31]. The acceptable cleave length (exposed fibre area without any coating) is 8 mm to 16 mm and the average splice losses are 0.02 dB or less for single mode fibres. By making use of high resolution direct core

monitoring image processing software the splicer aligns a pair of fibres in the horizontal and vertical planes. This software performs both the tasks of core alignment and splice loss estimation. After aligning the fibre cores, the fibres are joined together with heat from an electric arc to form a low loss fusion splice [31]. Afterwards a proof test may be performed to verify the strength of the splice and also its physical condition. The splice may then be protected by applying a fibre protection sleeve over the spliced area and inserting it into the built-in heat sink protector to prevent the sleeve from moving. Figure 6.2 (b) shows the components and parts which carry out the mentioned operations. The typical splice cycle time when the splicer is in quick splice mode is 11 seconds and 15 seconds for when it is in automatic splice mode. The Sumitomo electric splicer was used in this study to fix fibre breaks and also to construct an emulator from PMF and SMF. A full description of the instrument and several operations related to splicing, including how to splice different fibre types can be found in this document [31].

6.2 Broadband and laser sources

Optical sources play a fundamental role in fibre optics. They are important to either ascertain the optical characteristics of a DUT or FUT, or to use as sources of transport to transmit data with. Both laser and broadband sources are used in various applications concerning fibre optics. In this study several sources were used to make PMD measurements. The sources themselves and the application of the sources differed depending on the measurement method applied. The optical sources used in this study included the following; EXFO M2100 light emitting diode (LED), EXFO FLS-5800 CD/PMD analyzer source and the Agilent 8164A lightwave measurement system. This section takes on a brief discussion regarding optical sources followed by descriptions of each source and its specifications.

Optical devices generate light in different ways hence generating various spectra with unique characteristics. A tuneable DFB laser shown in figure 6.4 was used in this study. Tuning of a DFB laser is done by altering the temperature of the device or by altering the modulation rate of the current powering the laser. The acronym LED

stands for light emitting diode. A LED is a semiconductor device which emits light. Light is produced by a radiative recombination process by confining the charge carriers and the stimulated optical emission to the active region of the pn junction in LEDs [2]. There are two basic LEDs, surface emitters and edge emitters. Edge emitters consist of an active junction region, which is the source of incoherent light, and two adjacent guiding layers [6]. Their emission pattern is more directional than surface emitters. LEDs differ from lasers as good quality LEDs may be produced at a much lower cost than lasers and LEDs emit a bigger range of wavelengths compared to lasers.

The EXFO M2100 broadband light source is a high power EELED (edge emitting laser emitting diode) light source with a variable power output and a high dynamic range suitable for PMD measurements. The EXFO M2100 broadband light source is a C-band light source. It has a central wavelength around the 1550 nm region and a spectral width of 50 nm, its full spectrum is shown in figure 6.3 (c). The output light from the EELED source is polarized by a built in polarizer which makes it appropriate for PMD measurements as it is required that the input light to the DUT be polarized. This light source is also very small with a size of 6.5 cm × 18.5 cm × 26 cm and operating temperature range of 15^{o}C to 40^{o}C hence it qualifies very easily as a portable light source suitable for field measurements. The M2100 polarized broadband source was used in the FA setup to make PMD measurements.

The EXFO FLS-5800 CD/PMD analyzer source [32] viewed in figure 6.3 is a modulated, polarized broadband source which was specifically designed to be used with the EXFO FTB-5500 polarization mode dispersion analyzer. In general it is a broadband source which may be used for various fibre optic applications. Depending on the selected setting it can operate in the C-band, the L-band or in the C + L band, where the C-band is defined as the range 1550 ± 10 nm and the L-band as 1607.5 ± 17.5 nm. It has an output power of 4 dBm. Figure 6.3 shows the source spectra for the C-band, the L-band and for the C + L band.

(a)

(b)

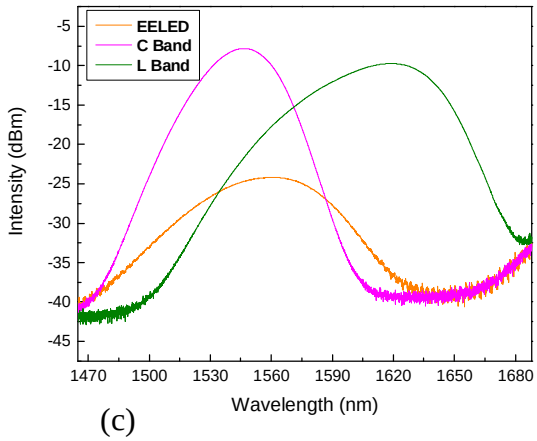

(c)

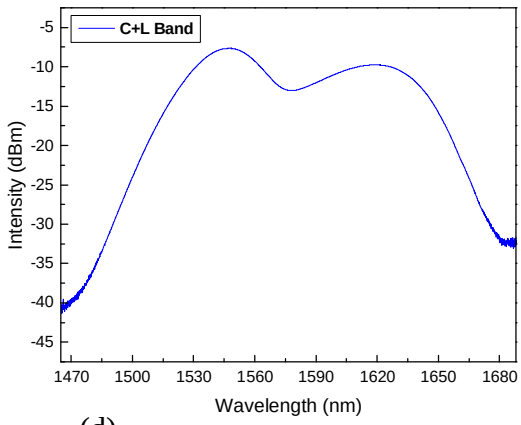

(d)

Figure 6.3 (a) M2100 LED broadband light source, (b) EXFO FLS 5800 polarized broadband light source, (c) optical spectra of the EELED source and the C- and L-band of the FLS 5800 light source, (d) optical spectrum of the C + L band of the FLS 5800 light source.

The fact that it is a broadband polarized source makes it an ideal source for PMD measurements such as for the interferometric and FA PMD techniques. General specifications include temperature operating conditions between 0 ^{o}C and 40 ^{o}C, a light weight of 3.2 kg and 11.7 cm by 22.2 cm by 33.3 cm in size. Hence it is very easy to move around and is very suitable for PMD measurements in the field. In this study the EXFO FLS 5800 CD/PMD analyzer source was used in both the FA setup and together with the generalized interferometric technique to perform PMD measurements on different fibre types.

Tuneable lasers are an essential component in polarimetric PMD measurement methods. Both the Jones matrix eigenanalysis technique and the Poincaré sphere analysis method make use of tuneable laser sources. In this study the Agilent 8164A

lightwave measurement system shown in figure 6.4 (a) was used for both of these techniques. The Agilent 8164A lightwave system consists, amongst others, of a tuneable distributed feedback (DFB) laser. Hence it is a polarized narrow-band single wavelength source which is able to sweep across a desired wavelength range. The Agilent 8164A lightwave measurement system weighs 20 kg and has the dimensions 145 mm × 426 mm × 545 mm. The tuneable laser has a range from 1459.2 nm to 1583.30 nm and it has a minimum wavelength resolution of 0.1 pm. Figure 6.4 (b) shows the spectrum of a single selected wavelength, 1550 nm, which was measured using an optical spectrum analyzer. From this spectrum it can be seen that the selected wavelength is well defined and has a high intensity narrow spectrum. The Agilent 8164A user's guide [33] explains in detail how to operate the laser.

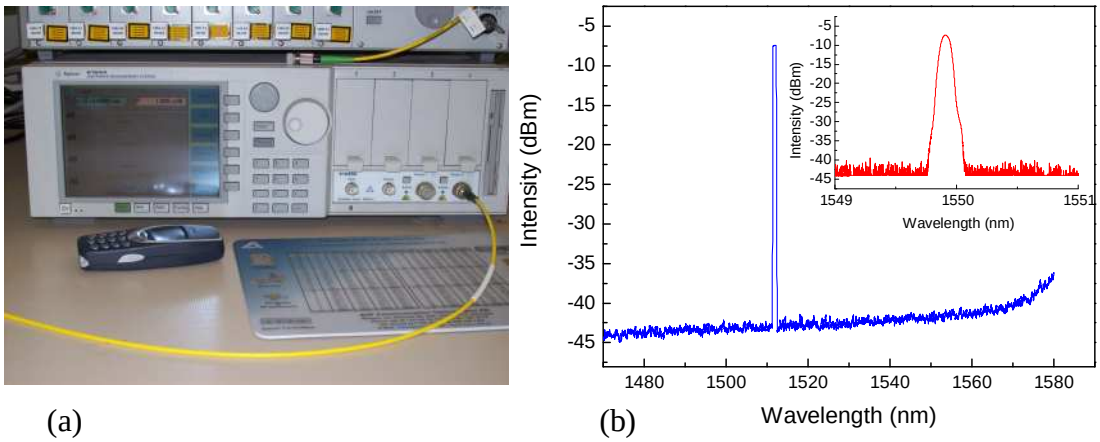

(a) (b)

Figure 6.4 (a) Photograph of the Agilent 8164A lightwave measurement system, (b) Intensity spectrum of the Agilent 8164A laser at a wavelength setting of 1550 nm.

6.3 PMD measurement equipment

6.3.1 Optical spectrum analyzer

An optical spectrum analyzer (OSA) is a device which measures optical power as a function of wavelength. It is used to characterize the spectral purity and power distribution of a light source, as well as to measure the transmission characteristics of optical devices. There are mainly two types of optical spectrum analyzers, namely the

interferometer-based OSA and the diffraction grating based OSA. The interferometric based OSA has two subcategories, the Fabry-Perot and Michelson interferometer based OSA. The Fabry Perot OSA has a fixed narrow spectral resolution which allows it to measure laser chirp. The nature of the intensity spectrum generated by the Michelson interferometer makes it very good for direct measurements for coherence length, as well as accurate wavelength measurements.

The Agilent 86142B series optical spectrum analyzer was used in this study to perform PMD measurements in the fixed analyzer setup. This OSA is a diffraction grating based OSA. Diffraction based OSAs use monochromators as tuneable optical filters. A diffraction grating which separates the light into different wavelengths is housed in the monochromator. The diffraction grating is positioned such that it directs specific wavelengths towards an aperture. As these wavelengths pass through the aperture they reach a photodetector. The current from the photodetector is converted to a voltage by a transimpedance amplifier and digitized. Any further signal processing is performed digitally. The grating is rotated in order to sweep all wavelengths across the photodetector. A ramp generator determines the horizontal location of the trace as it sweeps from left to right. The final result is an optical intensity vs wavelength trace [34]. The angle of the grating determines the wavelength that passes through the aperture and the slit width of the aperture determines the wavelength resolution. In reference [34] the types of optical spectrum analyzers are discussed and a whole chapter is dedicated to the diffraction grating based OSA.

The Agilent 86142B optical spectrum analyzer is a resourceful instrument in terms of characterization of optical spectra. In addition to the normal interface for characterization of optical spectra it has several less controllable applications. They are characterization of passive optical components, characterization of wavelength division multiplex systems, characterization of an optical amplifier and characterization of the spectra of light sources. Figure 6.5 shows a picture of the Agilent 86142B OSA with a polarizer directing light into the optical input of the OSA.

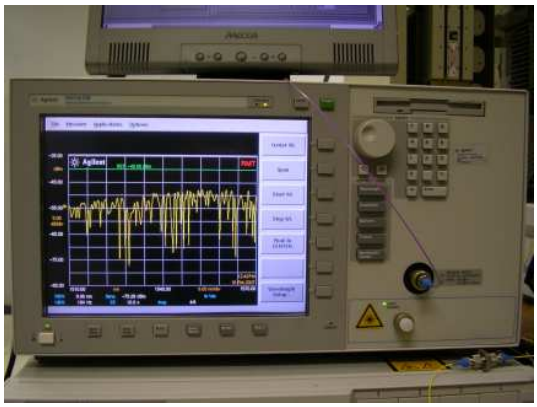

Figure 6.5 Photograph of the Agilent 86142B optical spectrum analyzer.

The soft key panels allows various parameters, for example the wavelength, the amplitude, the traces, markers and the bandwidth sweep, to be controlled and adjusted as desired.

Table 6.1 Agilent 86142B OSA instrument specifications found in reference [35].

Wavelength range	600 nm to 1700 nm
Reproducibility ≤ 1 min	± 0.002 nm
Span range	0.2 nm to full range and zero span
Accuracy depending on the source calibration and the wavelength range	± 0.01 nm to ± 0.2 nm
Absolute accuracy	± 0.5 nm
Maximum measurement power	+ 30 dBm total
Resolution bandwidth, FWHM (3 dB Bandwidth)	0.06, 0.1, 0.2, 0.5, 1, 2, 5, 10 nm
Dimensions	222 mm H × 425 mm W × 427 mm D
Weight	16.5 kg

Other settings like the number of trace points, single or multiple sweeps and trace averaging may also be adjusted as required. Data may be saved internally or onto a floppy disk for analysis. Table 6.1 lists a number of relevant instrument specifications

for the Agilent 86142B OSA. This OSA has a total wavelength range of 1100 nm, hence in the domain of PMD measurements a wide range of broadband sources may be used to perform PMD measurements. Specifications which play a major role in PMD measurements are the resolution bandwidth and the sweep rate or sweep time. Actual peaks and valleys may be overlooked and missed during a sweep if an inappropriate resolution bandwidth, generally too large a value, is set. The instrument always tries to use the fastest sweep time possible when it is in the auto-mode setting. The sweep time depends on the following instrument settings; wavelength span, resolution bandwidth, video bandwidth, sensitivity, trace length and power level. The sweep time ranges from 56.3 ms to a maximum value which depends on the number of trace points [35]. Whenever an inappropriate sweep time was used during a measurement, red text reading “oversweep” will occur on the screen of the OSA. Over sweeping can also affect the number of extrema in the transmission spectrum through a polarizer. Hence both these parameters need to be closely monitored. Reference [35] is the user’s guide of the Agilent 82142B OSA where all the instrument specifications may be found and it is also clearly explained how to operate the instrument. The Agilent 82142B instrument has a GPIB interface which may be used to connect it to a computer and presents the possibility of automating the FA setup. In this study a computer program using Labview was written to automate the data collection and PMD calculation. This part of the project will be discussed in chapter 7.

6.3.2 Generalized interferometric PMD measurement instrument

The generalized interferometric (GINTY) PMD measurement instrument known as the FTB-5500B polarization mode dispersion analyzer is based on the TIA-approved interferometric PMD measurement method. It presents a fast field-proof PMD measurement method [36]. The analyzer covers the O + C + L bands, has a dynamic range higher than 50 dB for long haul applications and has multiple measurement capability. Figure 6.6 shows such a unit. This particular analyzer averages over the entire source wavelength range without any filtering. The FTB-5500 PMD analyzer has the advantages of being able to measure the PMD of long fibre spans and is also

capable of withstanding small vibrations due to its fast measurement time. The FTB-5500 PMD analyzer module is inserted into a slot on the side of the platform.

Figure 6.6 Photograph of the FTB-5500B PMD analyzer

Before a PMD measurement the wavelength range, the fibre type, single or multiple measurements, averaging, saving instructions and several other parameters and options need to selected and specified. The instrument has various windows from where this may be done. The FTB-5500B PMD analyzer has an optical input at the open end of the module. The connection from the polarized broadband light source is connected to this input terminal.

Table 6.2 Technical specifications of FTB-5500B PMD analyzer.

Wavelength range	1260 to 1675 nm
Measurement range	0 to 115 ps
Measuring time	4.5 s
Absolute uncertainty (accuracy)	± (0.020 + 2 % of PMD)
Dimension	9.6 cm H × 7.6 cm W × 26.0 cm D
Weight	1.5 kg

After saving the data, the data needs to be extracted from the saved files using a specific procedure. There exists a file converter tool which exports PMD files to specific formats. For example from PMD-5500B to ASCII files. This exporting

process may be customized to your personal specifications. Table 6.2 contains a selected number of technical specifications of the FTB-5500B PMD analyzer. The analyzer accommodates a fairly wide wavelength range and as mentioned before and as verified by both the weight and dimension, the analyzer is a field proof unit. It has the ability to measure a very wide PMD range in a short period of time, 4.5 s for a single PMD measurement.

6.3.3 Polarization controller and analyzer

A polarization controller refers to an optical device which allows the operator to change the state of polarization of the incoming light as desired. Polarization controllers have both an input and an output port. They allow the user to have control over the state of polarization of the light source. Polarization analyzers measure the state of polarization (SOP) of the light. Hence they only have one input terminal.

In this study the Adaptif Photonics A3200 polarization controller seen in figure 6.7 was used for various applications.

Figure 6.7 Adaptif photonics A3200 polarization controller and A1000 polarimeter.

This controller contains five endless rotatable waveplates: Four quarter waveplates and one half waveplate. The waveplates are made up of lithium niobate ($LiNbO_3$) crystals and the state of polarization is given by the position of the waveplates in terms of five angles measured in radians. The state of polarization of the input light is

changed by applying a voltage to the crystal to change the crystal properties, which in turn alters the SOP of the input light. One complete rotation of a quarter waveplate changes the phase difference by $\pi/2$, while one complete rotation of a half waveplate changes the phase difference by π. The Polarization Navigator software (supplied by vender) is used to control the polarization controller. The SOP of the light may be changed manually by manually setting the five angles. Another option is the scrambling operation where polarization fluctuation is created by rotating the waveplates at different speeds. The sequence mode, changes the SOP by using an uploaded ASCII text file.

During this project the A1000 polarimeters from Adaptif Photonics were used to keep track of the SOP of an input light signal. Figure 6.7 shows a photograph of a polarization analyzer or polarimeter. The instrument has one light input terminal. By using the polarization controller and the polarimeter together, the polarization dependent loss (PDL) and polarization mode dispersion (PMD) application program may be used to do PDL and PMD measurements. The polarization Navigator software controls the whole operation and requires only a few parameters to be set. In this study the A3200 and the A1000 Adaptif photonics instruments were used to make PMD measurements. A study was also conducted where the wavelength was changed and the SOP measured with the change in wavelength. The polarization Navigator software displays this change visually on a Poincaré sphere and also indicates the current state of polarization of the input light signal by showing the path traced out by the E_x and E_y components of the electric field in the xy plane. More details concerning these instruments may be found in reference [37].

CHAPTER 7

AUTOMATION OF DATA COLLECTION AND PMD CALCULATION

Interfacing of computers with instruments has become a normative operation within the scientific community. Benefits of interfacing includes faster data acquisition and handling thereof. Hence the whole research process is sped up and the possibility of a larger spectrum of data analysis within a shorter timeframe becomes more probable. Over the years many computer programs have been designed for this particular operation and application. LabVIEW is one such program. It is a graphical programming language that uses icons for data flow programming. For this study a self assembled FA setup was used with an optical spectrum analyzer (OSA) as a detector. The OSA was interfaced with a computer via a GPIB port. A program was then written using LabVIEW, to automate the data collection and PMD calculation. This chapter sets out to provide specific details entailing the program structure and its operation.

7.1 Interfacing between computer and OSA

As mentioned in the previous chapter, the Agilent 86142B series optical spectrum analyzer was used in a self assembled fixed analyzer (FA) PMD measurement setup. The Agilent 86142B OSA shown and described in chapter 6 has a GPIB (general purpose interface bus) port for remote control at the back of the instrument. A GPIB with an external USB (universal serial bus) connection was plugged into the OSA GPIB port and the National Instruments (NI) 488.2 for Windows software installed.

The Agilent 86142B OSA instrument drivers were downloaded from the net and installed. A program using LabVIEW functions and drivers appearing as LabVIEW functions may then be written to control the instrument and to perform data analysis with the data recorded during the experimental procedure. By following these

procedures a program was written to control the Agilent 86142B OSA and to perform data analysis with the data recorded by the OSA and transferred to the computer. The subsequent sections describe the program operations and present the flow of the program from instrument initialization to data analysis and PMD calculation.

7.2 Program operation

The program used to interact with the Agilent 86142B OSA was written using LabVIEW. The main operations of the program are to: send a list of commands regarding measurement specifications, collect measurement data and lastly to calculate the measured PMD using extrema counting analysis. The program allows the user to enter the desired measurement parameters such as; start wavelength, stop wavelength, number of points that make up the intensity trace, number of averaging, whether the DUT has mode coupling or not, screen parameters, etcetera. Based on the set measurement parameters the OSA carries out a wavelength sweep after which the intensity data is returned to the program. Exact details of the program structure and operations may be found in Appendix 1.

The program requires an intensity trace without the polarizer in place. This trace is used to normalize the current intensity trace as described in chapter 5. Peak detector functions which are strategically incorporated into the program determine the number of extrema (number of peaks and valley's). Once the number of extrema is known then the program performs the calculation using extrema counting analysis equations and works out the PMD. Details of the program structure and operation are found in Appendix 1.

7.3 User interface description of the extrema counting analysis PMD measurement program

The program that was written is used to carry out PMD measurements using the FA technique. Therefore before starting the program, the FA setup must first be connected. Since the intensity spectrum needs to be normalized, two measurements are done: one without the polarizer and one with the polarizer in place. Basically the program initializes the instrument, then sets the necessary parameters that were specified, starts the sweeping process and then collects the data recorded by the OSA. Thereafter, the data is operated upon to generate a normalized intensity spectrum as a function of wavelength. The program then continues to calculate the PMD measured using the extrema counting analysis method. The number of extrema is determined by a peak detector function virtual instrument (VI). The peak detector VI counts either the number of peaks or the number of valleys found in the input signal or array depending on what is requested. Two of these functions were used, one for the number of peaks and the other for the number of valleys. The sum of the two yields the number of extrema. The PMD is then calculated by making use of equation 5.23 in chapter 5. This marks the point of termination where the program enquires whether the user would like to save any data. The session then finally closes after this request is attended to.

LabVIEW programs are called virtual instruments which contain two important components; the front panel and the block diagram. The front panel refers to the user interface and the block diagram contains the graphical source code which makes up the program being written which defines the functionality of the VI. Hence when operating the extrema counting analysis program, the user interacts with the front panel. On the front panel the user is able to specify the value of certain parameters pertaining to the experiment or PMD measurement to follow. The front panel also acts as a site where the user may view the results after the PMD measurement is done. This paragraph describes the user's interaction with the program. Figure 7.1 to 7.3 shows the four user interfaces that are found in the extrema counting analysis program.

Figure 7.1. User interface of the PMD extrema counting program currently displaying the menu page.

Figure 7.1 show the menu page which is mainly used to select one of the applications that the program has to offer. The three applications which are available are; get source spectrum, PMD extrema counting (no normalization) and PMD extrema counting (normalization). Upon selection of one of the three applications, that particular application will run. The next step is to go to the window of that particular application and set the parameters as required by the experiment. Figure 7.2 offers a pictorial view of the Get Source Spectrum application. The purpose of this application is to carry out a measurement of the source intensity over wavelength. Hence with regard to the FA technique this measurement is done without the polarizer in place. State resource name is the first control that appears on the user interface. The default resource name and primary address are already filled in. The details pertaining to this control are required for the purpose of initializing a session with the instrument. Below that is the file path indicator which will indicate where the file will be saved. Right at the bottom left is where the user may specify parameters specific to the experiment. The parameters include the starting and stopping wavelength, the trace average, the number of trace points and whether a single or continues sweep is to be performed. The top left window presents the user with the ability to customise the intensity scale of the OSA according to preference. All the parameters and results will appear in a window in the lower right corner. The results include an intensity

spectrum and the measurement data as well. Any additional notes to be saved may both be written and viewed in a sub-window in this same location.

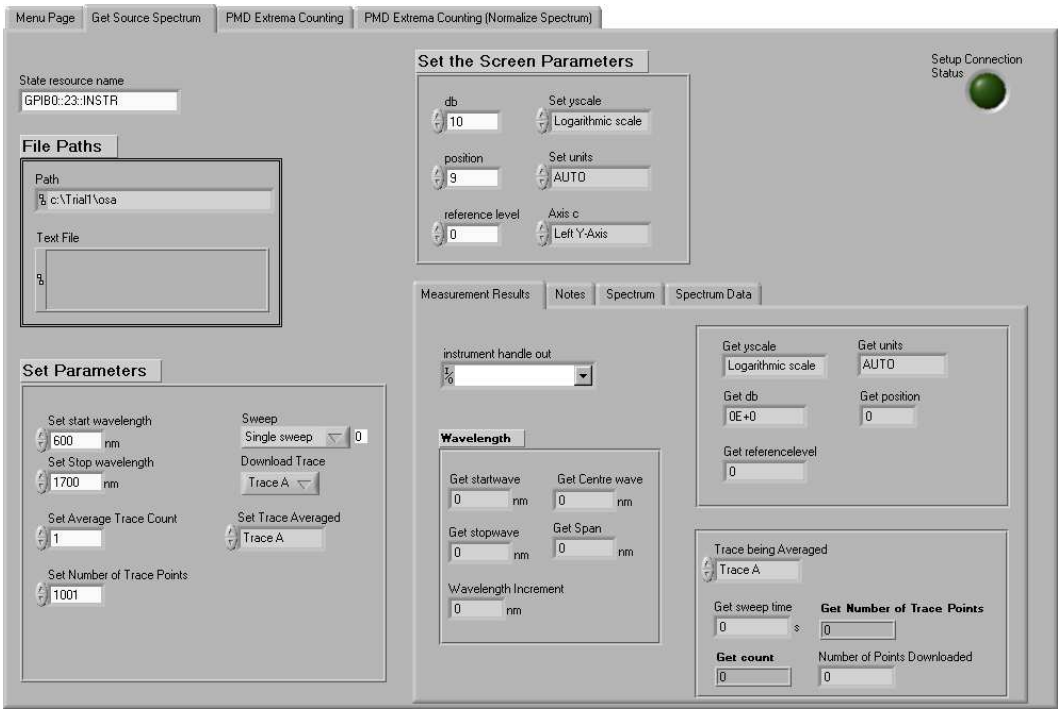

Figure 7.2. Displaying the user interface of the get source application.

After saving the data obtained from using the Get Source Spectrum application in a file, the PMD extrema counting (normalize spectrum) application may be used to carry out a PMD measurement. The PMD extrema counting (normalize spectrum) application is used when a polarizer is placed in front of the intensity spectrum. This application requires a pre-existing file consisting of an intensity spectrum from a previous measurement of the source intensity in the absence of a polarizer. Figure 7.3 shows the user interface of this particular application. In the top left corner the file path of the spectrum to be recalled may be filled out in a box segregated for this particular purpose. The user interface is pretty much the same as that of the get source spectrum application, except for a few key differences brought about by specifications required for PMD measurements. Right at the bottom left of the user interface shown in figure 7.3, two important parameters placed in a box need to be specified. Firstly it is required whether the fibre has mode coupling or no mode coupling because this information dictates which mode coupling factor to apply in the extrema counting analysis equation. Secondly, what is also of importance is the wavelength spacing to

be used by the peak detector function in order for it to find the number of peaks and valleys. The specified wavelength spacing should be no more than half of the half width of the peaks and valleys. This parameter will be explained in a later section. Having set all the necessary parameters the program may be run. All the measurement results can be found afterwards to the right on the user interface.

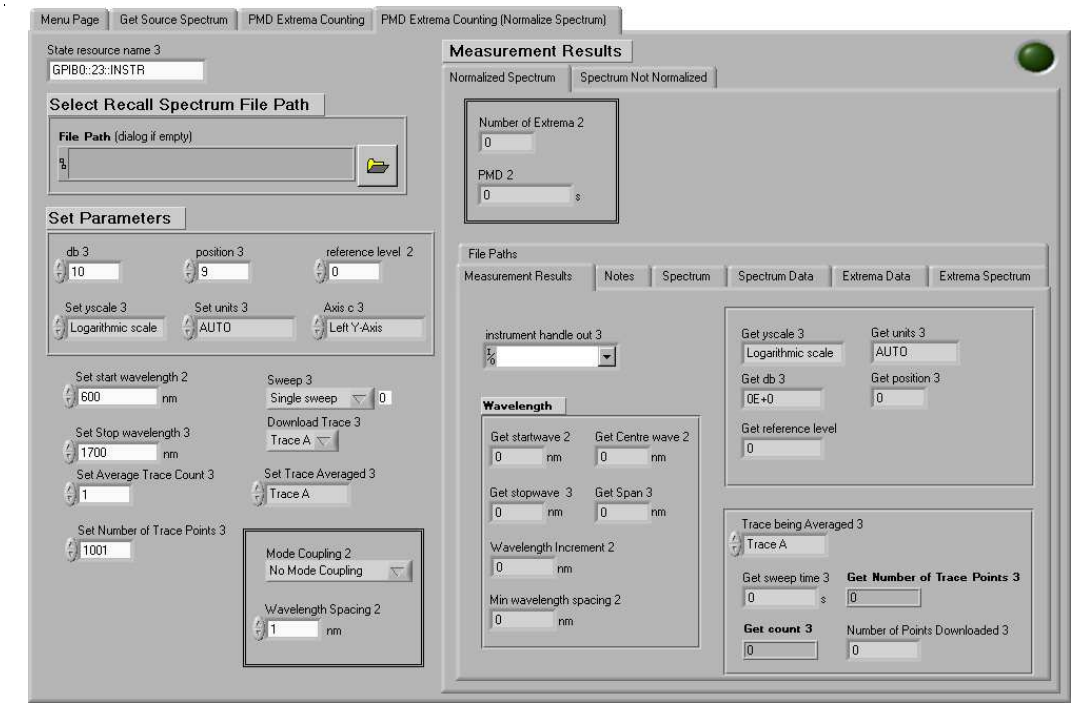

Figure 7.3 Displaying the user interface of the PMD extrema counting normalize spectrum application.

Note that both the number of extrema and the calculated PMD value will be displayed in a box at the top of the right hand side on the user interface. Other data displayed includes wavelength locations of all the extrema. The user will be prompted to save any wanted information. The information that could be saved comes in three categories of which all three may be chosen or declined. The first saved file contains all the wavelengths and their corresponding intensities for the normalized spectrum in the form of two columns or arrays. The second saved file consists of the same type of information, but for the PMD measurement where the intensity spectrum was not normalized. The third and last file houses a list of information, including user notes, in text form. Table 7.1 shows a typical example of the layout of such a file.

Table 7.1Typical illustration of PMD measurement data saved.

```
PMD   2.579159E-12
Start wavelength   1.518000E-6
Stop wavelength   1.598000E-6
Span   8.000000E-8
Number of Data Points    1001
Width used for extrema search  12.000000
Wavelength Range for Peaks     1.000000
Number of Extrema found        51
Trace Average      100


Summary
Date: 14/02/2007
EXFO M2100 1550 nm source.
Polarization Maintaining Fibre (1).
Bandwidth 3 nm.
```

The PMD Extrema Counting (No Normalization) application user interface has a similar appearance to the Normalize Spectrum application. The only difference is that in this application there is no need to recall any spectrum, hence the measurement and program operation is straight forward with no normalization done on the intensity spectrum. As described each user interface served a specific purpose with all the user interfaces sharing the common feature of user friendliness. The queries at the start of the program serve to make sure that the user has connected the setup and has provided the file path of the required spectrum in the case of the normalize spectrum application. The queries at the end of the program, allow the user to save the needed information.

CHAPTER 8

FIXED ANALYZER LAB RESULTS

Routine characterization of PMD in optical networks has become a necessity to keep track of the network quality. It follows that easy-to-apply PMD measurement techniques are required. What is also of importance is the characteristic of each PMD measurement technique. In addition to knowing what results the measurement technique yields, it is also important to establish the advantages and disadvantages of the PMD measurement technique. In this chapter the PMD measurement performance of the FA technique was investigated in a controlled laboratory environment by conducting PMD measurements on various fibre types. The chapter presents experimental results pertaining to the nature of the FA intensity spectra depending on the launch angle and also the fibre type. The FA technique is then compared with two commercially available PMD measurement techniques. A comparison of the three different FA data analysis methods is also presented. The FA technique has the added advantage of unveiling information regarding the length regime of the fibre or DUT. Hence this experimental information is also presented.

8.1 The effect of launch angle variation within polarization maintaining fibre on the FA intensity spectrum

Polarization maintaining fibre is a high birefringence fibre which has no mode coupling sites and maintains the original input state of polarization. The fibre has internal strain and asymmetry which splits the input pulse into two separate polarization modes. Depending on the input polarization of the fibre, only one polarization state will be transmitted with a change in wavelength if the input light is properly polarized and aligned with the polarization direction of the fibre. If the input polarization state is launched along the fast or slow axis of the polarization

maintaining fibre (PMF), then theoretically there will be no evolution of the input SOP with wavelength.

PMF may be made by inducing birefringence by applying stress on the core, placing it between or within glass elements of different chemical composition. Some PMFs originate from intentional asymmetry of the fibre core geometry that is, form birefringence. These techniques yield the same outcome as a difference in the refractive index between the orthogonal axes. Examples of PMF are shown in figure 8.1.

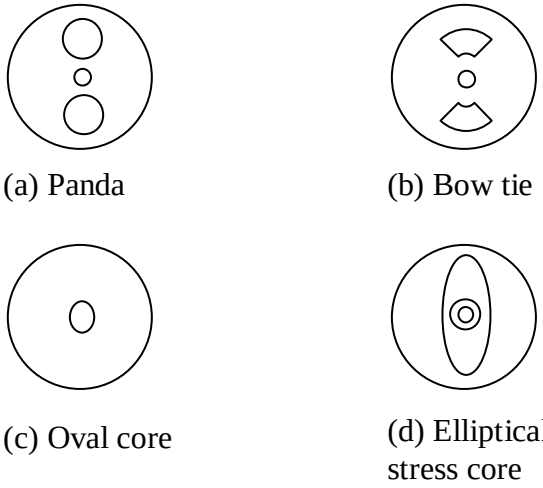

Figure 8.1 Examples of polarization maintaining fibres.

Polarization mode coupling sites are absent within PMF hence the principal states become the eigenmodes of the fibre [38]. Therefore PMF exhibits distinct fast and slow principal optical axes. It has a much larger and more uniform birefringence than the residual birefringence of ordinary single mode fibre. Light coupled into a length of PMF resolves into two orthogonal modes which propagate with different velocities throughout the fibre due to the difference in the birefringence. Consider a polarised broadband source. If the electric field intensity is equally distributed in the fibre between the two orthogonal modes then the input signal becomes depolarized, yielding a degree of polarization (DOP) of close to zero. When the electric field of the input light is completely aligned with the fast or slow axis of the PMF then the input polarization state is not altered at all and the DOP becomes unity.

During this investigation the conventional FA setup was connected using the polarized M2100 broadband light source and the optical spectrum analyzer (OSA) as a detector. The choice of fibre was PMF for its distinct and unique properties. Using a 50:50 coupler/splitter the light exiting the PMF was split between the optical spectrum analyzer and the polarization analyzer, which was used to monitor the DOP change for different input SOPs. Figure 8.2 shows the complete experimental setup including the computer interface with the OSA. This experimental setup was first used to establish the

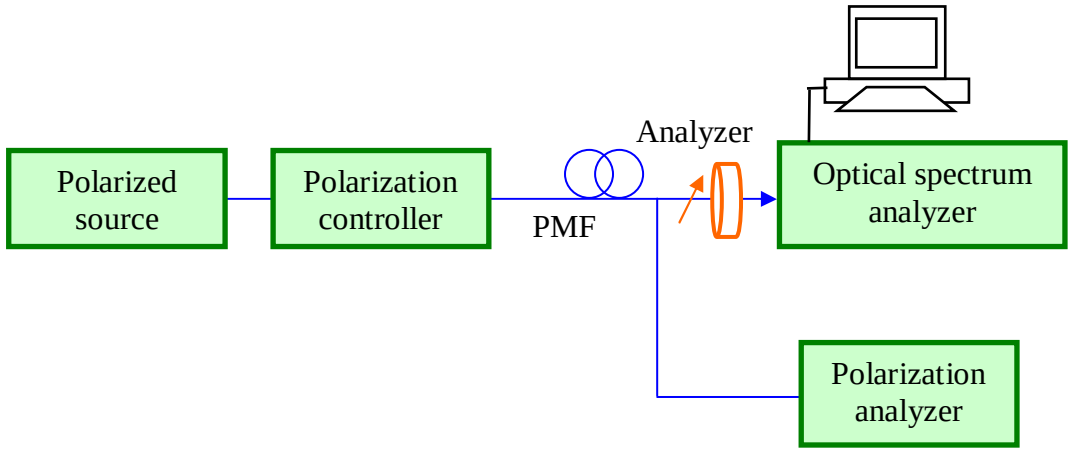

Figure 8.2 Conventional FA setup, including a polarization analyzer to keep track of the DOP.

location of the PSPs of the fibre on the Poincaré sphere. The polarization controller was then used to control the input SOP; three different SOP were sent through the PMF and the output intensity traces recorded.

Depending on the SOP launched into the PMF the optical energy will either propagate only in the slow mode, only in the fast mode or a fraction will be in the slow mode and the remaining fraction in the fast mode. A maximum DOP of 1 implies that all the light energy has been coupled into either the slow or the fast axis. Figure 8.3 shows the Poincaré sphere where the polarization controller randomly scrambled the SOP to generate as many different input SOPs as possible. All these SOPs were passed through the PMF and the output SOP measured with a polarization analyzer. The points at the end of the orange bundle touch the Poincaré sphere which implies that they have a DOP of 1. Therefore they represent the fast and slow axis and therefore the PSPs of the PMF. These PSPs are orthogonal in Jones space, and manifest as an

angle separation of 180^{o} on the Poincaré sphere in Stokes space. It is not possible to indicate specifically which end represents the fast axis and which end represents the slow axis from this diagram alone. The orange bundle cuts through the centre of the Poincaré sphere where the points towards the central region have a DOP of approximately zero. Minimum DOP implies that the light energy is equally distributed between the two orthogonal eigenmodes.

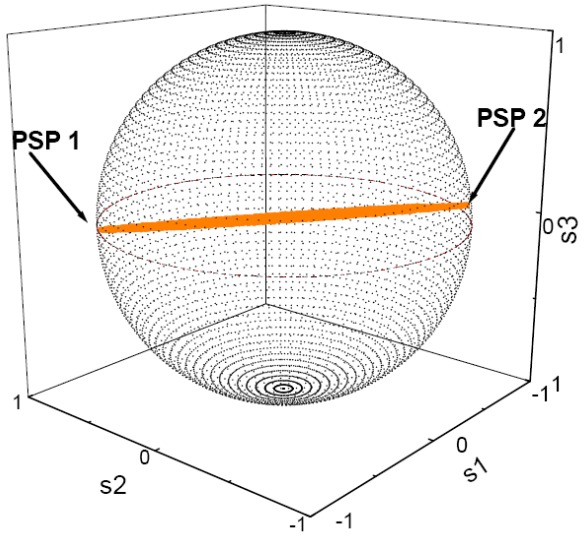

Figure 8.3 Location of the PSPs on the Poincaré sphere of a 2 m long PMF section.

This scrambling method illustrates that the two PSP are orthogonal and that the light has a DOP of unity when launched into one of the PSP and a minimum DOP when launched with equal intensity into the two PSP simultaneously.

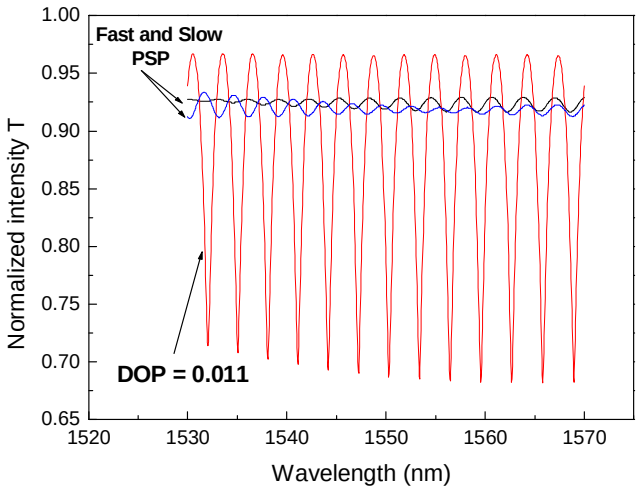

Figure 8.4 Intensity spectra of 2 m PMF for launch angles with maximum and minimum DOP.

The intensity distribution was then measured with an OSA as shown in figure 8.2. Wave plates inside polarization controller were individually adjusted and a polarization analyzer monitored the DOP and SOP. Using the setup indicated in figure 8.2 the wave plates were set such that the DOP was minimum and maximum touching points PSP1 and PSP2, as indicated in figure 8.4 where the two SOPs on the Poincaré sphere were orthogonal, and the intensity trace measured for each setting using the OSA. Figure 8.4 shows the intensity spectrum for a minimum DOP of 0.01 and also for a maximum DOP of 1.00. When both PSP were equally illuminated the DOP was 0.01 and showed the biggest variation in intensity, where the overall intensity variation is 0.285 as is observed in figure 8.4. Comparing the intensity variation, the normalized intensity along the fast and slow axis are 0.013 and 0.023 respectively, which shows a significant percentage difference of 92 % and 95 % with respect to 0.285 (DOP = 0). From figure 8.4 it is safe to conclude that SOPs launched into only the fast or slow axis yields minimum fluctuation nearing the expected theoretical straight line. The minimal fluctuation is explained by the fact that the SOP is independent of wavelength but remains in the fast or slow axis thus retaining the original input SOP. Hence there is no change in the intensity of the light as a result of a change in the wavelength. However experimentally it is evident that some fluctuation although small is present. This may be due to the uncertainty that all the light energy is launched into the fast or slow axis initially or by the fact that when the light exits the PMF then it passes through very short single mode fibre which may have a minute birefringence and mode coupling effects.

8.2 Effects of birefringence and mode coupling on the intensity spectrum

Using the conventional FA setup the effects that birefringence and mode coupling have on the intensity spectrum were then investigated. PMF has no mode coupling sites and has been shown to have a periodic intensity spectral signature. Viewed on the Poincaré sphere the output SOP rotates in a circular fashion about the PSP, hence the light intensity through the polarizer decreases and increases in a periodic fashion

as well. This periodic signature is characteristic of fibres with no mode coupling hence birefringence remains the only contributor to PMD. From the extrema analysis equation [13] it is evident that the extrema density increases linearly with PMD, therefore the more the number of extrema in the intensity spectrum the higher the measured PMD value. This is illustrated in figure 8.5, which shows the intensity spectra of two PMF sections plotted over the same wavelength range. The one fibre section is 2 metres long, figure 8.5 (a), and the other 20 metres long, figure 8.5 (b).

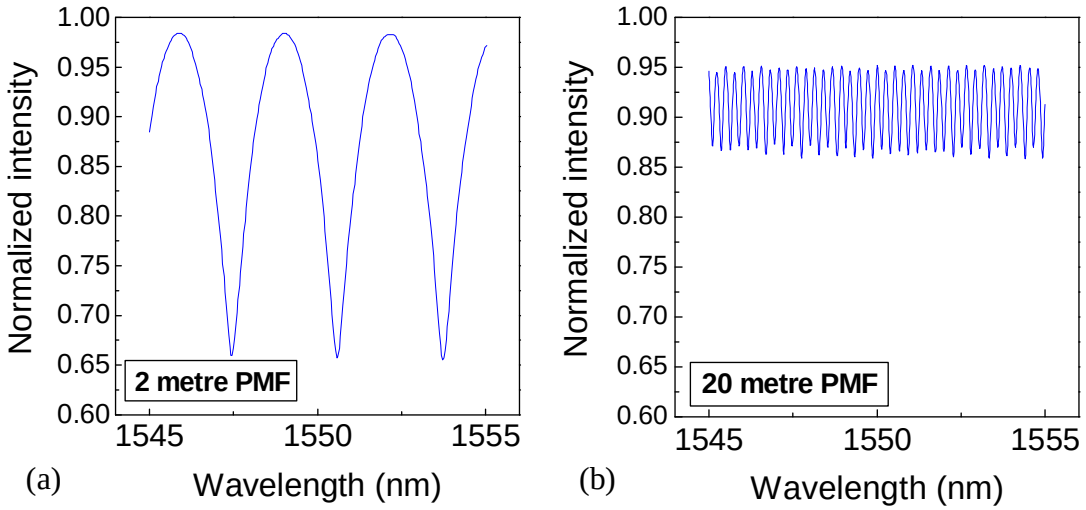

Figure 8.5 Intensity spectra of; (a) 2 m PMF and (b) 20 m PMF.

The high PMD value for the longer PMF sections is supported by the intensity signature of the 20 m PMF section which has a lot more extrema within the same wavelength window than the 2 m long PMF section. A longer PMF section allows the eigenmodes to propagate longer through the fast and slow axes, increasing the total time delay between the two modes. Since the increase in fibre length resulted in more extrema and hence an increase in the PMD value, it is concluded that increased exposure of the light signal to the birefringence alone generates a signature yielding an increase in the PMD value.

The effect of mode coupling on the transmission spectrum differs from that of birefringence. The following experiment shows that mode coupling influences the periodic nature of the intensity spectrum. PMD measurements were carried out on several fibre types using the FA PMD measurement technique. The conventional FA

setup was used with the EXFO M2100 polarized broadband source and the Agilent 86142B OSA as a detector. Intensity spectra of the various fibre types are shown in figure 8.6. The fibre shipping spool of 24.7 km figure 8.6 (a), the emulator figure 8.6 (c) and the fibre cable of 6 km (d) all have non-periodic spectra.

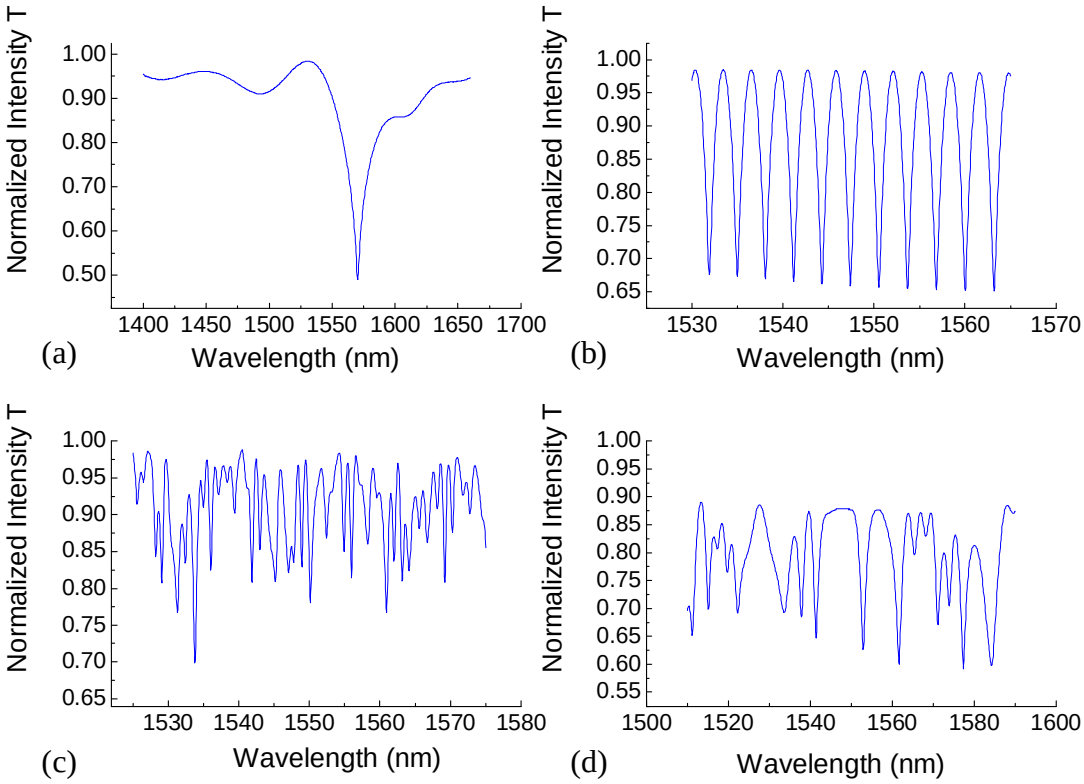

Figure 8.6 Intensity spectra of; (a) fibre shipping spool, (b) 2 m PMF, (c) emulator and (d) fibre cable.

Non-periodicity of each of these spectra may be attributed to mode coupling. The mode coupling present in the fibre shipping spool may be attributed to the fact that the fibre is tightly wound round the spool. Hence, pressure points on the fibre acting as mode coupling sites are created as the fibre crosses over itself. The emulator measured is made up of a concatenation of four PMF sections joined together by single mode fibre sections. Each site where two fibre pieces are joined together acts as a definite mode coupling site. Mode coupling sites of the fibre cable are most likely as a result of handling of the fibre (manufacturing process) and may also be as a result of wounding the cable up onto a big drum. Figure 8.6 (b) shows the intensity spectrum of one more fibre type, PMF. Absence of mode coupling within PMF gives a resultant periodic intensity spectrum. Hence it can be noted that the presence of mode coupling has a definite effect on the intensity spectrum of the DUT.

8.3 PMD measurement performance comparison: FA technique vs time and frequency based commercially available measurement techniques

The FA PMD measurement technique is a frequency domain measurement technique. It determines the average PMD of a DUT by measuring the transmission spectrum through a polarizer as a function of wavelength [13]. The technique has three analysis methods namely extrema counting, mean level crossing counting analysis [13] and the Fourier analysis method [15]. The two well established PMD measurement techniques used for comparison purposes are the Jones matrix eigenanalysis (JME) and the generalized interferometric (GINTY) PMD measurement techniques.

PMD measurements were performed on the same fibre types as in section 8.2 for the following techniques: The FA technique (FA), the generalized interferometric technique (GINTY) and the Jones matrix eigenanalysis technique (JME). Ten consecutive measurements were taken for each fibre type. The results are indicated in figure 8.7. The fibre types are abbreviated as fibre shipping spool (FSS), 2 m polarization maintaining fibre (PMF 2m), the emulator (EMU) and the fibre cable retains its name.

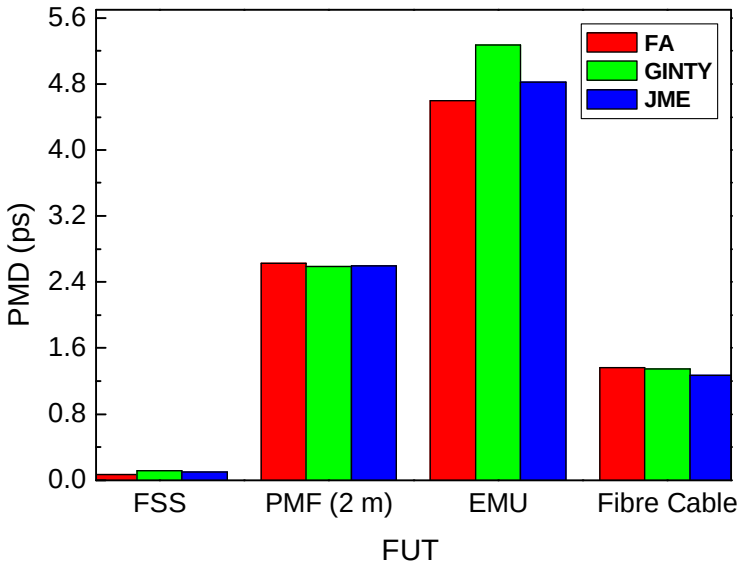

Figure 8.7 PMD comparison between FA (extrema analysis), GINTY and JME.

Extrema counting analysis was chosen to analyze the FA technique data. From figure 8.7 it is evident that the FA technique compared well with both the frequency and time domain techniques. The FA technique, represented by the red bar, gave similar PMD as that given by both JME and GINTY for all the fibre types.

Table 8.1 Summary of measured PMD values using FA, GINTY and the JME measurement techniques.

		FA	GINTY	JME
FSS	$<\Delta\tau>$ (ps)	0.07	0.115	0.097
	ε	0.01	0.004	0.007
	σ (%)	33.8	6.030	14.400
PMF (2 m)	$<\Delta\tau>$ (ps)	2.62	2.589	2.599
	ε	<0.01	0.002	0.001
	σ (%)	<0.76	0.154	0.039
PMF (20 m)	$<\Delta\tau>$ (ps)	30.13	30.314	30.136
	ε	0.20	0.009	0.009
	σ (%)	1.33	0.056	0.060
Emulator 1	$<\Delta\tau>$ (ps)	4.60	5.277	4.822
	ε	<0.01	0.099	0.005
	σ (%)	<0.43	3.751	0.207
Emulator 2	$<\Delta\tau>$ (ps)	4.80	5.947	6.175
	ε	<0.01	0.012	0.002
	σ (%)	<0.42	0.404	0.049
Fibre cable	$<\Delta\tau>$ (ps)	1.37	1.348	1.266
	ε	0.06	0.010	0.026
	σ (%)	9.07	1.480	4.030

Table 8.1 shows the average of ten PMD measurement results for each technique from which the half range (ε) defined as half the difference between the maximum and minimum, and the percentage error (σ) was calculated. The maximum PMD measured using FA method was 30.13 ps for the 20 m long PMF and the minimum 0.07 ps for the FSS. It should be noted that in some cases the FA technique did not measure any error (where the smallest decimal number was used to indicate error), however the JME and GINTY techniques were still able to detect the measured PMD change. A possible explanation is related to the extrema change that would occur in the event of a PMD change. The extrema counting analysis method can only detect a change in the PMD value for PMD changes greater than the difference between extrema n+1 and n,

used to calculate the measured PMD value. This explains why the half range (ε) of PMF (2 m), emulator 1 and emulator 2 are <0.01 ps for the FA technique, indicating the techniques inability to detect very small PMD changes.

Both the extrema counting and mean level crossing counting analysis methods depend on counting particular features present within the intensity spectrum. Hence both analysis methods operate within the frequency domain. The question which then arises is how would these two analysis methods compare with one another? FA generated intensity traces were collected using the conventional FA technique setup. Both the extrema counting and the mean level crossing analysis methods were used to analyze individual intensity traces. Figure 8.8 shows the results pertaining to this investigation.

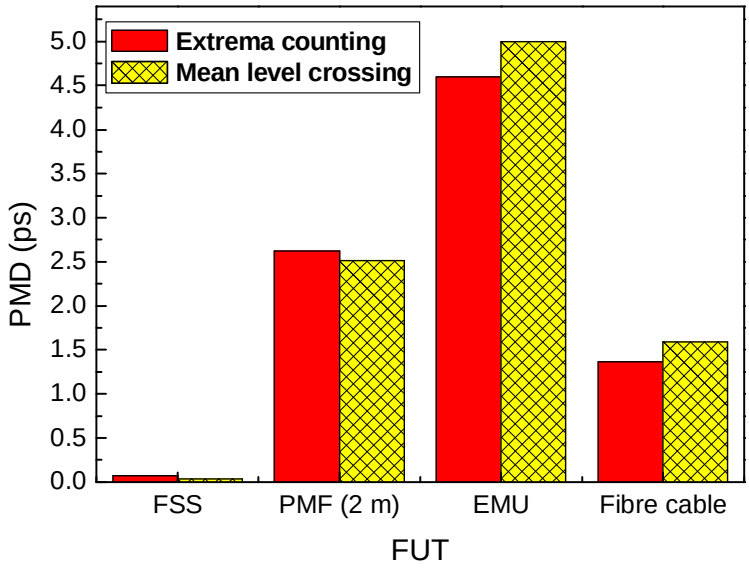

Figure 8.8 Comparison of extrema counting analysis and mean level crossing analysis.

From figure 8.8 it is evident that the extrema counting and mean level crossing analysis methods show little difference in the determined PMD value. This negligible difference in the calculated PMD value for various fibre types of various PMD values suggests that the mean level crossing analysis may also be used as a trusted technique to determine the DUT PMD.

8.4 Fourier analysis of the intensity spectra

FA generated intensity spectra may also be analyzed using Fourier analysis to extract the measured PMD value as explained in chapter 5. Fourier transformation of the normalized intensity spectra yields a resultant interferogram which gives information regarding the PMD value [15]. Intensity spectra of the already mentioned fibre types in chapter 8 were analyzed using Fourier analysis and the PMD results compared with those determined using the JME and GINTY.

Figure 8.9 (a) shows the intensity spectrum of PMF and (b) the resultant interferogram after a fast Fourier transform was applied to the intensity spectrum.

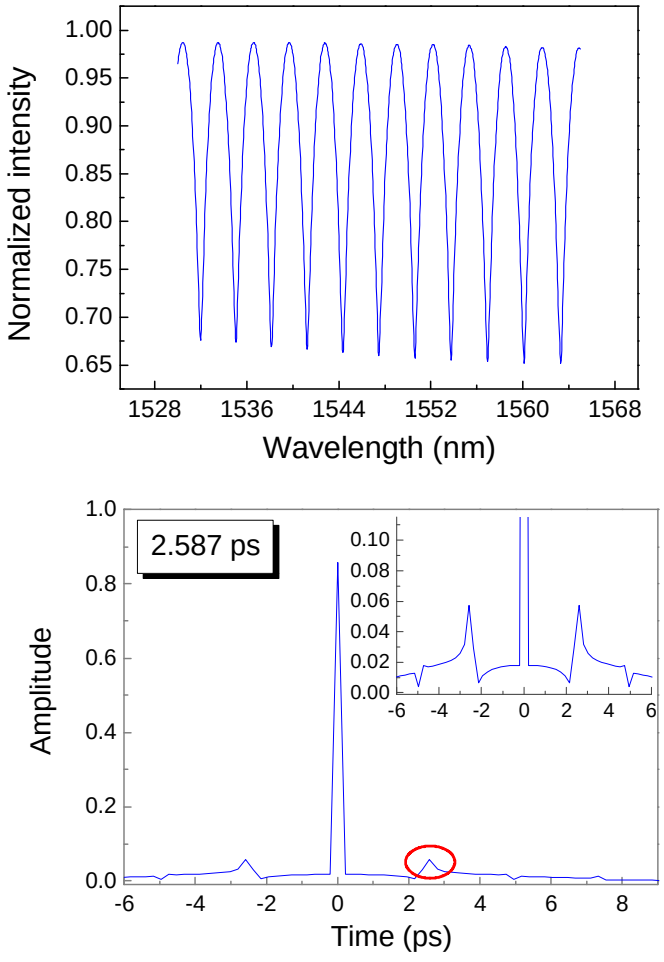

Figure 8.9 (a) Intensity spectrum of 2 m PMF and (b) Fourier transform of the intensity spectrum.

PMF has a periodic intensity spectrum and the resultant interferogram after the Fourier transform gives three spikes where the two satellite spikes give the information regarding the PMD. The position of the satellite peak to the right determines the PMD value of the measured component or fibre [7]. Depending on the periodic nature of the spectrum, the Fourier transform relates the frequency of the wave patterns in the spectrum to the DGD values. If the intensity trace is periodic having only one frequency a single peak representing the PMD appears. In figure 8.9 (b) the satellite peak is positioned at 2.587 ps, hence the PMF is established to have a measured PMD value of 2.587 ps. Figure 8.10 shows both the intensity spectrum and the interferogram of a 20 m long PMF section. From the interferogram it is noted that the PMF section has a PMD of 30.275 ps.

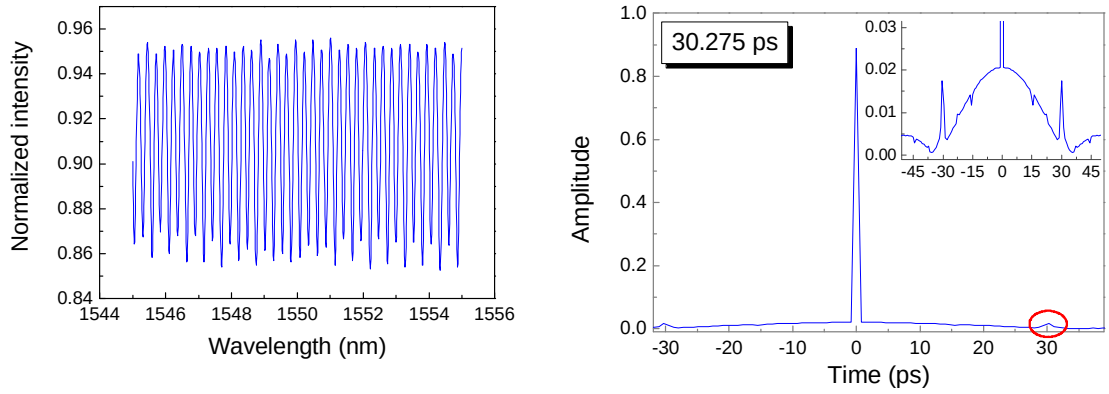

Figure 8.10 (a) Intensity spectrum 20 m PMF and (b) Fourier transform of intensity spectrum of 20 m PMF.

Interferograms of fibres with appreciable mode coupling have a lot more peaks producing a fringe envelope which is Gaussian in shape [15]. The half width of the Gaussian gives the measured PMD value [15]. Fourier analysis was performed on the intensity spectra of two emulators and a fibre cable. The emulators consisted of a concatenation of PMF sections joined with single mode fibre sections. Figure 8.11 shows both the intensity spectra and the resultant interferograms together with the Gaussian fit for the three mentioned FUT.

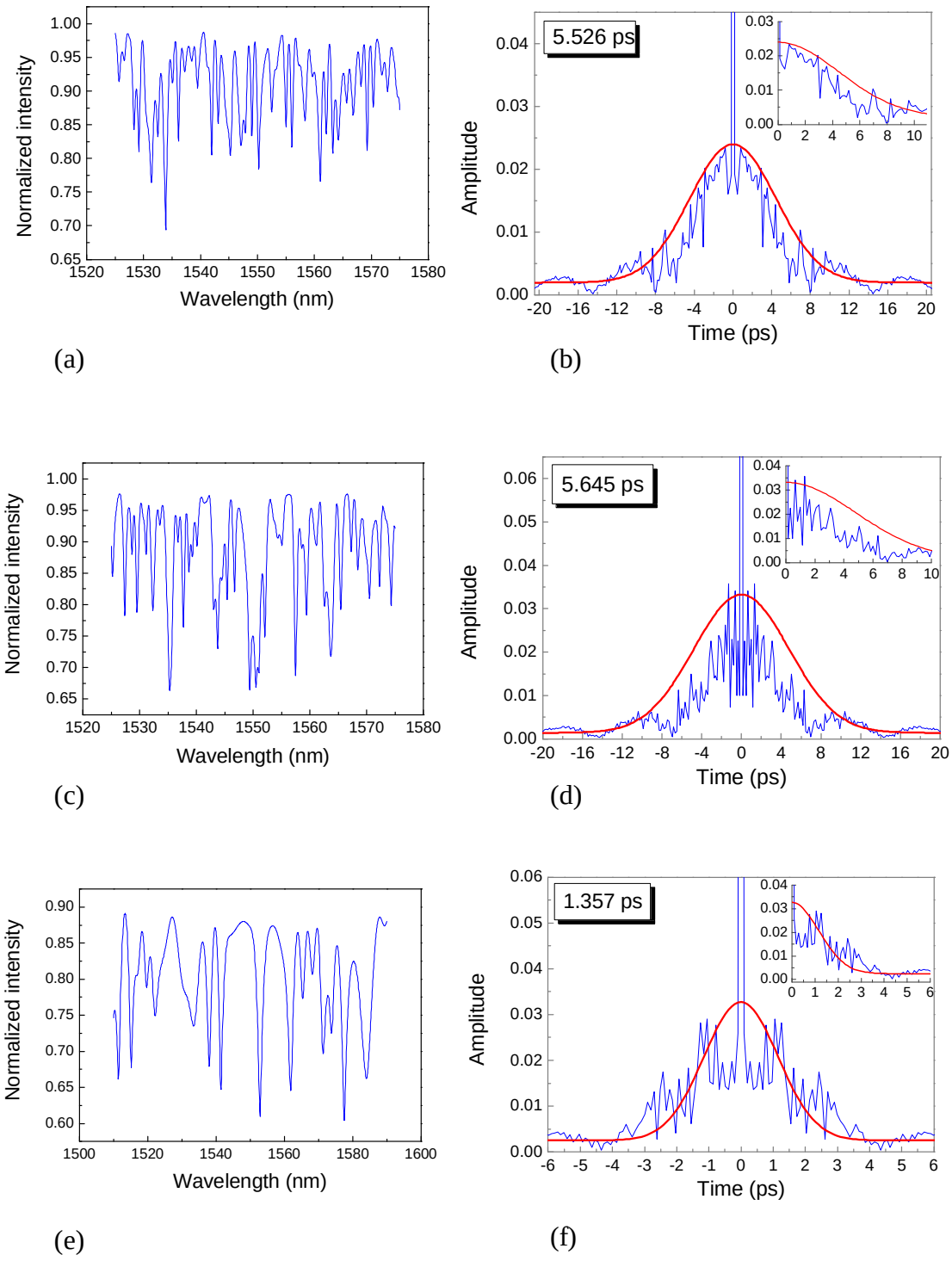

Figure 8.11 Intensity spectra and corresponding Fourier transform envelope of: (a) and (b) emulator 1, (c) and (d) emulator 2, (e) and (f) fibre cable.

The interferograms shown in figure 8.11 (b) and (d) are for the intensity traces of the two emulators. It is immediately evident that the interference envelope of both the emulators is Gaussian in shape. The second emulator had a lot more PMF sections coupled with the single mode fibre sections, hence more coupling sites which is

apparent in the well defined fringes in the interference envelope. The fibre cable has a less broad interference envelope shown in figure 8.11 (f) hence giving a PMD of 1.357 ps. A comparison of the FA technique using the Fourier analysis method shows good agreement with the interferometric technique. It can be seen in figure 8.12 that the FA Fourier analysis determined PMD value is very similar to the generalized interferometric determined PMD value. Gisin stated in a paper, [15], that the interference envelope from an interferometer is similar to the Fourier transform of the light intensity. As mentioned in this paper, the fringe envelope produced by Fourier transformation does give an accurate PMD value which shows great similarity to that produced by the interferometers.

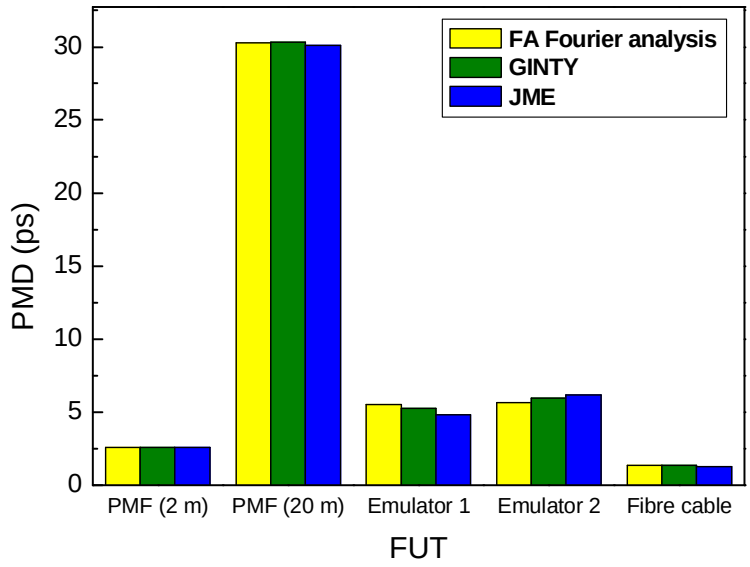

Figure 8.12 Comparison of the FA technique using Fourier analysis with the GINTY and JME techniques.

8.5 Length regime investigation for various fibre types

Birefringence induces a time delay between the orthogonal eigenmodes and mode coupling further complicates the effect of PMD. As a result of mode coupling and refractive index (RI) changes due to stress and temperature; PMD becomes a stochastic phenomenon, randomly changing due to external effects like temperature, pressure and vibrations. PMD no longer scales linearly with length but as the square root of length for appreciable mode coupling. Therefore it is important to know how a particular fibre scales with length. The FA technique has the added advantage of

giving a numerical value for the length regime of the fibre, hence giving an indication of the number of mode coupling sites present within the fibre. This very simple length regime determination technique was used to carry out an investigation regarding the length regime of the different fibre types.

When a fibre is in the long length regime, PMD scales as the square root of length and has a Maxwellian probability density function [13]. This gives an indication that the fibre has appreciable mode coupling sites. The ratio of the fibre length and the coupling length then tends to infinity. As shown in chapter 5, the ratio of the number of extrema and mean level crossing (N_e/N_m) gives a value of 1.54 for appreciable mode coupling. When the fibre is in the short length regime then PMD varies linearly with length and is deterministic [13]. To indicate the short length regime the ratio of the fibre length and the coupling length is equal to zero. For negligible mode coupling the FA technique gives the ratio N_e/N_m as unity.

FA intensity traces were obtained for each fibre type. The number of extrema and number of mean level crossings were then counted and the ratio of the two determined. From this ratio it is possible to classify whether the fibre scales in the long length regime or the short length regime. Table 8.2 shows the fibre types with both the number of extrema (N_e) and number of mean level crossings (N_m) found in the intensity trace and the N_e/ N_m ratio. The unity ratio of the PMF is immediately evident indicating that PMF has negligible mode coupling and thus it is in the short length regime. The fibre shipping spool (FSS), fibre cable and the emulator (EMU) all have ratios different to one suggesting that they must all possess appreciable mode coupling sites. Just as the intensity trace of the fibre gives an indication of the presence or absence of mode coupling, the ratio gives a numeric indication.

Table 8.2 Summary of ratio regarding the length regime for various fibre types.

DUT	**Extrema**	**Mean level crossing**	**N_e/N_m**
FSS	5	2	2.5
PMF (2 m)	23	22	1.05
Emulator	70	49	1.43
Fibre cable	32	25	1.28

Figure 8.13 gives a graphic view of the level of the ratio for the presence of mode coupling and also in the absence of mode coupling. The emulator, FSS and the fibre cable ratios all differ from the unity ratio line. It is not clear whether ratios above one and increasing imply that the mode coupling site density within a fibre is increasing as well.

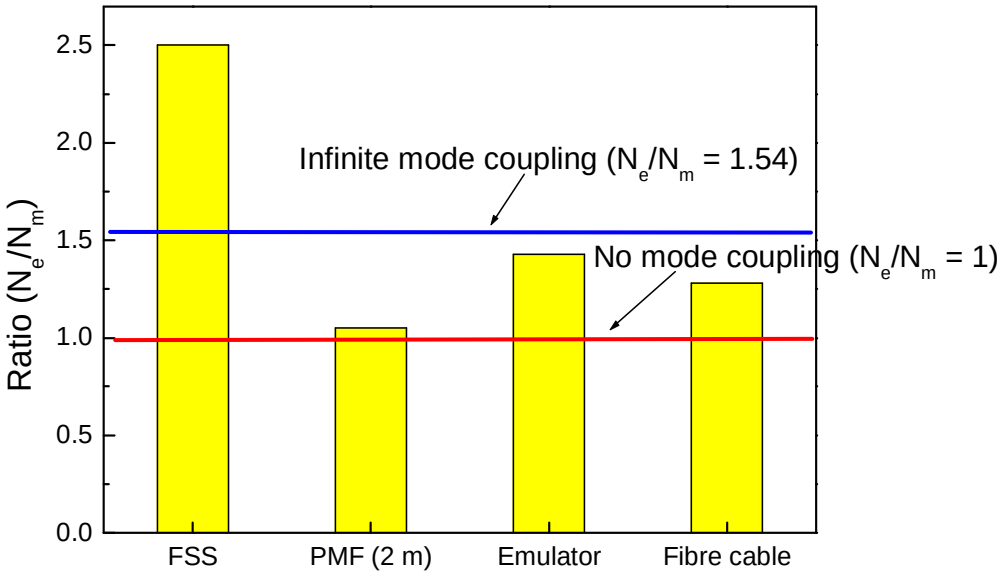

Figure 8.13 The N_e/N_m ratios for various fibre types. Also indicated are the values for which infinite mode coupling and no mode coupling.

8.5 Summary

This chapter focused mainly on the PMD measurement performance of the home built FA technique in the laboratory. Using PMF it has been demonstrated that the intensity fluctuation with wavelength does have a strong dependence on the launch angle. Thus if all the light is launched into only the fast axis of the PMF then the intensity fluctuation is minimal compared to when it is launched such that both the fast and slow axis are equally illuminated. PMD measurements were performed on six fibre types where each had a unique and distinct intensity spectrum, which depends on the

magnitude of the birefringence and the degree of mode coupling present within the fibre. Both the extrema counting and mean level crossing analysis methods showed good agreement with the familiar and trusted commercially available JME and GINTY PMD measurement techniques. Furthermore, Fourier analysis of the intensity spectra agreed well with the generalized interferometric technique in particular. The last section of this chapter focuses on the length regime of each of the investigated fibre types. It was shown that the simple ratio of the number of extrema against the number of mean level crossings can indicate whether the FUT is classed in the long length regime or in the short length regime.

CHAPTER 9

A COMPARISON OF PMD MEASUREMENT RESULTS OF BURIED DEPLOYED FIBRE, FIXED ANALYZER VS COMMERCIALLY BASED TECHNIQUES

This chapter focuses on field measurements of PMD on buried deployed fibres on the Telkom network using the FA technique and commercially available PMD measurement techniques. Due to the nature and length of the deployed Telkom fibre it gives a real representation of PMD measurement challenges with regard to PMD measurement performance of the various PMD measurement techniques. This investigation aims to determine the performance of the FA technique on real deployed fibres in optical networks. The FA technique and the JME and GINTY measurement techniques were compared. When using a specific measurement technique it is also of importance to have knowledge and understanding of the technique's characteristics. Several characteristics of the FA technique pertaining to PMD measurements were investigated using buried deployed Telkom fibre. These characteristics included wavelength window size, sampling and launch angle variation.

9.1 PMD measurement performance of the FA technique on buried deployed cables

(a) Suitability of FA techniques for deployed fibre cables

Deployed fibre cables differ in their PMD fluctuation and SOP (state of polarization) variation. Basically fibre cables are either deployed aerially on poles or they may be buried and placed under ground. Aerial cables are disturbed by external effects and are subject more to vibrations, movement and a change in temperature. This causes the output SOP to fluctuate considerably and in turn results in more variation in the measured PMD value. Buried deployed Telkom fibre is a lot more stable regarding external effects; hence the SOP and the overall measured PMD value fluctuate less. A

lot of study has been performed regarding the fluctuation of SOPs and the measured PMD value in deployed aerial and buried fibre cables for the purpose of PMD compensation and in an attempt to enable a better understanding of PMD. In order to carry out routine characterization of PMD in deployed fibre types, suitable measurement techniques need to be employed. Hence the specifications and characteristics of the PMD measurement technique need to suit the fibre deployment method under investigation.

The FA technique has the limitation of requiring that the PMD of the DUT being measured remain constant over a certain time period. Hence the fibre must be in a very stable environment regarding temperature changes and also mechanical disturbances. This reduces the chance of performing accurate PMD measurements on aerial fibre using the FA technique. The main reasons for this limitation of the FA technique are the continuous and rapid SOP and PMD fluctuation. Cameron [39] reported PMD measurements performed on both buried and aerial deployed fibre using the interferometric technique. He found that changes in PMD occur in the buried fibre every 60 to 90 minutes, and that for the aerial fibre is about 5 minutes when the temperature changes rapidly. This led to the conclusion that a strong correlation exists between the PMD fluctuation and temperature change, hence it was concluded that the major contributor to the PMD fluctuation in the aerial fibre was the change in temperature. Due to the nature of the FA technique data acquisition, SOP stability over a sufficient time period is imperative. Waddy *et al.* [40] observed SOP fluctuation in an aerial fibre over a six day period using a polarimeter. They found the fastest SOP change to be 1.824 seconds. It was also observed that the fast SOP fluctuations occur during the day time and less SOP changes occur during the night when the temperature is lower. Knowing that the average PMD does change very rapidly and more so the SOP, it can be concluded that the FA technique is not an appropriate technique to perform PMD measurements on aerial fibre. This is because the intensity manifestation as a result of SOP fluctuation would be affected by the changing SOPs resulting into erroneous PMD measurement results. Thus PMD measurements were only performed on buried deployed cables.

(b) FA technique compared with JME

Due to the fibre stability in terms of strain and temperature a buried deployed cable 28.8 km in length was used to conduct comparative PMD measurements. The cable links Sidwell and Linton Grange, in Port Elizabeth, which are 14.4 km apart and is looped to make an overall length of 28.8 km. The FA technique measurement performance was compared to the JME technique and then to the GINTY technique. For FA technique comparison with JME, the conventional FA setup using the M2100 broadband source was used to do PMD measurements over a 60 nm wavelength range from 1510 nm to 1570 nm. The JME setup involved a polarimeter and polarization controller from Adaptif, and the Agilent 8164A tuneable laser source. The same wavelength range from 1510 nm to 1570 nm was kept for the measurements using JME. Thirty sequential PMD measurements were made on three different buried deployed Telkom fibre links using both techniques. Figure 9.1 shows the intensity spectrum of each buried fibre link.

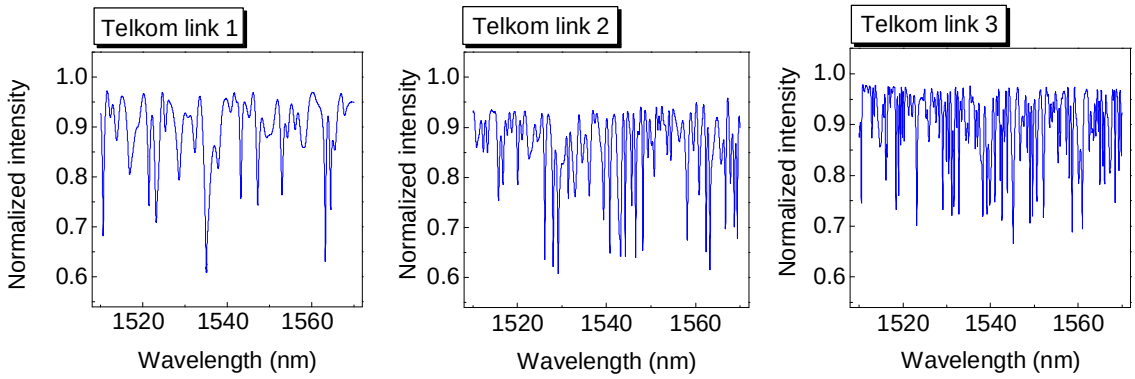

Figure 9.1 Normalized intensity spectra for 3 different buried deployed Telkom fibre links.

Both the extrema and mean level crossing density increase from link 1 to link 3, hence the calculated PMD value will also increase according to this link sequence. The non-periodic signature evident in the intensity trace of all three links proves that a significant amount of mode coupling sites are present within the fibre links. The measurement period for 30 PMD measurements was approximately just less than 30 minutes. As the fibre type was buried fibre the expected PMD and SOP change is negligible over 30 minutes. Colour maps of the intensity trace prove that the intensity fluctuation during the 30 minute PMD measurement period is very slight if any for each individual wavelength. Each intensity spectrum comprises of 5000 points. A set

of 200 points representing specific wavelengths were selected from each of the 30 traces and the normalized intensity plotted in a colour map. Figure 9.2 shows two such maps, one for link 1 and another for link 3 which has a much higher PMD value. The colour map for link 2 it not shown here but it has the same trend as link 1 and 3. Both figure 9.2 (a) and (b) show that the normalized intensity stays fairly constant for all wavelengths over the period of time during which the PMD measurements were conducted. This is represented by the unchanging colour lines formed from the left to the right of the measurement number. Hence the normalized intensity remains constant to a high degree over the 30 minutes measurement time for both the low and high PMD links.

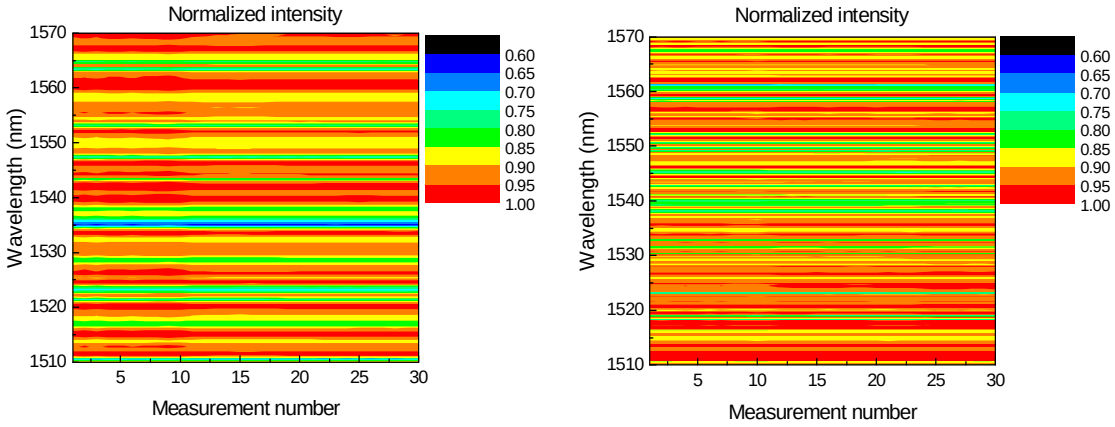

(a) Link 1 (b) Link 3

Figure 9.2 Contour colour map of (a) Link 1 [PMD = 3.218 ps], (b) Link 3 [PMD = 9.679 ps] consisting of the normalized intensity of 200 wavelengths for 30 measurements.

Using extrema counting analysis and mean level crossing analysis the FA technique raw data was analyzed and compared to the PMD measurement results from the JME technique. Figure 9.3 shows the PMD measurement comparison of the FA and JME techniques, where the FA technique is represented by the red bars and the JME by the blue and green bars.

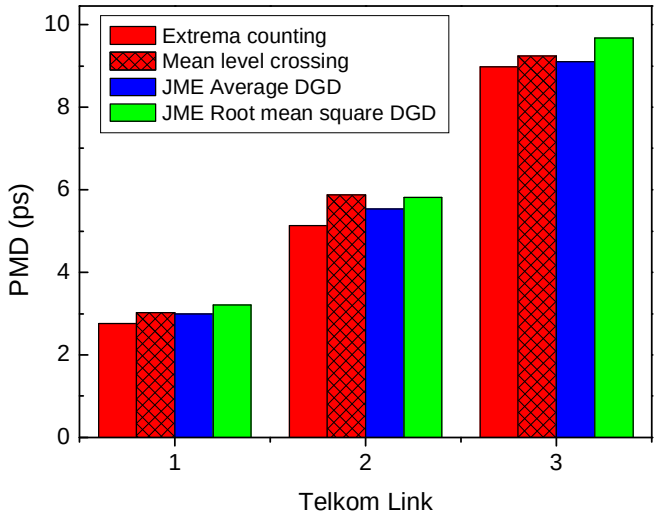

Figure 9.3 PMD measurement results of Telkom buried deployed fibre links for FA and JME techniques.

Both the extrema counting and mean level crossing analysis methods compare very well with both the RMS and average DGD values found using the JME technique. According to the FA extrema counting analysis the three links gives PMD values of: 2.76 ps, 5.13 ps and 8.98 ps. Table 9.1 gives a summary of the PMD measurement results including the error determined from the 30 measurements performed. The abbreviations used in the table are: Ext for extrema, MLC for mean level crossing, Std for standard, AVG DGD for average DGD and RMS DGD for root mean square DGD.

The high (0.16 ps half range error) and low (< 0.01 half range error for the MLC FA method) error values found for the FA technique compared to the JME technique again suggest that the FA technique either slightly over estimates or slightly underestimates the change in the PMD value. The JME technique is fairly consistent, indicating from the low errors that the PMD changes only slightly in the buried deployed fibre link. These measurement results are in agreement with theoretical predictions performed by Heffner *et al.* [24] where a fibre was modelled using 2000 birefringent fibre sections of randomly chosen DGD and angles. The FA technique using extrema counting was found to compare well with the JME technique.

Table 9.1 Summary of results for the FA (Extrema - Ext, mean level crossing – MLC) vs JME methods (AVG DGD AND RMS DGD refers to average DGD and root mean square DGD respectively).

	Link 1			
	FA		**JME**	
	Ext	**MLC**	**AVG DGD**	**RMS DGD**
Mean PMD (ps)	2.76	3.02	2.986	3.218
Half range (ps)	0.11	< 0.01	0.042	0.005
Std deviation	0.08	< 0.01	0.015	0.002
Ratio (N_e/N_m)	1.42 ± 0.04			
	Link 2			
	FA		**JME**	
	Ext	**MLC**	**AVG DGD**	**RMS DGD**
Mean PMD (ps)	5.13	5.87	5.527	5.812
Half range (ps)	0.05	< 0.01	0.004	0.003
Std deviation	0.02	< 0.01	0.003	0.002
Ratio (N_e/N_m)	1.36 ± 0.01			
	Link 3			
	FA		**JME**	
	Ext	**MLC**	**AVG DGD**	**RMS DGD**
Mean PMD (ps)	8.98	9.24	9.106	9.679
Half range (ps)	0.16	0.08	0.022	0.028
Std deviation	0.08	0.08	0.014	0.021
Ratio (N_e/N_m)	1.51 ± 0.03			

In an attempt to answer whether the results will agree if two measurement techniques were used to measure PMD, P. A. Williams summarized the theoretical and experimental results of four PMD measurement techniques [25]. It is mentioned that the average DGD from JME and the extrema analysis give the same PMD value theoretically. This was confirmed in the same article, [25], from a large data pool indicating that the average DGD from JME and the FA technique with extrema analysis do give similar measured PMD values. From figure 9.3 it is indeed evident that there is a definite similarity between the FA extrema counting analysis PMD value (red bar) and the JME average DGD (blue bar).

Determination of the length regime entails a very simple procedure regarding the ratio of the number of extrema and the number of mean level crossings as discussed previously, chapter 5 section 5.1. It is well known that in the long length regime PMD scales as the square root of length and has a Maxwellian probability density function (pdf). Poole and Favin [13] showed that the ratio of the extrema and mean level crossings are more than 50 % greater in the long length regime than in the short length regime provided that the statistical uncertainty of the measurement procedure is less than 50 % [13]. Table 9.1 shows the extrema, mean level crossing ratio of the links to

be 42 %, 36 % and 51 % greater than that of negligible mode coupling for the buried deployed fibre links 1, 2 and 3, giving an indication that all three links have a considerable amount of mode coupling sites present within the fibre link. PMD increases from link 1 to link 3 however this does not match the pattern for the ratio where link 2 has the second highest PMD but the lowest ratio. The low ratio suggests that link 2 has the least amount of mode coupling sites present within the link.

Results from this study show that the intensity spectra remain unchanging and constant for individual wavelengths throughout the measurement time of approximately 30 minutes for the buried deployed fibre links. This suggests that the PMD should also remain fairly unchanging. Slight changes in the PMD indicated by the JME technique are evident though. These changes may occur as a result of temperature changes or vibrations. The results pertaining to the comparison of the FA technique with the JME technique regarding PMD measurement performance show that the FA technique does give similar results to that of the JME technique. In particular a very good agreement was found between the FA extrema counting analysis PMD measurement value and the average DGD found from JME. Finally length regime analysis gives an indication that all three fibre links do fall under fibres scaling in the long length regime hence housing considerable mode coupling.

(c) FA technique compared with GINTY

Both the FA technique and the generalized interferometric (GINTY) PMD measurement technique use broadband sources. Hence comparative PMD measurement performance measurements between the FA and GINTY techniques could be done using the same optical source. This gives the advantage of exposing both techniques to the same optical characteristics at the same time and also resulting in PMD measurements being carried out at the same time. The Fourier analysis method is recorded in literature where its theoretical and experimental similarity with the interferometric technique is mentioned [15, 19, 25, 26, 28, 41]. PMD measurements were carried out on three buried deployed Telkom fibre links using the FA and the GINTY PMD measurement techniques. All three analysis methods (Extrema counting, mean level crossing and Fourier analysis) were applied to the FA data and compared with the GINTY PMD measurement results.

The conventional FA technique setup was applied where the EXFO FLS 5800 CD/PMD analyzer broadband source was used. PMD measurements of the link were carried out at the same time. In order to feed the optical source exiting the FUT to the OSA and the GINTY instrument simultaneously, a 50/50 beam splitter was placed right after the FUT. The schematic of this setup is shown in figure 9.4.

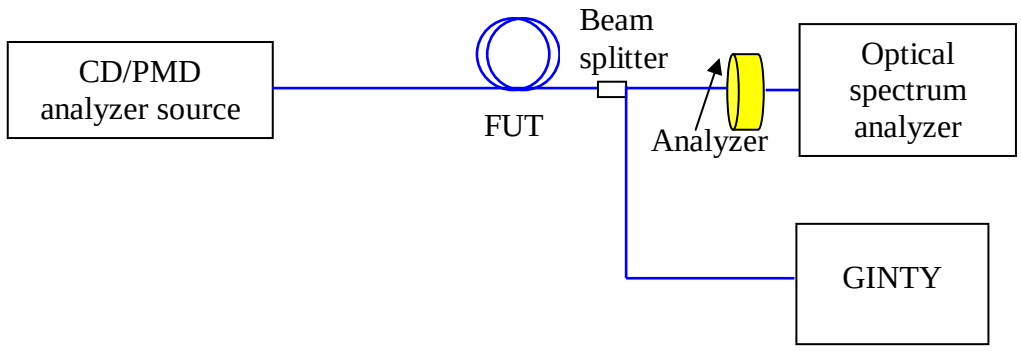

Figure 9.4 Conventional FA technique setup with the addition of the GINTY technique for comparative PMD measurements

This arrangement was used to conduct 30 consecutive PMD measurements for each of the three fibre links. Both the FA and GINTY technique were set to perform repeated measurements. The OSA measured the intensity of wavelengths within the range 1513 nm to 1652 nm. Signatures of the intensity spectra are presented in figure 9.5 together with the Fourier interference envelope and the Gaussian fit.

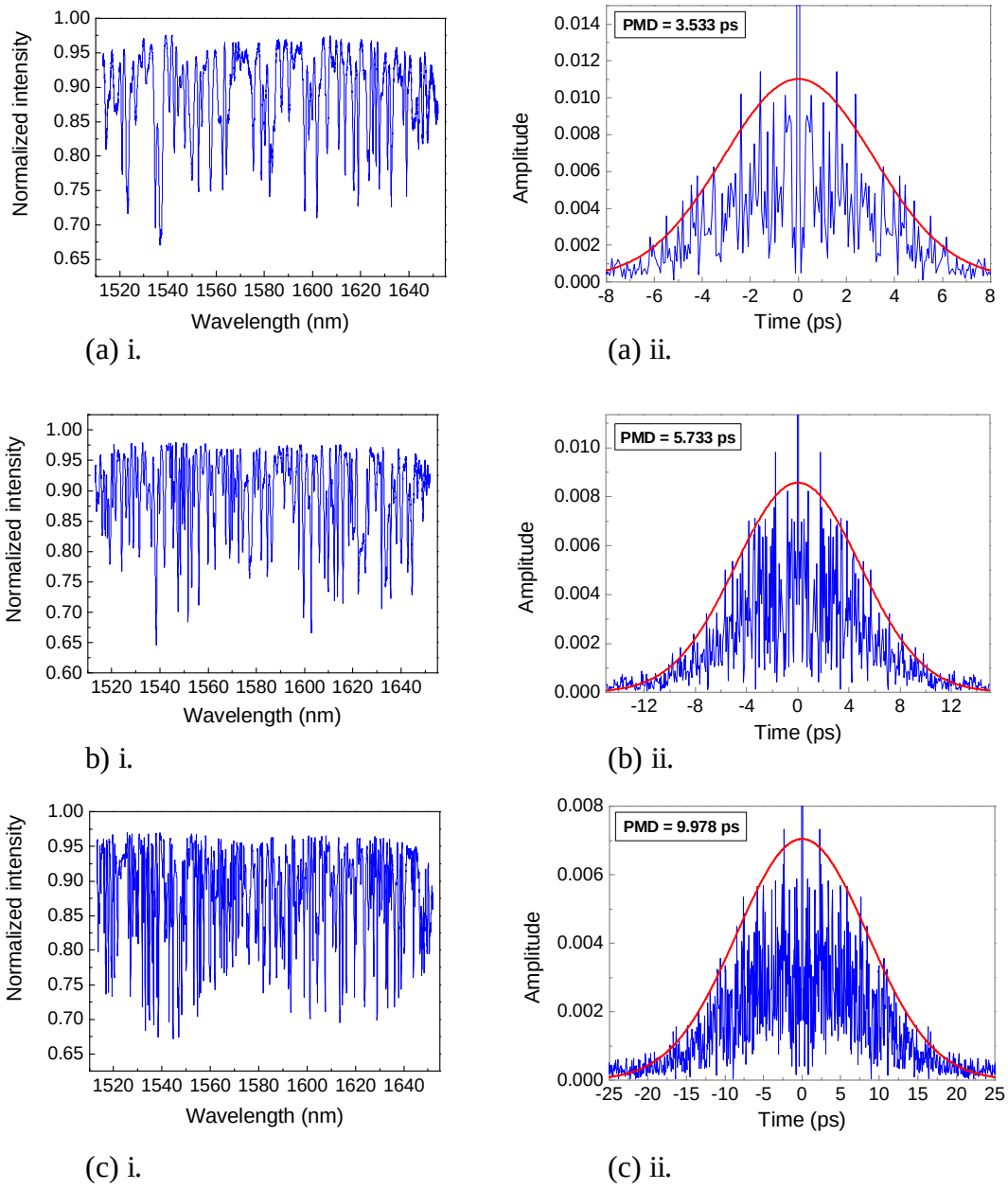

Figure 9.5 Intensity spectra and corresponding Fourier transform envelope with Gaussian fit: (a) link 1, (b) link 2 and (c) link 3.

According to the Fourier analysis method link 1 has a PMD of 3.53 ps, link 2 a PMD of 5.73 ps and link 3 has a PMD of 9.98 ps. The pattern of an increase in the number of extrema and a corresponding increase in the number of interference fringes with a broadened Gaussian pattern is proportional to an increase in the PMD of the links. N. Gisin *et al.* shows that the information provided by the interferometric technique is identical to that provided by the FA technique up to the Fourier transform of the intensity spectrum [15]. It is mentioned that the interference envelope collected from

the interferometer is the same as a Fourier transform of the light intensity, hence the Fourier transform of the transmitted light intensity through a polarizer should yield the same interference envelope. However the difference between the two techniques is noted. The FA technique like any other polarimetric technique requires the FUT to be motionless, while the interferometric technique is non-sensitive to vibrations [15]. They also caution that an insufficient number of points may result in high frequency cut off, leading to incorrect PMD values [15]. In this study the intensity spectra consisted of 5000 points. Heffner also takes up the same task and shows that data provided by the interferometric technique is directly related to data from the FA technique by a Fourier transform [41]. Figure 9.6 shows bar graphs of the magnitude of the PMD delay for the three buried fibre links which were investigated. It is clear that in general the FA technique compares very well with the GINTY PMD measurement technique. In particular the Fourier analysis method yields a PMD value which is very similar to the GINTY PMD measurement technique.

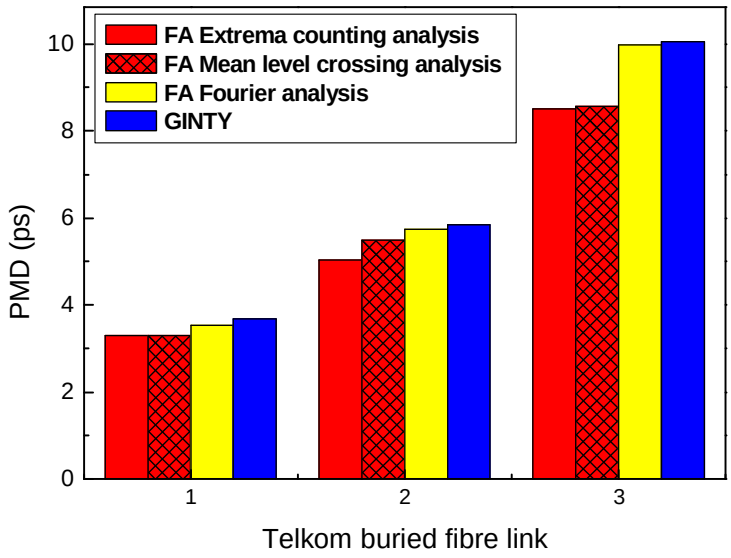

Figure 9.6 PMD measurement results of Telkom buried deployed fibre links for FA and GINTY techniques.

These results are also summarized very clearly in table 9.2 where the percentage difference in the PMD between the FA Fourier analysis method and GINTY were 4.4 % for link 1, 1.95 % for link 2 and 0.63 % for link 3. All three fibres are again predicted to be in the long length regime with link 2 showing lower degree of mode coupling within the fibre.

Table 9.2 Summary of results for the FA vs GINTY measurement techniques.

	Link 1			
	FA			GINTY
	Ext	MLC	FFT	
Mean PMD (ps)	3.303	3.295	3.533	3.683
Half range (ps)	0.050	0.076		0.009
Std deviation (ps)	0.029	0.041		0.005
Ratio	1.56 ± 0.02			
	Link 2			
	FA			GINTY (ps)
	Ext (ps)	MLC	FFT	
Mean PMD (ps)	5.040	5.491	5.733	5.845
Half range (ps)	0.049	0.077		0.011
Std deviation (ps)	0.033	0.051		0.006
Ratio	1.43 ± 0.02			
	Link 3			
	FA			GINTY (ps)
	Ext (ps)	MLC (ps)	FFT (ps)	
Mean PMD (ps)	8.504	8.561	9.978	10.041
Half range (ps)	0.099	0.153		0.034
Std deviation (ps)	0.060	0.109		0.019
Ratio	1.54 ± 0.01			

Theoretically it has been predicted that the numerical factor relating the frequency and time domain PMD measurements is 1.085 [19]. Since extrema counting analysis gives the average measured PMD value, the ratio of the PMD value given by GINTY to that given by extrema counting analysis should equate to this numerical value. Figure 9.7 shows the ratio of the PMD value for both GINTY to extrema counting analysis and GINTY to mean level crossing analysis. This is plotted against the predicted numerical value of 1.085 as shown in figure 9.7. From this, analysis gives the maximum percentage difference as 8.85 % for the ratio formed using extrema counting and 8.11 % for the ratio formed using mean level crossing analysis. If it is assumed that the theoretical ratio is correct, than the slight deviation of the ratio determined from the experimental results serves as an indication that the extrema counting and mean level crossing analysis methods do provide a similar average PMD value according to PMD measurements operating in the frequency domain.

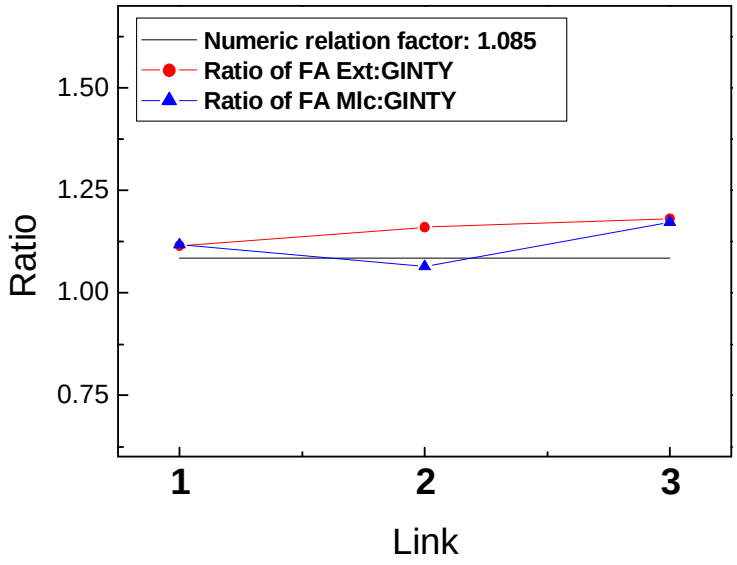

Figure 9.7 Comparison of the ratio of extrema counting PMD value with the GINTY PMD value with the numerical factor relating time and frequency domain PMD measurements.

PMD measurements were conducted simultaneously using the same optical broadband source for both the FA and GINTY techniques. It was found that the FA technique compared very well with the GINTY PMD measurement technique. In particular the Fourier analysis method gave very similar PMD values to that of the GINTY technique. By including the numerical factor which relates PMD measurements operating in the frequency domain to those operating in the time domain, it was found that both the extrema counting and mean level crossing analysis methods do give very similar PMD values to those of GINTY.

9.2 Wavelength window variation investigation

PMD measurements may be performed using wavelength windows of different sizes keeping in mind that a broadband source is required when an OSA is used as a detector. An interesting question arises as a result of using windows of various sizes for PMD measurements. The question enquires whether the measured PMD value is a function of wavelength window size and if so, is the fluctuating PMD value significant? These queries were investigated by performing PMD measurements for various wavelength window sizes and carrying out PMD analysis.

PMD measurements were again performed on link 2 of the selected buried deployed Telkom fibre links, using the conventional FA setup and the JME technique. The FA data was analyzed using extrema counting analysis because this analysis method yields the average PMD value. PMD measurements were performed for various wavelength windows within the range 10 nm to 100 nm, in increments of 10 nm. The range of the first wavelength window was 1525 nm to 1535 nm and the second was from 1520 nm to 1540 nm. Hence the range of the last wavelength window was from 1480 nm to 1580 nm where the central wavelength is 1530 nm. Figure 9.8 shows the PMD measurement results for all the wavelength windows for both the FA and JME techniques.

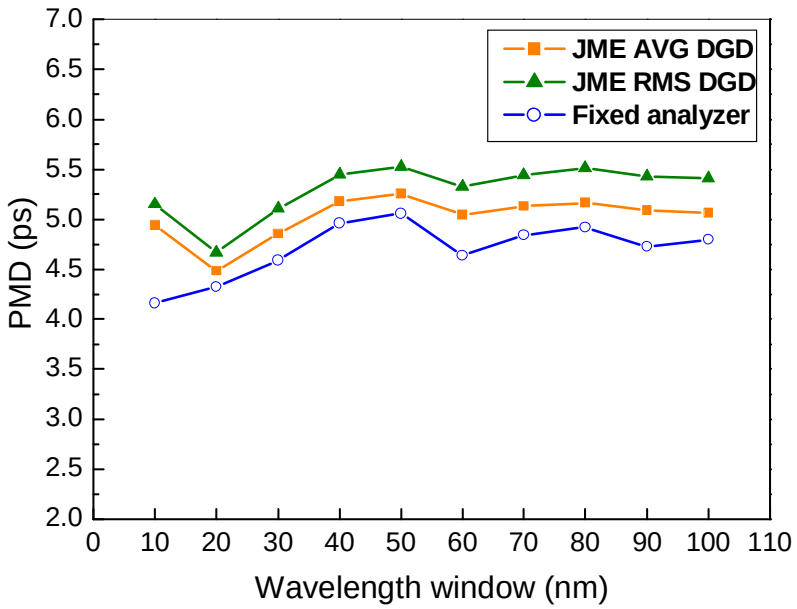

Figure 9.8 PMD for wavelength windows within the range 10 nm to 100 nm.

From figure 9.8 it is very evident that the FA technique does follow the trend of the JME technique for the pattern traced out for PMD vs wavelength window. In general the number of extrema and the number of mean level crossings depend on the product of the magnitude of the average PMD and the size of the frequency window [14], hence the smaller the PMD the larger the required wavelength window. PMD is either averaged over time or over wavelength. The FA technique averages PMD over wavelength. Thus the smaller the PMD value to be measured the wider the

wavelength range should be in order to take more wavelengths contributing to the determination of the measured PMD value into account. From figure 9.8 it can be seen that the PMD value is stable above 60 nm. Below the 60 nm wavelength window the PMD starts to drop and starts fluctuating. Overall there is not much variation for all the windows within the wavelength window range of 10 nm to 100 nm. The PMD variation for all the wavelength windows is 0.77 ps for the RMS DGD, 0.86 ps for the AVG DGD and 0.90 ps for extrema counting analysis.

It was found that there is no variation in the intensity of a particular frequency with a change in the wavelength window within the measurement time. Analysis of the trend of the PMD with wavelength window variation confirms that there is a decrease in the stability of the PMD value as the wavelength window decreases for any particular PMD value being measured. Hence it is advisable to use as many wavelengths as possible especially when low PMD values are measured.

9.3 The effects of sampling

Sampling plays a major role in all measurement techniques, and the FA technique is no exception to this rule. When doing FA technique measurements sampling does affect the resultant PMD value. Incorrect sampling leads to biased PMD values which are different to the true PMD value. Hence it is imperative to understand the effects that sampling has on the PMD value so that correct sampling can be performed when carrying out PMD using the FA technique.

Williams and Wang investigate the effects of sampling on the PMD value and discuss a simple correction algorithm which removes the effects of these biases within ±1.7% [14]. It is reported that both the number of extrema and the number of mean level crossings depend on the sampling density which is a function of the number of points used, the PMD to be measured and the frequency window [14]. It is expected that sampling with too few points underestimates the PMD value. However sampling too densely is redundant, it leads to a magnification of the effect of noise and also extends the measurement time. It is reported that in order to minimize the uncertainty at least

$2\langle\Delta\tau\rangle\Delta\omega$ frequency points are required in the makeup of the intensity trace [14]. By making use of this expression a quick calculation by substituting in a PMD value of 5 ps and a wavelength range of 60 nm from 1510 nm to 1570 nm predicts the number of points to be 477 points.

PMD measurements were again performed on link 2 using the FA technique. This time the number of points was varied from 50 to 10000 points. Both extrema counting and mean level crossing analysis were performed on the intensity trace. For confirmation of the PMD value JME measurements were conducted on the link as well. Figure 9.9 shows the results of all the PMD values determined for different number of points used.

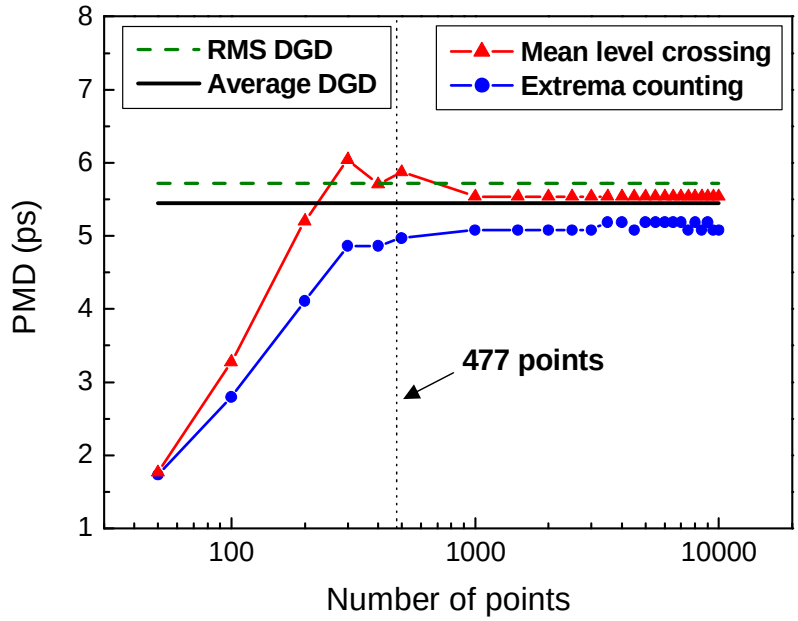

Figure 9.9 PMD values for number of points which make up the intensity spectrum, ranging from 50 to 10000 points.

From figure 9.9 it is very clear that under sampling, using too few points, underestimates the PMD value. This underestimation of the PMD effect starts occurring for below 500 points. This suggests that the expression $2\langle\Delta\tau\rangle\Delta\omega$ does give a very good indication of the minimum number of points to be used. In figure 9.10 this expression is used to plot the recommended minimum number of points to use for different PMD values within the range 1 to 10 ps and for a fixed wavelength range of

60 nm (from 1510 nm to 1570 nm). If the PMD to be measured was 4 ps then just less than 500 points would still have given correct PMD values according to figure 9.10.

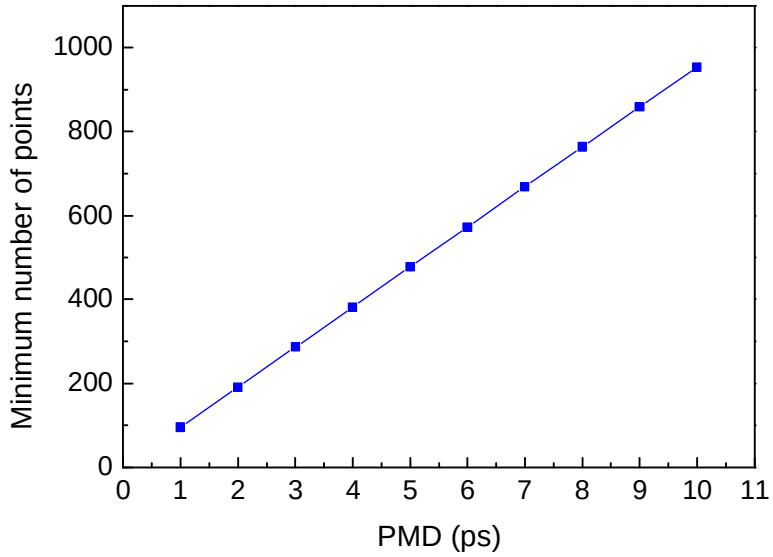

Figure 9.10 Recommended number of points for a wavelength window of 60 nm dependent on the PMD.

Over-sampling leads to the introduction of noise which will definitely affect the PMD value to be determined. Noise signatures may be mistaken for extrema or mean level crossings, increasing the PMD and thus overestimate the PMD value.

Sampling as in any other measurement techniques plays a major role in the FA techniques determination of the PMD value. Hence it is important to sample correctly, steering clear of both under and over-sampling. William and Wang's technique for determining the optimum number of points to use does seem to give a good indication of the number of points to use.

9.4 Investigation of input polarization scrambling

Polarization scrambling has been proven to play a role concerning determination of the average PMD value. PMD measurement results depend on the specific SOP input into the fibre under test. An intuitive explanation of the effect on PMD measurement results with respect to the FA technique is given in this section. The effect of input

scrambling was investigated using manual polarization scramblers at the input of the FUT. The polarization state was changed between each measurement and not while the measurement took place. These scramblers allow for a random 96 polarization states to be set.

In literature the effects which cause the input SOP within optical fibres to evolve is not only attributed to temperature changes or external mechanical perturbations but also due to the topology of the fibre. Researchers have shown that the angle of rotation of linearly polarized light propagating down the fibre is a direct measure of Berry's phase [42]. Tomita and Chiao report experimental verification of Berry's topological phase [43]. The authors prove that the input SOP evolve solely due to the overall geometry of the fibre of the path taken by the light [43]. The topological nature of this phase is confirmed by the results that good agreement was found between the measured rotation angles and those predicted by Berry's phase for fibre following a helix path. In many SOP scramblers the polarization state of the light is controlled using stress birefringence. Frins and Dultz also determine the rotation of the polarization plane of light travelling in a single mode fibre that lies in a space curve [29]. This in turn led to the invention of the manual polarization scrambling cubes.

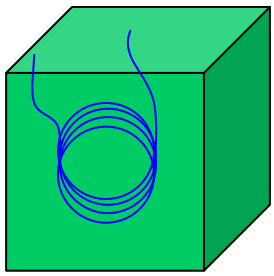

Figure 9.11 Manual polarization scrambling cube.

A polarization scrambling cube consists of a cube with single mode fibre wound into a loop housed inside the cube. The loop occupies a specific plane within the cube. Various orientations of the cube specify the random polarization states. There exist a total of 96 possible orientations for the cube and the plane the fibre loop occupies, resulting in a total of 96 random polarization states.

The conventional FA setup was assembled with the manual polarization scrambling cube placed just in front of the input to the fibre under test. PMD measurements were conducted for a total of 96 random input polarization states using the FA technique. Link 2 of the buried deployed Telkom fibre was again chosen for this investigation.

Results for both extrema counting analysis and mean level crossing analysis are shown in figure 9.12 and figure 9.13 respectively. Both analysis methods basically show the same fluctuation in the PMD value. This fluctuation is a manifestation of the variation of the input SOP and hence signifies the importance to average the PMD over a range of input SOPs.

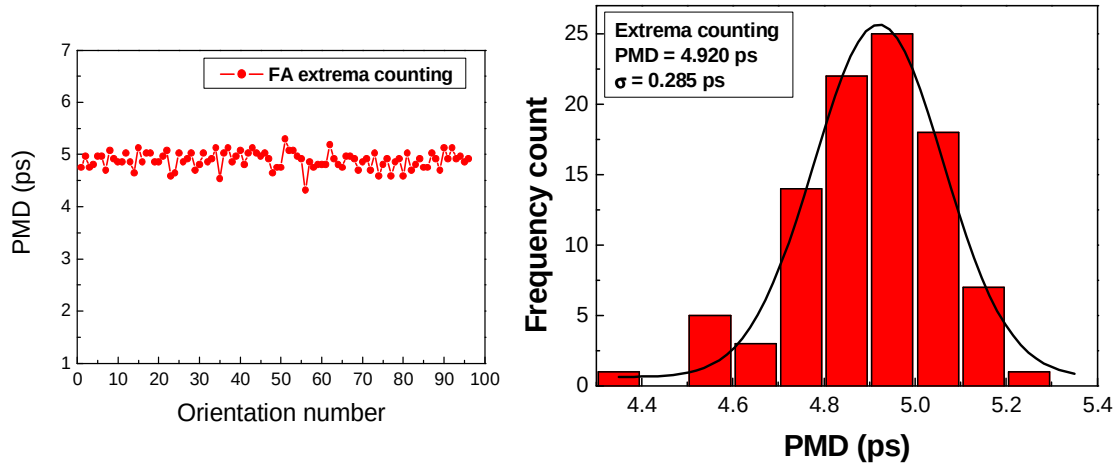

Figure 9.12 FA extrema counting method: (a) PMD values for various random polarization states, (b) histogram of PMD values for various random polarization states.

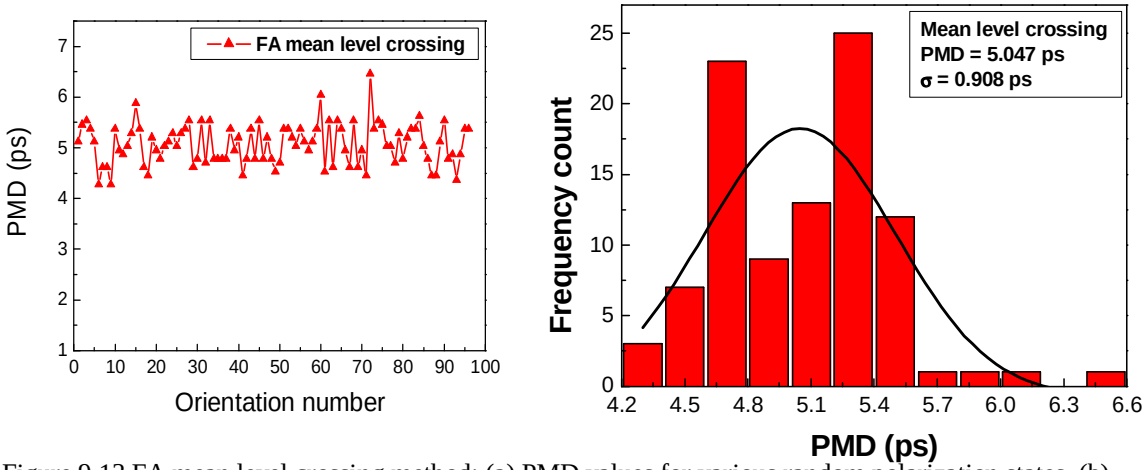

Figure 9.13 FA mean level crossing method: (a) PMD values for various random polarization states, (b) histogram of PMD values for various random polarization states.

The fluctuating PMD may be explained by the principle of operation of the FA technique. As discussed before, a broadband source (in the case where an OSA is used as a detector) sends a polarized wavelength packet down an optical fibre where the PMD transforms the input SOP as a function of wavelength. A detector measures the manifestation of the fluctuating SOP due to PMD as an intensity fluctuation with wavelength. The fluctuating transmitted intensity through the polarizer is a result of the path traced out by the SOP. By positioning the manual scrambler at the input of the FUT, the position of the starting SOP of the trajectory traced out on the Poincaré sphere changes. Hence there should be 96 random input SOPs, implying 96 starting SOP positions. The manifestation of the fluctuating SOP as fluctuation of transmitted intensity through a polarizer will thus differ for a different input SOP. Figure 9.12 (b) and 9.13 (b) shows histogram plots of the PMD for different input SOPs. Both extrema counting and meal level crossing analysis give a Gaussian distribution where the centre PMD value specifies the average PMD value and the FWHM (σ) the error. Extrema counting gives the measured PMD value averaged over 96 polarization states as 4.920 ps ± 0.285 ps and mean level gives the PMD value to be 5.047 ps ± 0.908 ps, where the measurement error is the standard deviation. The JME technique determines the average DGD to be 5.236 ps and the RMS DGD as 5.506 ps. These results imply a 2.6 % and an 11.9 % difference between the extrema counting analysis PMD value and the average DGD and the RMS DGD value respectively. The range of the PMD values for extrema counting is 0.973 ps and for mean level crossing it is 2.175 ps, which gives percentages differences of 18.4 % and 33.7 %. Hence it becomes apparent that the measured PMD value is biased to the input SOP therefore a PMD value averaged over a range of random SOP gives a more accurate representation of the true PMD value.

9.5 Summary

This chapter concentrated on PMD measurements performed on buried deployed Telkom fibre with a particular focus on the FA measurement technique. The FA data was analyzed using the extrema counting, mean level crossing and Fourier analysis

methods. Other investigations included the wavelength window variation, sampling density and input polarization scrambling upon which conclusions were reached.

The FA technique compared well with both the JME and GINTY PMD measurement technique. In particular the extrema counting analysis method from the FA technique gave very similar PMD values to the average DGD from the JME technique whereas the Fourier analysis method from the FA technique agreed very well with GINTY technique. According to the ratio stemming from the FA technique all three buried fibre links were found to be in the long length regime.

In general it has been shown that the minimal fluctuation of the PMD value was observed with a change in the wavelength window size where the selected range of wavelength windows was from 10 nm to 100 nm. For the measured link with a PMD within the range of 5 ps, a decrease in the measured PMD value was observed for windows smaller than 50 nm. The effect of sampling density was also addressed where both over- and under-sampling have been proven to affect the measured PMD value negatively. Williams and Wang's modest prediction of the minimum number of points to use does seem to serve as a good indicator. Polarization manual scrambling has been shown to yield a percentage difference between the maximum and minimum PMD values for extrema counting analysis. Hence scrambling needs to be taken into consideration when doing PMD measurements using the FA technique.

CHAPTER 10

COMPARATIVE INVESTIGATION OF THE TRANSFORMATION OF THE FLUCTUATING SOP TO A FLUCTUATING INTENSITY SIGNAL

The FA technique uses two different detectors depending on the source used. When a broadband light source is used the preferred detector is an optical spectrum analyzer. In the case of a tuneable laser a power meter is used to detect the intensity of the transmitted light through a polarizer. In this chapter PMD measurements using the FA technique where a tuneable laser source was used as a detector are discussed. PMD measurement performance comparison between the FA technique and a particular Poincaré sphere method developed for this study is done. The Poincaré sphere method differs from the FA technique in terms of the results that it offers regarding the PMD dispersive effect. The nature of the setup introduces an interesting question regarding what information can be extracted before and after the polarizer. This chapter looks into this query and other consequent questions.

10.1 Introductory concepts

The FA technique records the intensity of the transmitted light through the polarizer for each wavelength, where each wavelength is related to a specific SOP. The polarimetric techniques record the SOP of the light as a function of wavelength. There exist several Poincaré sphere techniques where the fundamental aim remains to determine the DGD as function of optical angular frequency using the normalized Stokes parameters to calculate the rate of change of the SOPs with angular optical frequency. These techniques differ with respect to the algorithms used to determine what the rate of change is from the normalized states of polarization. Considering the experimental setup of the FA and Poincaré sphere analysis (PSA) method the fundamental difference concerning acquisition of data which exists between the two

methods, is that in the one method a polarizer is placed in front of the detector and not in the other method. The other difference that exists is related to the data being recorded. The FA technique records the intensity transmitted through the polarizer which is a result of the changing SOP caused by the PMD within the fibre while the PSA method records the SOP change directly. Therefore it may be said that the FA technique is an indirect method of determining the PMD of the FUT. This chapter seeks to investigate the effects of collecting data before and after the polarizer pertaining to the determination of PMD.

In 1988 Poole first introduced Poincaré sphere analysis (PSA) method [9]. This method requires at least one of the input polarization states to be circular, after which it allows for the determination of the DGD and PSPs. Cyr then introduced a Poincaré sphere analysis (PSA) method which requires only linear input states of polarization [12, 44]. This PSA method uses the same raw data as the JME technique to calculate the PMD. Both techniques have the inherent advantage of yielding the DGD as a function of frequency. Cyr proved the mathematical equivalence of this particular PSA method to the JME technique [12, 44]. A simulation of 20 concatenated waveplates with random delays and orientations of birefringent axes was used to generate raw data. Using this raw data the DGD vs frequency figures generated using the PSA and JME techniques were proven to be identical [12, 44]. Thus it can be said that the accuracy of this PSA method is of the same order as that of JME. The PSA techniques described require at least three input polarization states as is the case with the JME technique. This deviates from the aim of this investigation, which is to sweep across a wavelength range using only one input state of polarization.

10.2 Experimental procedures

In this investigation PMD measurements were conducted using the FA technique and the PSA method simultaneously. Conventional PSA methods such as those introduced by C. D. Poole and N. Cyr [9, 44] require three input states of polarization due to the calculations involved. The PSA method developed for this investigation requires only one input SOP, further details may be found in Appendix 2. This was specifically

done so as to perform the FA measurement at the same time and also allows for a simultaneous measurement of polarization mode dispersion. This section discusses the experimental setup in detail.

For this particular investigation the conventional FA setup was assembled where a tuneable laser was used as the source, requiring a power meter as a detector shown in figure 10.1.

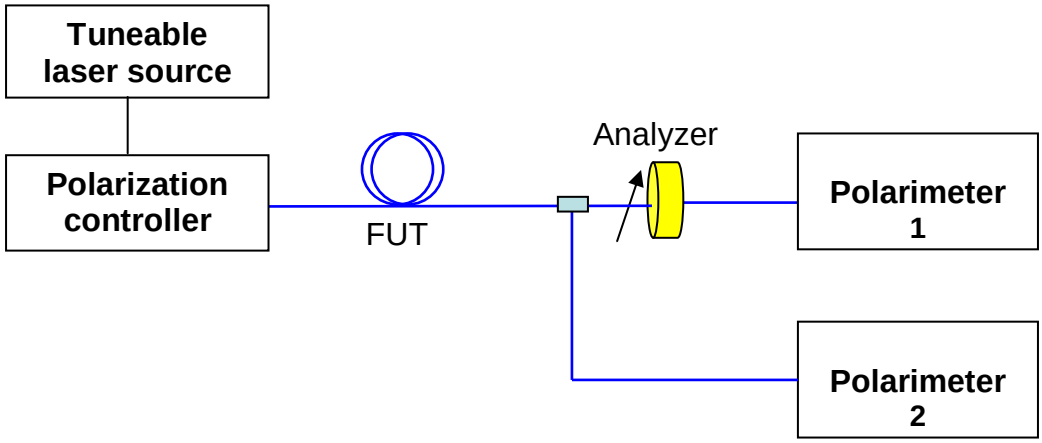

Figure 10.1 Conventional FA setup with a tuneable laser source coupled with a convention PSA measurement setup.

Figure 10.1 shows the entire setup as used during this investigation. A 50/50 beam splitter was used to split the signal into two polarimeters. No additional power meters were necessary since the Adaptif Photonics A1000 polarimeter has a built-in power meter. Polarimeter 1 was used to detect the transmitted intensity through a linear polarizer, while polarimeter 2 records the evolving SOP as a function of wavelength. The polarization controller shown in figure 10.1 controls the launch SOP. A wavelength range of 1510 nm to 1570 nm was used with a step of 0.1 nm. The sweep speed was set at 1 nm/s. These parameters determine the time taken for an entire sweep to complete, which is 60 seconds.

PMD measurements were done on polarization maintaining fibre (PMF) 2 metres in length. Measurements were also conducted on an emulator consisting of a concatenation of PMF and single mode fibre sections. Extrema counting and mean level crossing analysis methods were used to extract the PMD value. The PSA

technique yields more information regarding the polarization group delay. From the technique it is possible to obtain the DGD as a function of wavelength and also the PSPs. The adapted PSA technique developed for this study was used to determine both the DGD and the PSP of the different fibre types and the emulator.

10.3 Comparison of FA and PSA techniques with JME method verification

Measured PMD results for 2 metre PMF

PMF is a standard optical fibre which should give consistent results regarding PMD. The expected transmitted intensity signature is periodic in nature. This same trace was mapped out using the tuneable laser source as seen in figure 10.2. The signature is periodic in form as expected. The number of extrema and the number of mean level crossings amount to the same number, hence since no mode coupling sites are present in PMF the measured PMD value reduces to the same value of 2.57 ps ≈ 2.6 ps.

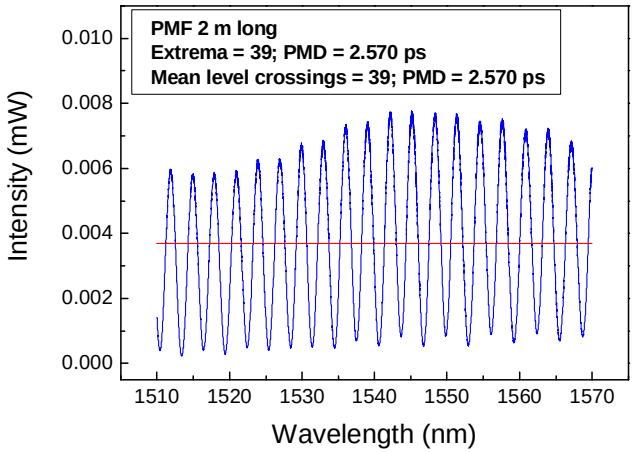

Figure 10.2 Intensity over wavelength spectrum for a 2 metre long PMF section.

The JME technique determined the average PMD value to be 2.564 ps and the root mean square DGD as 2.564 ps as well. Hence there is a very good comparison between the FA technique determined PMD value and that of JME with only a 0.2 % difference in the PMD value.

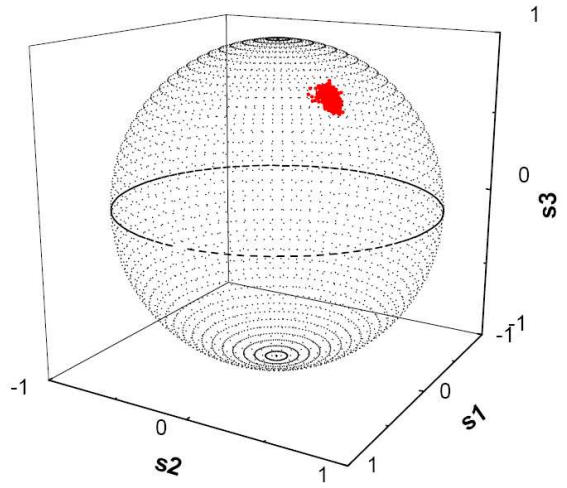

Figure 10.3 SOP location of the light transmitted through a polarizer with a change in wavelength for 2 metre long PMF section.

Figure 10.3 shows the transmitted SOP through the polarizer. This specific polarizer has PMF at the output directing the light away from the polarizer in order to maintain the SOP exiting the polarizer. From figure 10.3 it is clear that the SOP through the polarizer remains fixed with a change in wavelength.

While the SOPs were kept constant by the polarizer allowing only a change in the intensity, the variation of the SOPs was recorded at the output of the coupler. Together with the wavelength this data was fed into the PSA algorithm program. Figure 10.4 shows the DGD vs wavelength trace for the 2 metre long PMF determined using the PSA technique, in blue, and also the JME technique, in red.

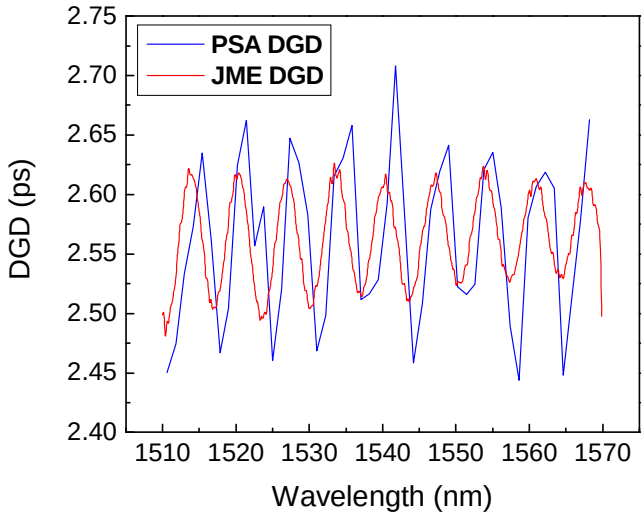

Figure 10.4 PSA and JME determined DGD over wavelength change for a 2 metre long PMF section.

The PSA and JME traces resemble each other very much, showing the same trend in the DGD variation with wavelength and also falling in a very similar DGD band. The PSA method showed a DGD variation range of 0.264 ps and the JME method 0.145 ps.

Table 10.1 Summary of FA, PSA and JME methods PMD measurement results for a 2 m long PMF.

FA		**PSA**		**JME**	
Extrema counting analysis	**Mean level crossing analysis**	**Average DGD**	**RMS DGD**	**Average DGD**	**RMS DGD**
2.57 ps	2.57 ps	2.562 ps	2.563 ps	2.564 ps	2.564 ps

The mean DGD given by the PSA method is 2.562 ps and the root mean square DGD is 2.563 ps. The average DGD gives the PMD value as 2.564 ps for JME and 2.562 ps for PSA, yielding a PMD difference of 0.02 ps. Hence the percentage difference is 0.08 %. These results agree with PMD and DGD calculations using theoretical simulations by N. Cyr *et al*. [44] where it was proven that the two techniques produce the same PMD value and DGD over wavelength trace. Experimental investigations have shown that the Poincaré sphere method gave the same average PMD value as that given by the FA extrema counting analysis method [45]. In reference [19], different laboratories also showed good comparison of PMD between the principal states analysis method, the FA technique and an interferometric technique. Further analysis of the PSA method yields the PSPs. Figure 10.5 shows the PSPs for the 2m long PMF determined using the developed PSA method and also the JME technique.

The PSP computed through by the adapted PSA method (blue points) is exactly 180^{o} that using the JME technique (green points). Since both techniques determine only one PSP and it is known that a PSP set is orthogonal in the absence of polarization dependent loss, 180^{o} apart on the Poincaré sphere, hence the orthogonal mate of both the JME and PSA determined PSP must appear 180^{o} on the other side of the Poincaré sphere.

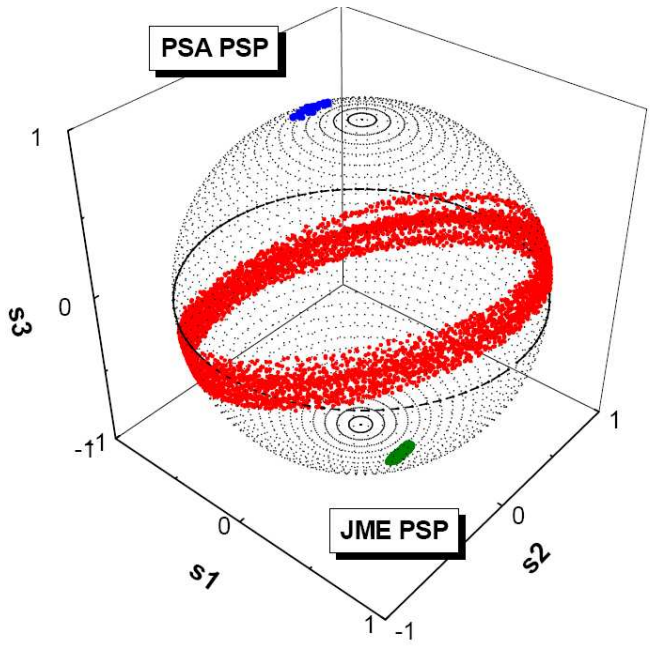

Figure 10.5 Rotation of SOP and location of PSP obtained using the JME and PSA method.

As the PSPs in figure 10.5 are orthogonal it can be concluded that the PSA and the JME methods agree to a high degree.

10.4 Summary

In this chapter the FA method in conjunction with a developed PSA method was investigated using the setup pertaining to a tuneable laser source. The issues of measured PMD value comparison and differences in the results offered regarding the polarization time delay within various fibre types was addressed. The tuneable laser source setup together with the power meter as a detector presented the same results as those found previously using the broadband source together with the OSA. In general from the results it can be concluded that the FA technique agrees very well with the average PMD determined by the developed PSA method which in turn agrees very well with the JME technique, hence correlating with previous studies reported in literature. From the results presented the developed PSA method proved adequate in computing the DGD over wavelength and the PSPs, more so for PMF, showing good agreement with the standard JME technique. Further theoretical and experimental investigation is required in order to determine whether the possibility of determining

the DGD and PSP from the intensity spectra is lost during transmission of the light through the polarizer.

CHAPTER 11

CONCLUSIONS

This dissertation investigates the PMD measurement performance of the FA measurement technique. The FA technique setup was assembled and the first FA PMD measurements were performed in South Africa. Characteristics pertaining to PMD measurements of the FA technique were addressed. In general it has been shown that the FA technique is a very effective technique for determining the average PMD of a link. The technique has three analysis methods which all agreed very well with the JME and GINTY PMD measurement techniques on the measured PMD value. The FA technique is easy to implement and does not take a long time to perform PMD measurements. It proved to be suitable for field measurements as well. The FA technique has the added advantage of making use of cheaper instruments and also that of giving numerical information regarding the length regime of the fibre.

The effect that the launch angle variation has on the transmitted intensity spectrum was demonstrated in chapter 8. Polarization maintaining fibre was used for this purpose. It was observed that by aligning the input SOP with one of the PSP, a minimum fluctuating intensity trace resulted. This omnipresent fluctuation may be attributed to the fact that realistically speaking it is not possible to launch all the light into only the fast or slow axis. If this ideal situation were possible then a straight line would appear on the intensity trace and the PMD of the PMF would be zero, as no time delay occurred between the orthogonal polarization modes. When the input light signal was launched such that both PSPs were equally illuminated, the DOP was minimum yielding an intensity trace which gave a percentage difference of 92% and 95% with respect to the intensity variation produced by launching the light into either the fast or slow axis.

PMD measurements were performed in the lab on different fibre types. PMF is known not to have any mode coupling sites present when not under strain. All the other fibres investigated had mode coupling sites present, produced from either strain or splicing

or as a result of the manufacturing process. This allowed for the effects that birefringence and mode coupling has on the intensity spectrum to be made visible. The amount of birefringence determines the number of extrema present within the transmitted spectrum and mode coupling affects the periodicity of the intensity spectrum.

A good agreement was found in the comparison between the PMD values determined using the FA technique, and the GINTY and JME techniques. In particular the extrema counting analysis method and the JME measurement technique agreed very well, and the Fourier analysis FA method and the GINTY PMD measurement technique showed similar measured PMD values.

The FA technique was further used to give some insight into the length regime of the different fibre types. This techniques, showed PMF to be in the short length regime and the rest (6 km fibre cable, fibre shipping spool and an emulator made up of a concatenation of PMF and single mode fibre sections) to be in the long length regime, that is having appreciable mode coupling sites.

The FA technique also performed very well in the field on buried deployed Telkom fibre links. For this study the same wavelength range was used for the FA and the JME measurements. In addition, the same source and wavelength window was used in the comparison between the FA and GINTY techniques. The techniques agreed well as before. The FA Fourier analysis method has the advantage of giving a graphical representation of the mode coupling characteristics of the FUT. The Fourier analysis method also allows filtering out high frequency features, induced by noise or vibration that would be detected as peaks and valleys by the extrema-counting analysis method, Derickson [6]. It was found that the Fourier analysis method agreed particularly well with its counterpart the GINTY technique.

The question of whether the intensity at a particular wavelength and hence the PMD changes with a variation of the wavelength window size was also addressed. It was found that, the smaller the PMD value the larger the required wavelength window size. The PMD trend with wavelength window appeared similar for the FA and the JME techniques. The smaller the wavelength window for the particular PMD which

was being measured the more the PMD value started showing signs of deviating from the true PMD value.

Williams and Wang [14] discussed the effects of sampling and presented an equation to determine the number of points to use for a given PMD value and wavelength range. In chapter 9 it is shown how the number of points collected for the intensity spectrum can lead to incorrect PMD values. The equation presented by Williams and Wang also proved to be reliable, hence it may be used to determine the number of points to use when performing PMD measurements.

State of polarization (SOP) scrambling plays a role when performing PMD measurements using the FA technique. This was clearly shown in chapter 9 where the PMD fluctuated and depended on the input state of polarization. Hence it is recommended that the average PMD value, determined from PMD values for all the input states, serves as a better indicator of the true PMD of the FUT.

An additional study included in this dissertation is a comparison between the FA technique and our developed Poincaré sphere analysis method. The fundamental experimental difference between the techniques is the fixed polarizer placed in front of the detector for FA measurements. Hence this investigation essentially looks into the impact of collecting data before and after the polarizer. Both the FA technique and the developed Poincaré sphere analysis method determine the average measured PMD value. The FA extrema counting analysis method agreed well with the average DGD given by the developed Poincaré sphere analysis method. However the Poincaré sphere analysis method does give additional information in the form of DGD over wavelength and the evolution of the PSPs.

This work proves that the FA method is able to determine the average PMD accurately and the technique showed good reproducibility of the measured PMD value. The FA method has the added advantage of giving numerical information regarding the length regime. The highest PMD value that the FA technique can measure is limited by the spectral resolution of the source/detector combination [13]. For low PMD values, the FA technique is limited by the size of the wavelength window used. Using extrema counting to achieve a standard deviation of 20 % the

frequency window is given by, 33 divided by the average PMD value. Hence extremely broadband sources are required for very low PMD value, for example for a PMD of 0.1 ps a source width of 350 nm is required [13]. The technique has the drawback of requiring stable measurement conditions. Hence it is not suitable for performing measurements on aerial fibre.

APPENDIX 1

Program structure and operation

After the appropriate application has been selected and all the relevant parameters have been set the user may start the program by clicking the run button. This sets the program in motion which will in turn initialize a session with the Agilent 86142B optical spectrum analyzer (OSA) described in chapter 6. The graphical source code was written in the block diagram. This section presents a detailed explanation of the main operating procedures the program follows. The flowchart shown in figure A1.1 will diagrammatically illustrate the sequence of operations performed by the program.

A list of fifteen LabVIEW functions originating from the Agilent 86142B OSA instrument drivers were used and coupled with general LabVIEW VI's which were mainly incorporated for the purpose of data handling, computations and saving preferences. The list of functions used are as follows; initialize, vertical scale, get vertical scale, set wavelength start and stop, get wavelength start and stop, get centre wavelength and span, set sweep time, get sweep time, set number of trace points, get number of trace points, average trace, get average trace, start sweep, download traces and close.

The flowchart type structure in figure A1.1 shows the sequence of the program operation. As seen in figure A1.1 the flowchart consists of 15 blocks indicated by numbers placed next to each block. The operational explanation of the flowchart will focus on the PMD measurement normalize spectrum application of the program. Each application starts with a sequence of questions following each other. Subsequent questions appear depending on answers given to previous questions asked. These questions are there to assist the user in making sure that all the requirements for the experiments are met. For example one of the questions asked by the normalize spectrum application is, 'Has the spectrum to be recalled been selected?' Depending on the answer the program will either run or execute with a suggestion for the user to provide the file path of the required spectrum. The program then initializes a session

with the instrument placing the OSA in the remote control setting. Operations 2 to 4 consists of sending all the parameters needed to be set on the OSA for application and also reading all the set parameters sent by the OSA to the computer. Block 5 in the flowchart represents the next step which generates the wavelength array. This is done by a For loop which uses the starting and stopping wavelength together with the number of points to calculate the increments of the wavelength. The increments are then in turn used to generate the wavelength array by adding multiples of the increments to the starting wavelength. The next operations are starting a sweep and downloading the measured intensity of the wavelengths from the OSA.

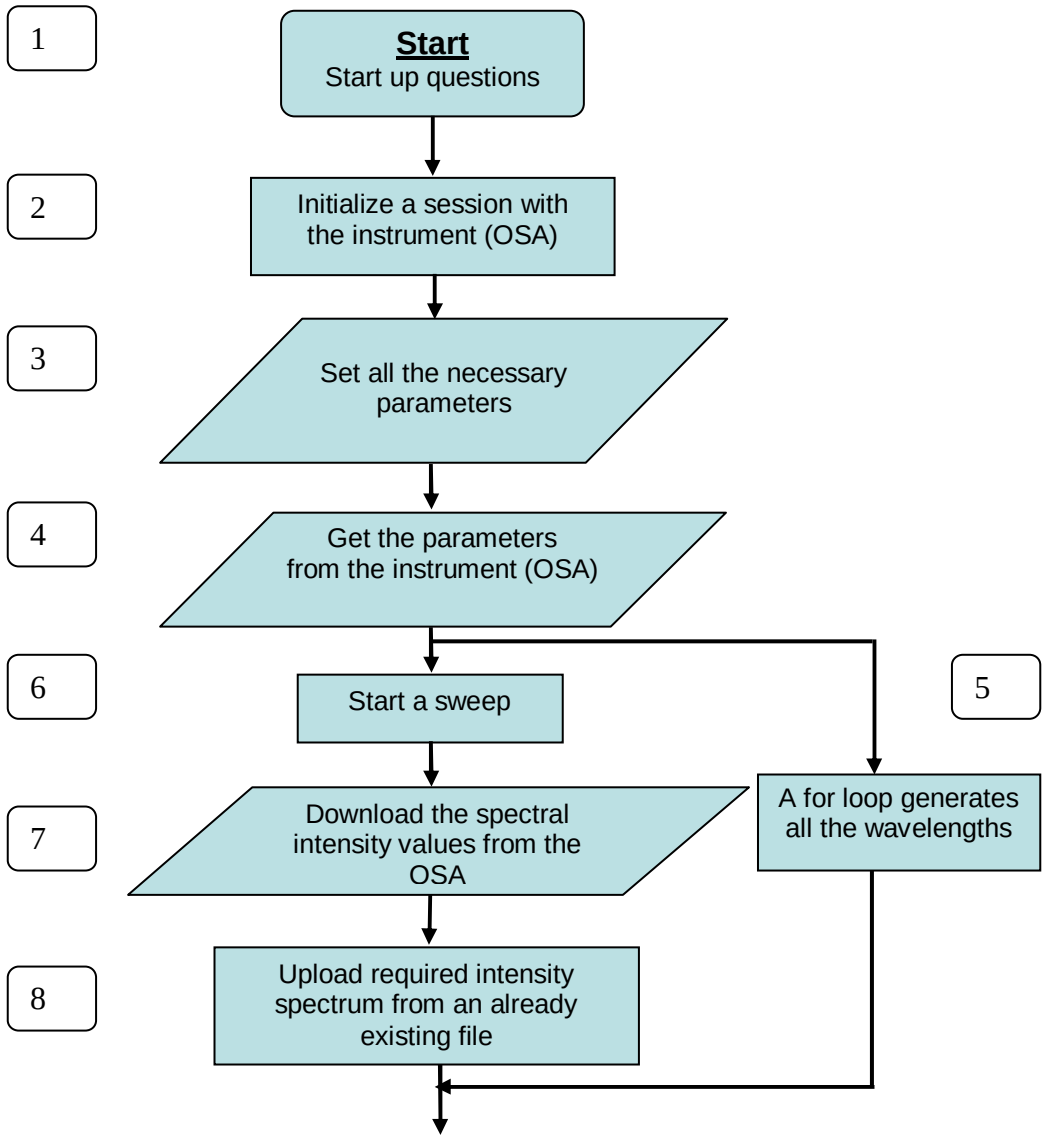

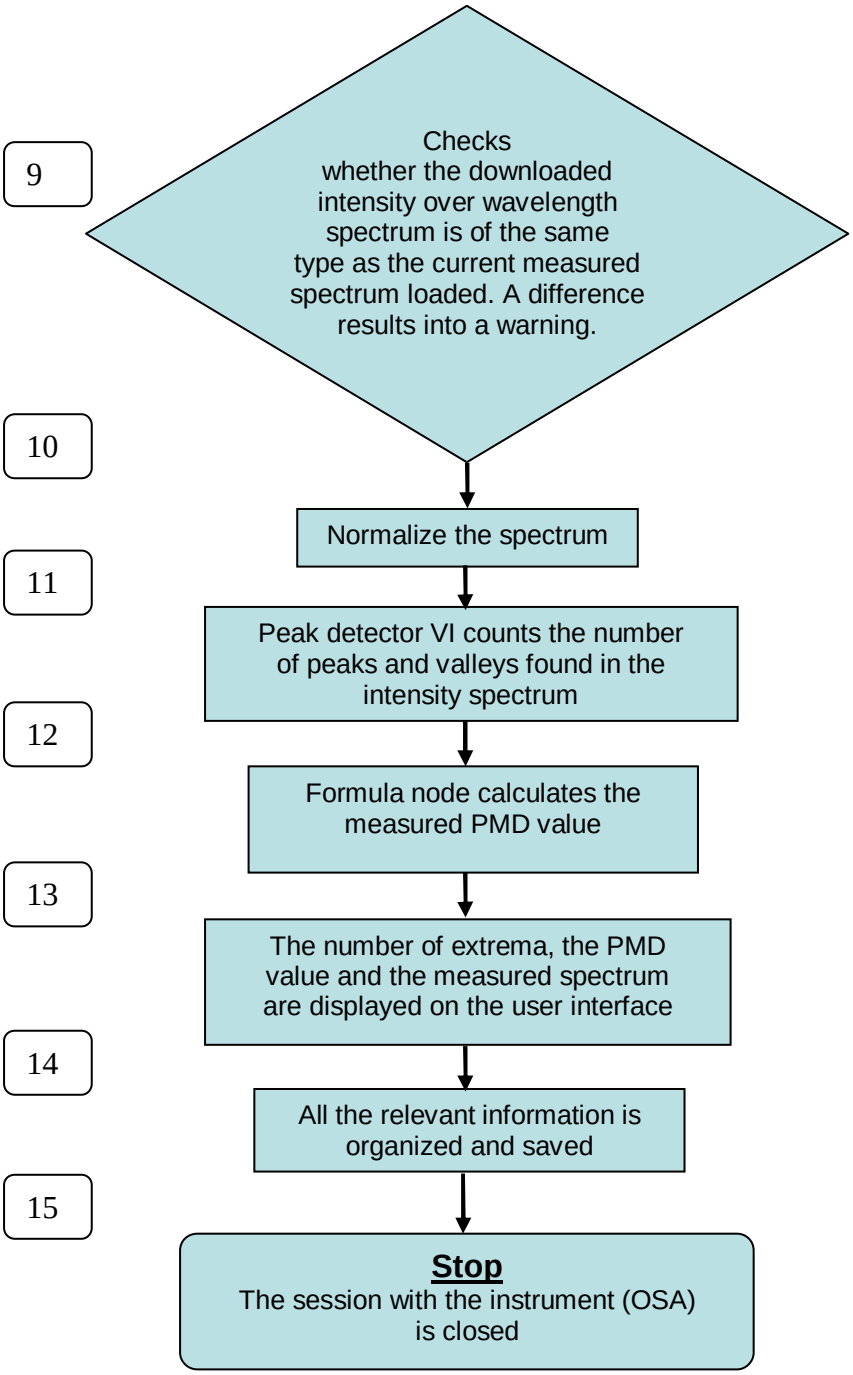

Figure A1.1. Flowchart type structure given a descriptive summary of the program operation.

This is then followed by uploading the existing file which is an intensity spectrum of the source without the polarizer in place. Normalization in then performed by dividing the two spectra as previously explained. A special feature added to this program is its ability to determine whether the spectra are compatible. This is done by comparing the start and end wavelength, according to the number of points in the loaded

spectrum with those of the current measurement. If the comparison fails a warning appears otherwise the program continues running. A peak detector VI then operates on the normalized spectrum and counts the number of peaks and valleys in the spectrum. The peak detector VI either counts the number of peaks or valleys hence two peak detector functions are required each counting either peaks or valleys with the addition of the two giving the number of extrema. The peak detector VI requires three inputs: the width, threshold and array to be operated on. This VI is based on an algorithm that fits a quadratic polynomial to sequential groups of data points. The width specifies the number of data points used. For the purpose of this program the width input was converted to wavelength spacing. This is simply done by multiplying the width with the wavelength increment to get the wavelength spacing. The wavelength spacing must then be no more than then half the half-width of the smallest peak. The threshold rejects peaks and valleys which are too small; any peak with a height lower than the threshold is rejected and any valley with a height greater than the threshold is rejected as well. For each VI the threshold was set such that for the peak detector the threshold was ten minus the lowest intensity value and for the valley detector the threshold is ten plus the highest intensity value. The next operation is the calculation of the PMD value which is represented by block 12 on the flowchart. A formula node uses the extrema counting analysis equation discussed in chapter 5. Finally both the number of extrema and the PMD value are displayed together with a full view of the intensity spectrum. Any data to be saved is organized and saved in a well ordered fashion by the program. The program then ends by closing the interactive session with the OSA. When using this program besides following good FA method experimental procedure it is of great importance that an appropriate wavelength spacing is chosen for counting the number of extrema. This is more so important for PMD measurements conducted on fibres showing a high degree of mode coupling as the peak half width of the peaks show a greater variation in size than in fibres with no mode coupling.

The program has proved to be successful at being able to handle PMD measurements on different fibre types and calculating exact and correct PMD values. A variation of this program was also written in order to perform continuous PMD measurements, meaning that the user may specify the number of PMD measurements that should be done. This variation allows the user to specify any number of measurements and also

to dictate the time interval between consecutive measurements. The data is saved after each measurement.

The extrema counting analysis method program has simplified PMD measurements and the calculation of the measured PMD value. The program removes the tedious task of counting the number of extrema and substituting this value into the equation. Throughout this study PMD measurements using the FA technique were made using this program and the continuous measurement version of it.

APPENDIX 2

Theoretical description of adapted PSA method

A2.1 (a) Theoretical background

For the purpose of this investigation a PSA data analysis method was developed in order to analyze the raw data obtained from experiment. The raw data consisted of the Stokes parameters of the SOPs as they evolve with wavelength. The whole algorithm depends on vector analysis where the fundamental purpose is to determine the rate of rotation of the SOPs with wavelength. As mentioned in previous chapters, frequency domain techniques determine the DGD from the rate of rotation about the PSPs where the equation describing this is

$$\Delta\tau = \frac{\Delta\theta}{\Delta\omega}. \qquad \text{(A2.1)}$$

This equation is the focus of the PSA method. SOPs evolve on the Poincaré sphere following a particular path depending on the magnitude of the birefringence and the degree of mode coupling sites present within the FUT. For the particular case of no mode coupling sites present within the FUT the SOPs will evolve continuously about a common axis formed by the line joining the two principal states of polarization which are orthogonal, implying 180^{o} from each other on the Poincaré sphere. In the presence of mode coupling the SOPs frequently change direction deviating from what would have been a circular trajectory. Figure A2.1 shows the experimental results for SOPs traced out on a Poincaré sphere for an emulator (made up of a concatenation of single and PMF sections) within the wavelength range 1510 nm to 1570 nm.

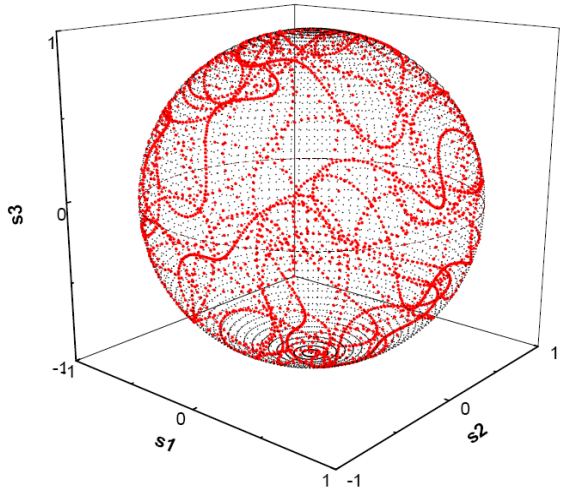

Figure A2.1 SOP trace of an emulator for a wavelength scan from 1510 nm to 1570 nm. The path is made up of 3000 points.

Figure A2.1 clearly shows that the SOP path changes direction, hence complete circles are not evident. Considering the fact that the PSPs remain constant over a small wavelength range to the first order [38], a small arc may be viewed as a circle through which the line joining the two PSPs will point through its centre. The line pointing through the centre of the circle gives the coordinates of the PSP and points in the same direction as the PMD vector. The rate at which the SOP changes with frequency for any arc determines the DGD.

Suppose the SOP traces out a path on the Poincaré sphere. A small section of this path will give an arc, which if the SOP continued on the path would form a circle where the centre of the circle gives the PSP and the rate of change with wavelength gives the DGD. The schematic drawn in figure A2.2 shows a small section of a possible path from point A to point B traced out on a Poincaré sphere. In figure A2.2 the centre of the arc is indicated by X and the centre of the Poincaré sphere by O. Points D, B, X, A all lie on the surface of the Poincaré sphere.

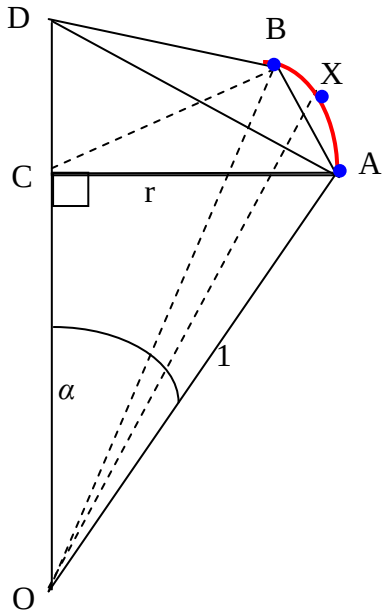

Figure A2.2 Schematic of the resultant vectors from an arc traced out on the Poincaré sphere from point A to point B.

The algorithm chooses three points on the arc. These three points are used to construct two vectors which point away from the centre point. Hence the coordinates of B, X and A are used to make the vectors $\overline{XB} = \overline{B} - \overline{X}$ and $\overline{XA} = \overline{A} - \overline{X}$. The method of using the three points to determine the vectors was suggested by T. Gibbon [46]. The algorithm then runs through a sequence of four steps.

1) Determining the PSP.

The cross product of vector $\overline{XB} = \overline{B} - \overline{X}$ an $\overline{XA} = \overline{A} - \overline{X}$ give a vector $\overline{C}$ whose unit vector gives the coordinates of the PSP.

$$\overline{XB} \times \overline{XA} = \overline{C}$$

$$\frac{\overline{C}}{\left|\overline{C}\right|} = \hat{n}$$

2) Find the angle α using the law of cosines.

The vector $\overline{DA} = \overline{A} - \overline{D}$ is found by using $\hat{n}$ and then used to calculate the angle α.

$\overline{DA} = \hat{n} - \overline{A}$, where $\left|\overline{DA}\right| = DA$

$$\alpha = \cos^{-1}\left(\frac{(OD)^2 + (OA)^2 - (DA)^2}{2(OD)(OA)}\right) = \cos^{-1}\left(\frac{1+1-(DA)^2}{2}\right)$$

3) Finding the radius r of this circle.

$$\sin\alpha = \frac{r}{1}$$

$$r = \sin\alpha$$

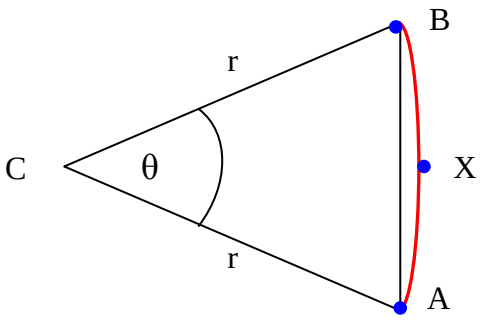

Figure A2.3 Arc AB traced out with a change in wavelength together with the resultant angle θ.

4) Calculating θ and then the DGD.

$$\overline{OA} - \overline{OB} = \overline{AB}$$

Then $\theta = \cos^{-1}\left(1 - \frac{(AB)^2}{2r^2}\right)$

$$\Delta\tau = \frac{\Delta\theta}{\Delta\omega}$$

This developed PSA technique determines both the DGD as a function of wavelength and also the PSP. The drawback of this technique regarding its calculations is that it makes the assumption that the SOPs are not depolarised. PMD does depolarize the input SOPs to a certain extent depending on the magnitude of the PMD.

A2.2 (b) Calculation of DGD and PSP using developed PSA method.

Theoretical calculations were done using equation A2.1 and the PSA developed algorithm. For this purpose a set of 90 SOPs were generated for a wavelength range starting from 1510 nm to 1529.8 nm. Figure A2.4 shows all 90 SOPs lying on the equator.

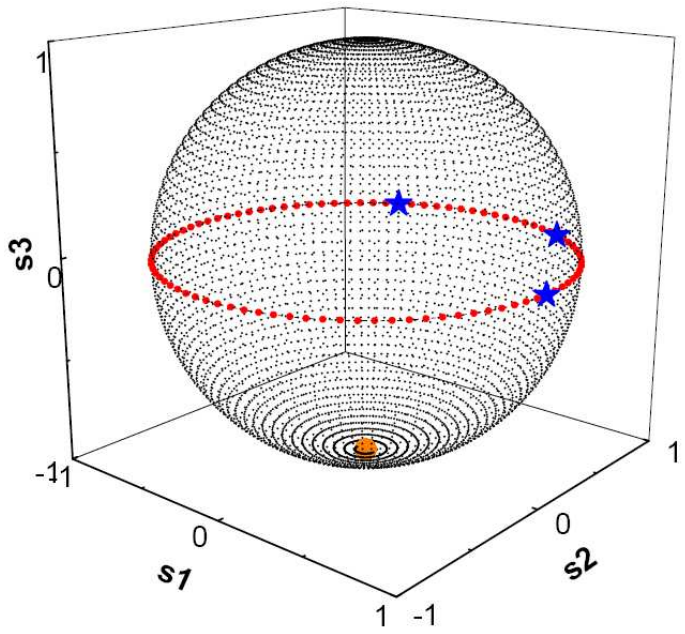

Figure A2.4 Theoretical test data set consisting of 90 SOP points (red points).

Manual calculation:

Since there are 90 points in 360°, for every point moved 4° are covered. If every fifteenth point is going to be used then the point span will be 30 points which is equivalent to 120°. Substituting all these parameters into equation A2.1 gives the following result.

$$\Delta\tau = \frac{\Delta\theta}{2\pi c}\left(\frac{\lambda_1\lambda_2}{\Delta\lambda}\right) = \frac{120^o}{2*180^o*c}\left(\frac{\lambda_1\lambda_2}{\Delta\lambda}\right) = 1.297\times10^{-13}\,s$$

Algorithm calculation:

The three chosen points also shown in figure A2.4 represented by blue stars and their corresponding wavelengths are:

A: (1, 0, 0) and 1510 nm

X: (0.5, 0.866, 0) and 1519.9 nm

B: (-0.5, 0.866, 0) and 1529.8 nm

$\overline{XA}$ = (1, 0, 0) - (0.5, 0.866, 0) = (0.5, -0.866, 0)

$\overline{XB}$ = (-0.5, 0.866, 0) - (0.5, 0.866, 0) = (-1, 0, 0)

$\overline{XA} \times \overline{XB}$ = (0.5, -0.866, 0) x (-1, 0, 0) = $0\hat{s}_1 + 0\hat{s}_2 + (-0.866)\hat{s}_3 = -0.866\hat{s}_3$

The PSP is then

$\hat{n} = \overline{XA} \times \overline{XB} \Big/ \left|\overline{XA} \times \overline{XB}\right| = -1\hat{s}_3$

The one PSP is plotted in figure A2.4 (orange dot) where its orthogonal mate should be located at the other pole of the sphere as it is 180^o away from the PSP.

$\overline{DA}$ = (1, 0, 0) – (0, 0, -1) = (1, 0, 1)

$\left|\overline{DA}\right|$ = DA = 1.414

$$\alpha = \cos^{-1}\left(\frac{2-(DA)^2}{2}\right) = \cos^{-1}\left(\frac{2-\left(\sqrt{2}\right)^2}{2}\right) = 1.571$$

r = sin(α) = sin(cos^{-1}(0)) = 1

$\left|\overline{AB}\right|$ = | (-0.5, 0.866, 0) – (1, 0, 0) | = 1.732

$$\theta = \cos^{-1}\left(1-\frac{(AB)^2}{2r^2}\right) = 2.094$$

Substituting this into equation 10.1 gives the DGD to be 1.297 x 10^{-13} s, giving an identical result for the PMD value as given by the manual calculation. The PSA method algorithm requires a lot of computations depending on the number of data points recorded. The chosen number of wavelength and SOP data points was 6000 for this investigation; hence a computer program was required to assist in making these computations. A program based on the PSA method algorithm was developed using LabVIEW 7.1. The program does all the computations and yields both the DGD vs

wavelength and PSP values. It only requires the total number of data points and the specified increments to be used.

APPENDIX 3

Research Outputs

Publications in conference proceedings

Gamatham, R. G. G., Gibbon, T. B., Wu, L. and Leitch, A. W. R. (2007), "Investigation of the Fixed Analyzer Technique for Polarization Mode Dispersion Measurements on Optical Fibres", Southern Africa Telecommunication Networks and Applications Conference 2007 (SATNAC 2007).

"A Comparative Investigation of PMD Measurement Performance with a Focus on the Fixed Analyzer Measurement Technique", Gamatham, R. G. G., Wu, L., Gibbon, T. B., and Leitch, A. W. R., ALC symposium 2008 (Kariega game reserve).

Oral presentations

"Investigation of the Fixed Analyzer Technique for Polarization Mode Dispersion Measurements on Optical Fibres", Gamatham, R. G. G., Gibbon, T. B., Wu, L. and Leitch, A. W. R., SATNAC 2007.

"A Comparative Investigation of PMD Measurement Performance with a Focus on the Fixed Analyzer Measurement Technique", Gamatham, R. G. G., Wu, L., Gibbon, T. B., and Leitch, A. W. R., ALC symposium 2008 (Kariega game reserve).

Poster presentation

"Characterization of Polarization Mode Dispersion in a Buried Optical Cable using the Fixed Analyzer Technique", Gamatham, R. G. G., Gibbon, T. B., Wu, L. and Leitch, A. W. R., SAIP Annual Conference 2007. (Awarded second prize in the Lasers, Optics and Spectroscopy category).

REFERENCES

1. **Agrawal, G. P.** (2002), "Fiber-Optic Communication Systems", Third edition, John Wiley & Sons.

2. **Keiser, G.** (2000), "Optical Fiber Communication", Third edition, McGraw-Hill Companies.

3. **Yariv, A.** (1997), "Optical Electronics in Modern Communications", Oxford University Press.

4. **Hecht, J.** (1999), "Understanding Fiber Optics", Third edition, Prentice Hall.

5. **Pedrotti, F. L.** and Pedrotti, S. J. L. S. "Introduction to Optics", Second edition, Prentice Hall 1987.

6. **Derickson, D.** (1998), "Fiber Optic Test and Measurement", Prentice Hall.

7. **IEC TR 61282-9 Technical Report** (2006-2007), Guidance on Polarization Mode Dispersion measurement and theory, 1st edition 2006-2007.

8. **Damask, J. N.** (2005), "Polarization Optics in Telecommunications", Springer Science + Business Media.

9. **Poole, C. D.**, Bergano, N. S. and Wagner, R. E. and Schulte, H. J. (1988), "Polarization Dispersion and Principal States in a 147-km Undersea Lightwave Cable", *J. Lightwave Technol.*, Volume 6, No. 7, pp 1185-1190.

10. **Williams, P. A.,** (2004) "PMD measurement techniques avoiding measurement pitfalls", *J. Opt Fiber Com Reports*, Rep. 1, pp 84-105.

11. **Namihira, Y.** and Maeda, J. (1992), "Comparison of various Polarization Mode Dispersion measurement methods in Optical Fibres", *Electron. Lett.*, Volume 28, No. 25, pp 2265-2266.

12. **Cyr, N.**, Girard, A. and Schinn, G. W. (1999) "Stokes Parameter analysis method, the consolidated test method for PMD measurements", *NFOEC Proc., Tech. Digest*, Volume II, pp 280.

13. **Poole, C. D.** and Favin, D. L. (1994) "Polarization-Mode Dispersion Measurements Based on Transmission Spectra Through a Polarizer", *J. Lightwave Technol.*, Volume 12, No. 6, pp 917-929.

14. **Williams, P. A.** and Wang, W. M., "Corrections to Fixed Analyzer Measurements of Polarization Mode Dispersion", *J. Lightwave Technol.*, Volume 16, No. 4, April 1994, pp 534-554.

15. **Gisin, N.**, Passy, R. and Von der Weid J. P. (1994), "Definitions and Measurements of Polarization Mode Dispersion: Interferometric Versus Fixed Analyzer Methods", *IEEE Photon. Technol. Lett.*, Volume 6, No. 6, pp 730-732.

16. **Heffner B. L.** (1992), "Automated Measurement of Polarization Mode Dispersion Using Jones Matrix Eigenanalysis", *IEEE Photon. Technol. Lett.*, Volume 4, No. 9, pp 1066-1069.

17. **Heffner B. L.** (1993), "Accurate, Automated Measurement of Differential Group Delay Dispersion and Principle State Variation Using Jones Matrix Eigenanalysis", *IEEE Photon. Technol. Lett.*, Volume 5, pp 814-817, No. 7.

18. **Jones R. C.** (1947), "A New Calculus for the Treatment of Optical Systems VI. Experimental Determination of the Matrix", *J. of the Opt. Soc. of America*, Volume 37, Number 2, pp 110-112.

19. **Gisin, N.**, **Passy, R., Blasco, P., Van Deventer, M. O., Distl, R., Gilgen, H., Perny, B., Keys, R., Krause, E., Larsen, C. C., Mörl, K., Pelayo, J. and Vobian, J.** (1995), "Definition of polarization mode dispersion and first results of the COST 241 round-robin measurements", *Pure Appl. Opt.*, Volume 4, pp 511-522.

20. **Ghatak, A. J.** and Thyagarajan, K. (1998), "Introduction to Fiber Optics", Cambridge University Press (1998).

21. **Cyr, N.** (2004), "Polarization Mode Dispersion Measurement: Generalization of the Interferometric Method to Any Coupling Regime", *J. Lightwave Technol.*, Volume 22, No. 3, pp 794-805.

22. **Gisin, N.**, Von der Weid J. P. and Pellaux J. P. (1991), "Polarization Mode Dispersion of Short and Long Single-Mode Fibers", *J. Lightwave Technol.*, Volume 9, No. 7, pp 821-827.

23. **Perny, B.**, Zimmer, C., Prieto, F. and Gisin, N. (1996), "Polarization mode dispersion: Large scale comparison of Jones matrix eigenanalysis against interferometric measurement techniques", *Electron. Lett.*, Volume 32, No. 7, pp 680-681.

24. **Heffner, B. L.** (1996), "PMD measurement techniques – a consistent comparison", *OFC Technical Digest*, pp 292-293, March 1996.

25. **Williams, P. A.** (1997), "Summary of current agreement among PMD measurement techniques", IEC, SC86, WG1, September 1997, Edinburgh, Scotland.

26. **Peters, J. W.**, Özgür, M. R. and Gebizlioğlu, O. S. (2005), "Field Measurements of PMD Using Four Common Measurement Techniques", *Opt. Society of America*.

27. **Williams, P. A.,** (1996), "TIA round robin for the measurement of PMD", SOFM 1996, NIST Special Publications 905, pp 125-129.

28. **Olsson, B. E.**, Karlson, M. and Andrekson, P. A. (1998), "Polarization Mode Dispersion Measurement Using a Sagnac Interferometer and a Comparison with the Fixed Analyzer Method", *IEEE Photon. Technol. Lett.*, Volume 10, No. 7, pp 997-999.

29. **Frins, E. M.** and Dultz, W. (1997), "Rotation of the Polarization Plane in Optical Fibers", *J. Lightwave Technol.*, Volume 15, No. 1, pp 144-147.

30. **Namihira, Y.** and Nakajima, K., J. (1994), "Comparison of various Polarization Mode Dispersion measurement methods in 1600 km EDFA system", *Electron. Lett.*, Volume 30, No. 14, pp 1157-1159.

31. Direct Core Monitoring, Optical Fiber Fusion Splicer, SUMIOFCAS, "MicroCore", TYPE-37 TYPE-37B, Guide to Operation.

32. **CD/PMD Analyzer Source**, FLS-5800, User Guide.

33. **Agilent 8163A/B** Lightwave Multimeter, Agilent 8164A/B Lightwave Measurement System, & Agilent 8166A/B Ligtwave Multichannel System.

34. **Optical spectrum analysis application note** 1550-4, Agilent Technologies, 1996.

35. **Agilent 86140B** Series Optical spectrum Analyzer's User's Guide.

36. **Polarization Mode Dispersion Analyzer FTB-5500B**, EXFO User Guide.

37. **Adaptif photonics** User's Guide.

38. **Poole, C. D.** and Wagner, R. E. (1986), "Phenomenological Approach to Polarisation Dispersion in Long Single-Mode Fibres", *Electron. Lett.*, Volume 22, No. 19, pp 1029-1030.

39. **Cameron, J.**, Bao, X. and Stears, J. (1998), "Time evolution of polarization mode dispersion for aerial and buried cables", *OFC Technical Digest*, pp. 240-241.

40. **Waddy, D.**, Lu, P., Chen, L. and Bao, X. (2001), "The Measurement of Fast State of Polarization Changes in Aerial Fiber", OFC 2001, Volume 4, Issue, 2001, pp ThA3-1 – ThA3-3.

41. **Heffner, B. L.** (1994), "Single-mode propagation of mutual temporal coherence: equivalence of time and frequency measurements of polarization-mode dispersion" *Opt. Lett.*, Volume 19, No. 15, pp 1104-1106.

42. **Chiao, R. Y.** and Wu, Y. S. (1986), " Manifestation of Berry's Topological Phase for the Photon", *Phys. Rev. Lett.*, Volume 57, Number 8, pp 933-936.

43. **Tomita, A.** and Chiao R. (1986), "Observation of Berry's Topological Phase by Use of an Optical Fiber", *Phys. Rev. Lett.*, Volume 57, Number 8, pp 937-940.

44. **Cyr, N.** (1999), "Equivalence of Poincaré sphere and Jones matrix analyses for Determination of PMD", *OFMC Convention, Nantes, France* 1999.

45. **Galtarossa, A.**, Gianello, G., Someda, C. G. and Schiano S. M. (1996), "In-Field Comparison Among Polarization-Mode-Dispersion Measurement Techniques", *J. Lightwave Technol.*, Volume 14, No. 1, pp 42-49.

46. **Gibbon, T. B.** (2003), "The Measurement of Polarization Mode Dispersion in an Optical Fibre", Dissertation, NMMU, December 2003.